ISTANBUL TECHNICAL UNIVERSITY ★ GRADUATE SCHOOL OF SCIENCE ENGINEERING AND TECHNOLOGY

THE BEHAVIOR OF QUAY WALLS DURING EARTHQUAKES

M.Sc. THESIS

Doruk DİKER

Department of Civil Engineering

Soil Mechanics and Geotechnical Engineering Programme

Thesis Advisor: Prof. Dr. Ayfer ERKEN

DECEMBER 2015

ISTANBUL TECHNICAL UNIVERSITY ★ GRADUATE SCHOOL OF SCIENCE ENGINEERING AND TECHNOLOGY

THE BEHAVIOR OF QUAY WALLS DURING EARTHQUAKES

M.Sc. THESIS

Doruk DİKER
(501131304)

Department of Civil Engineering

Soil Mechanics and Geotechnical Engineering Programme

Thesis Advisor: Prof. Dr. Ayfer ERKEN

DECEMBER 2015

İSTANBUL TEKNİK ÜNİVERSİTESİ ★ FEN BİLİMLERİ ENSTİTÜSÜ

RIHTIM DUVARLARIN DEPREM SIRASINDA DAVRANIŞI

YÜKSEK LİSANS TEZİ

Doruk DİKER
(501131304)

İnşaat Mühendisliği Anabilim Dalı

Zemin Mekaniği ve Geoteknik Mühendisliği Programı

Tez Danışmanı: Prof. Dr. Ayfer ERKEN

ARALIK 2015

Doruk DİKER, a **M.Sc.** student of ITU **Graduate School of Science Engineering and Technology** student ID **501131304**, successfully defended the **thesis** entitled "**THE BEHAVIOR OF QUAY WALLS DURING EARTHQUAKES**", which he prepared after fulfilling the requirements specified in the associated legislations, before the jury whose signatures are below.

Thesis Advisor : **Prof. Dr. Ayfer ERKEN** ....
İstanbul Technical University

Jury Members : **Assoc. Prof. Dr. Ayşe EDİNÇLİLER BAYKAL**....................
Boğaziçi University

Asst. Prof. Dr. Berrak TEYMÜR ....
İstanbul Technical University

Date of Submission : 27 November 2015
Date of Defense : 25 December 2015

To my mother and my father,

FOREWORD

This master of thesis has been prepared for submission to Istanbul Technical University, Civil Engineering Department, Soil Mechanics and Geotechnical Engineering Programme.

I would like to express my sincere thanks to my advisor Prof. Dr. Ayfer ERKEN, for her guidance, for sharing her knowledge and constructive cricitism to help me complete this thesis on time.

I would like to present my deepest thanks to Behnam ROMOUZİ-KOUCHEHBAGH (B.Sc.) for sharing his knowledge and helps about finite element programme. I also exhibit my sincerest thanks to Research Asst. Gülçin NOMALER for helps about finite element programme.

Finally, I would like to present my special thanks to my mother Nermin DİKER and my father Mehmet Faysal DİKER. You were my most important support for all my life. I could not succeed without your supports. Also, I exhibit my deepest appreciation to all my family members including my grandmother, my aunts, my uncles and my friends for their supports.

December 2015

Doruk DİKER
(Civil Engineer)

TABLE OF CONTENTS

Page

ABBREVIATIONS

B : Width of wall
CPT : Cone Penetration Test
CRR : Cyclic Resistance Ratio
CSR : Cyclic Stress Ratio
H : Height of wall
HS : Hardening Soil
HSsmall : Hardening Soil small strains
LE : Linear Elastic
N : Standard Penetration Test Blow Count
SPT : Standard Penetration Test
US : United States

LIST OF TABLES

Page

LIST OF FIGURES

Page

THE BEHAVIOR OF QUAY WALLS DURING EARTHQUAKES

SUMMARY

Soils show different behavior under dynamic loading conditions compared to static loading conditions. While designing structures and their foundations, both static and dynamic loading conditions must be considered. Dynamic loads such as earthquake loading affect the behavior of soil and should be examined before design. In port structures, quay walls are affected by lateral spreading during earthquakes. Due to the liquefaction in reclaimed backfill or foundation soils, quay wall movements take place. This type of failure caused wall damages costing 10 billion US Dollars in 1995 Kobe Earthquake.

In this study, general informations about soil liquefaction and its mechanism are presented. In addition, factors triggering liqufaction, liquefaction behavior of soils, liqufaction potential of soils, liquefaction induced displacements, residual strength of soils and evaluation of liquefaction potential are briefly explained. Moreover, lateral spreading, quay wall displacements due to earthquake, liquefaction induced lateral spreading prediction methods, quay wall displacement prediction methods, settlement prediction methods are explained and brief information about 1995 Kobe Earthquake is given. Furthermore, a quay wall damaged during 1995 Kobe Earthquake is modeled in finite element programme PLAXIS. Model parameters are determined by using Standard Penetration Test (SPT) data. The displacements that are calculated with finite element programme are compared to observed displacements and analytical and empirical methods. Moreover, the effect of different earthquake motion to wall displacement is studied. Kocaeli Earthquake (1999), Chi-Chi Earthquake (1999), Northridge Earthquake (1994) and Friuli Earthquake (1976) accelograms are used as different input motions and their effect to quay wall displacement is analyzed. Besides, the effect of densification in reclaimed backfill and foundation soil is studied. Also, the effect of dimension ratio B/H is analyzed. Finally, a damaged quay wall at Kushiro Port during 1993 Kushiro-oki earthquake is modeled and wall displacements are determined. In conclusion, Mononobe-Okabe method is not sufficient for quay wall design as it ignores liquefaction behavior. Local site effects should be evaluated and finite element analyses should be performed to understand wall behavior during earthquakes.

RIHTIM DUVARLARIN DEPREM SIRASINDA DAVRANIŞI

ÖZET

Depremler doğadaki endişe verici felaketlerden biridir ve yıkıcı hasarlara neden olabilir. Neredeyse her kıtada, depremler şehirleri ve köyleri tahrip eder. Uygun mühendislik çözümleri uygulanmadığı sürece depremler ağır hasarlara, sayısız ölümlere ve milyonlarca dolarlık ekonomik kayıplara neden olacaktır. Zararlara neden olan ana sebepler, zemin sıvılaşmaları, taşıma gücü kayıpları, şev göçmeleri, yüzey kırılmaları ve kum kaynamalarıdır.

Zeminler dinamik yüklemeler altında statik yüklemelere göre daha farklı davranış gösterirler. Yapıların ve temel sistemlerinin tasarımı sırasında hem statik hem dinamik yükleme koşulları göz önüne alınmalıdır. Deprem yükleri gibi dinamik yükler zemin davranışını etkiler ve tasarımdan önce incelenmelidir.

Suya doygun kumlu zeminlerde deprem sırasında sıvılaşma ortaya çıkabilir. Deprem sırasında dalga yayılımı nedeniyle boşluk suyu basıncı artar. Sismik yüklemenin hızlı olması nedeniyle zemin drenajsız koşullarda yüklenir ve oluşan boşluk suyu basıncı sönümlenemez. Zemindeki efektif gerilme, artan boşluk suyu basıncı nedeniyle zamanla azalır. Bu nedenle zeminde önemli mukavemet kayıpları meydana gelir ve bu olaya sıvılaşma denir. Malzeme özellikleri zeminin sıvılaşma davranışını belirler. Gevşek yerleşimli kohezyonsuz zeminler sıvılaşmaya daha yatkın iken sıkı yerleşimli zeminler deprem sırasında sıvılaşmayabilir. Fakat, eğer yükleme koşulları uygunsa, oluşan aşırı boşluk suyu basıncı sebebiyle yumuşama gözlemlenebilir.

Sıvılaşma nedeniyle büyük deformasyonlar ortaya çıkabilir ve bu deformasyonlar ağır yapı (binalar, köprüler, barajlar, yollar, demiryolları, limanlar vs.) hasarlarına ve altyapı (boru hatları, elektrik ve internet ağı, su isale hatları vs.) hasarlarına neden olur. Sıvılaşmanın neden olduğu deformasyonlar akma göçmeleri, yanal yayılmalar, taşıma gücü kayıpları, gömülü yapıların kabarması, zemin oturmaları ve zemin salınımlarıdır.

Yanal yayılmalar alt tabakada bulunan zeminin sıvılaşması nedeniyle üstte yer alan zemin tabakasının kayması olarak tanımlanabilir. Sıvılaşmanın neden olduğu yanal yayılmalar iki gruba ayrılabilir: zemin yüzeyinin eğimli olması nedeniyle ortaya çıkan yerdeğiştirmeler ve rıhtım duvar kaymalarının neden olduğu yerdeğiştirmeler. İlk grupta zemin yüzeyi eğim nedeniyle şev boyunca aşağı doğru hareket eder. İkinci grupta ise rıhtım duvar ve rıhtım duvarın arkasında yer alan zemin sıvılaşma nedeniyle denize doğru hareket eder.

Rıhtım duvarlar deprem sırasında duvarın arkasında bulunan gevşek ve suya doygun zeminin sıvılaşması nedeniyle hasar görebilir. Denize doğru kaymalar, duvar dönmeleri ve oturmalar deprem sırasında ve sonrasında ortaya çıkabilir. 1964 Niigata

Depremi, 1986 Kalamata Depremi, 1995 Kobe Depremi, 1999 Chi-Chi Depremi ve 1999 Kocaeli Depremi limanlarda bulunan istinat yapılarına ciddi hasarlar vermiştir. Duvar geri dolgusundaki ya da temel zeminindeki sıvılaşmalar nedeniyle duvarlarda yer değiştirmeler ortaya çıkmıştır. Bu tip göçmeler 1995 Kobe Depreminde 10 milyar Amerikan Doları zarara neden olmuştur.

Limanlarda yer alan dayanma yapılarının sismik performansı oldukça fazla önem arz etmektedir, zira liman tipi yapılar ticarette çok büyük öneme sahiptir ve uzun vadeli pahalı yatırımlar olarak inşa edilmektedirler. Deprem sırasında limanlarda oluşacak hasarlar ülkelerin ekonomilere ciddi zararlar verebilir ve ekonmik krizlere sebep olabilir. Ayrıca, felaketzede ülkelerin deprem sonrasında deniz yoluyla gönderilen yardımları kabul etmesini zorlaştırır. Bu sebeplerden ötürü, rıhtım duvarların davranışı dikkatlice analiz edilmelidir.

Deprem sırasında sıvılaşma nedeniyle meydana gelen yanal yayılmaların belirlenmesi önemlidir. Bu sebeple çeşitli araştırmacılar tarafından yanal yayılmaların neden olduğu deformasyonları tahmin etmek için analitik, deneysel ve fiziksel yöntemler geliştirilmiştir. Deneysel yöntemler diğer yöntemlere göre daha basit ve daha az komplekstir. Ayrıca deneysel yöntemler deplasmanlara ve çeşitli geometrik parametrelere ve zemin parametrelerine dayanır. Bununla beraber, deprem sırasında ortaya çıkan oturmaları belirlemek için çeşitli deneysel yöntemler de önerilmiştir. Bu yöntemler hem inşa edilmiş yapılardaki potansiyel zararları belirmek için hem de tasarım aşamasında kullanılabilir.

Bu çalışmada, zemin sıvılaşması ve sıvılaşma mekanizması hakkında genel bilgiler verilmiştir. Ayrıca sıvılaşmaya neden olan faktörler, zeminlerin sıvılaşma davranışı, zeminlerin sıvılaşma potansiyeli, sıvılaşmanın neden olduğu deplasmanlar ve zeminlerin rezidüel mukavemeti kısaca açıklanmıştır. Daha sonra depremlerin neden olduğu yanal yayılmalar, rıhtım duvar deformasyonları, yanal yayılma sıvılaşma tahmin metotları, rıhtım duvar deplasman tahmin metotları ve oturma tahmin metotları hakkında kısa bilgiler verilmiştir ve 1995 Kobe Depremi kısaca sunulmuştur.

1995 Kobe Depremi sırasında hasar görmüş bir rıhtım duvar sonlu eleman programı PLAXIS ile modellenmiştir. Model parametreleri Standart Penetrasyon Testi (SPT) dataları kullanılarak belirlenmiştir. Sonlu eleman programı ile hesaplanan deplasmanlar, sahada ölçülen deplasmanlar ve analitik yöntemler ile hesaplanan deplasmanlar ile karşılaştırılmıştır.

Ayrıca farklı deprem hareketlerinin duvar deplasmanına etkisi incelenmiştir. Kocaeli Depremi (1999), Chi-Chi Depremi (1999), Northridge Depremi (1994) ve Friuli Depremi (1976) kayıtları kullanılmış ve duvara etkisi incelenmiştir. Duvarın yanal ve düşey yerdeğiştirmeleri sonlu eleman programı kullanılarak hesaplanmıştır.

Bunlara ek olarak, dolgu zeminde ve temel zemininde sıkılaştırma etkisi analiz edilmiştir. Farklı zemin tabakaları farklı iyileştirme koşulları için sıkılaştırılmıştır. İlk durumda duvar geri dolgusu iyileştirilmiştir. İkinci durumda temel zemini iyileştirilmiştir. Üçüncü durumda ise duvarın topuk kısmı altında yer alan temel zemini kısmi olarak iyileştirilmiştir. Geri dolgu zemininin sıkılaştırılması deformasyonları % 40, temel zeminin iyileştirilmesi deformasyonları % 15 ve temel zeminin kısmi olarak iyileştirilmesi deformasyonları %10 azaltmıştır.

Ayrıca, duvar boyutlarının etkisi (B/H oranı) incelenmiştir. Duvarın yatay ve düşey yerdeğiştirmeleri sonlu eleman programı kullanılarak hesaplanmıştır. Sıvılaşmanın olduğu durumlarda B/H oranının önemli bir etkiye sahip olmadığı görülmüştür.

Son olarak Kushiro Limanında bulunan ve 1993 Kushiro-oki depreminde hasar görmüş bir duvar sonlu eleman programında analiz edilmiş, deplasmanları hesaplanmıştır. Kushiro Limanında görülen deformasyonlar Kobe Limanında görülen deformasyonlara göre daha azdır çünkü Kushiro Limanındabulunan zemin tabakaları Kobe Limanına göre daha sıkıdır.

Sonuç olarak, Mononobe-Okabe yöntemi sıvılaşma durumlarını dikkate almaması nedeniyle rıhtım duvar tasarımı için yeterli değildir. Sismik tasarım katsayıları aşıldığında, yıkıcı hasarlar ortaya çıkmaktadır. Yerel zemin etkileri değerlendirilmeli ve duvar davranışını anlamak için sonlu eleman analizleri gerçekleştirilmelidir.

1. INTRODUCTION

1.1 Definition of Problem

Earthquakes are one of the most concerning disastrous events in nature and can cause catastrophic damages. Almost every continent, earthquakes can destroy cities and villages. As long as appropriate engineering solutions are not applied, earthquakes will lead to heavy damages, numerous deaths and economical loss of million dollars. Main reasons of damages are soil liquefaction, loss of bearing capacity, slope failures, surface refractions and sand boiling.

Large deformations occur due to liquefaction and these deformations lead to heavy damage of structures (buildings, bridges, dams, roads, railways and ports etc.) and infrastructure (lifelines such as pipelines, power and internet network, transportation lines, water and sewage etc.). Liquefaction induced deformations are flow failures, lateral spreading, loss of bearing capacity, uplift of buried structures, settlements (ground subsidence) and ground oscillations.

Prediction of displacements due to lateral spreading is a challenging problem in geotechnical engineering. Analytical, empirical and physical methods have been proposed by several researchers to predict displacements. Also, finite element method can be used for modeling lateral spreading problems.

Seismic performances of waterfront retaining structures on ports are very significant because this type of structures has massive importance on trade and they are built as costly long-term investments. Failures during earthquakes at ports can damage economy of a nation and may lead to economical crisis. Also, makes it difficult for disaster-stricken countries to accept help using seaway after earthquakes. For these reasons, seismic behavior of quay walls should be analyzed carefully.

Kobe Earthquake hit Japan on 17 January 1995. The magnitude of the earthquake was 7.2 on the Richter scale. Quay walls in Kobe Port displaced seaward about maximum 5 m and about 3 m in average, inclined 4 degrees in the direction of sea (Inagaki et al., 1996). Artificial islands, Port Island and Rokko Island, are severely damaged during earthquake due to liquefaction. Total damage on waterfront area cost more than 10 billion US Dollars.

There are other cases that quay walls are damaged due to earthquakes. In 1964 Niigata Earthquake, 92.4% of harbor structures were severely damaged (Hayashi et al., 1966). In 1986 Kalamata Earthquake, block type quay walls moved around 15 cm and rotated 4-5 degrees towards sea and settlements on backfill were observed varying around 20 cm to 0 cm at the distance of 30 m to 40 m. (Pitilakis and Moutsakis, 1989). In 1999 Chi-Chi Earthquake, caisson quay walls displaced towards sea 1 m in average because of liquefaction of loosely filled sand behind wall due to strong shaking (Chen and Huang, 2000). In 1999 Kocaeli Earthquake port structures were damaged extensively. Quay walls at Derince Port moved towards sea and settlements were observed on backfill. All artificial filled areas moved into sea.

1.2 Purpose of Thesis

The objective of this study is to model quay wall behavior during earthquakes. A damaged quay wall in Kobe is modeled in finite element programme PLAXIS. The displacements that are calculated with finite element programme are compared to observed displacements, analytical methods and empirical methods.

Moreover, the effect of earthquake motion to wall displacement is studied. Kocaeli Earthquake (1999), Chi-Chi Earthquake (1999), Northridge Earthquake (1994) and Friuli Earthquake (1976) accelograms are used as different input motions and their effect to quay wall displacement is analyzed.

Besides, the effect of densification in reclaimed backfill and foundation soil is studied. Effects of densification of foundation, densification of backfill and partial densification of foundation are analyzed.

Also, the effect of dimension ratio B/H is analyzed. For different B/H ratios such as 0.66, 0.80, and 1.00 analyses are performed.

Furthermore, a damaged quay wall at Kushiro Port is analyzed. Three different earthquake records are applied as dynamic multipliers, including Chi-Chi (1999), Northridge (1994) and Friuli (1976) earthquakes. Horizontal and vertical displacements of caisson quay wall are calculated.

In addition, lateral displacements of caisson quay wall during 1995 Kobe earthquake calculated with analytical and empirical methods. Displacements in horizontal direction calculated with Richards-Elms (1977), Whitman-Liao (1979), Franklin-Chang (1985), Iai et al. (1997), Iai et al. (1999), LSI, Hamada (1994), Multi Linear Regression (MLR) and EPOLLS method.

Lastly, settlements beneath caisson during 1995 Kobe Earthquake are also calculated with empirical methods. Tokimatsu and Seed (1987), Ishihara and Yoshimine (1992) methods are used in settlement calculations.

1.3 Scope of Thesis

This thesis consists of five chapters. In the first chapter, definition of problem is given. Purpose of thesis and scope of thesis are explained.

In the second chapter, brief information about dynamic behavior of soils and soil liquefaction are given. Behavior of sand-like and clay-like soils under cyclic loadings is explained. Soil liquefaction and its mechanism, factors triggering soil liquefaction, liquefaction potential of soils, liquefaction induced failures and residual strength of liquefied soils are presented.

In the third chapter, literature review is given. Lateral spreading and its effects to engineering structures are explained. Mechanism of liquefaction induced lateral spreading, liquefaction induced quay wall damages, lateral spreading displacement prediction methods, quay wall displacement methods and liquefaction induced settlement prediction methods are presented. Also, brief information about 1995 Kobe earthquake is given in this chapter.

In the fourth chapter, finite element method and case studies are presented. Constitutive soil models, selection of soil model and model parameters, Hardening soil with small strains model in PLAXIS and determination of model parameters are explained. Also, case studies are presented in this part.

In the fifth chapter, reached conclusions are presented.

2. DYNAMIC BEHAVIOUR OF SOILS AND SOIL LIQUEFACTION

2.1 Introduction

Dynamic behavior of soils under cyclic loading and soil liquefaction due to seismic loadings are given in this chapter. Definition of soil liquefaction and its mechanism, factors triggering soil liquefaction, liquefaction potential of soils, liquefaction induced failures and residual strength of liquefied soils are presented.

2.2 Dynamic Behavior of Soils

Soils show different behavior under dynamic loading conditions comparing to static loading conditions. While designing structures and their foundations, both static and dynamic loading conditions must be considered. Dynamic loads such as earthquake loading, wave loading, machine foundations, blasting and traffic loading affect the behavior of soil and should be examined. Safety against failure must be ensured and allowable displacements must not be exceeded both in static and dynamic conditions.

During and after earthquakes, strength loss or extreme deformations may cause ground failures or instability. Evaluation of dynamic behavior of soils is significant for the estimation of potential deformations and strength loss. The estimation procedures are different for sandy and clayey soils.

Boulanger and Idriss (2004) state that dynamic behavior of fine grained soils and coarse-grained soils are different under cyclic loadings. The behavior of low-plasticity silts and clays, which are in the transition zone between “sand like” and “clay-like”, is more complex. The authors used “sand like” and “clay-like” terms to define the stress-strain behavior under cyclic and monotonic loading which are similar to sands and clays.

Particle size, grain size distribution and relative density affect strength and compactibility of sands and “clay-like” soils. For clays, plasticity index is important.

According to Boulanger and Idriss (2004), the important points for the behaviour and engineering properties of sands are:

- The stress-strain behavior of sands is mainly related to relative density (D_R) and confining pressure.
- Sands usually have a small enough compressibility because relative density does not change in significant amount while effective consolidation stress is increasing.
- For sands, there is no relationship between relative density and confining stress history.
- For sands, conventional tube sampling methods may possibly cause disturbance. Sands lose most of effective stress and become undisturbed by vibration and strains during sampling process.
- The determination of cyclic loading behavior of sands can not be obtained reliably because of the effects of the disturbance. Frozen sampling methods give more reliable results, but it is not often used due to the cost of this technique.
- The penetration resistances of SPT and CPT are sensitive to relative density and other characteristic parameters of sands, tests can be used for correlation for other parameters such as internal friction angle and cyclic resistance ratio.
- Because of the reasons given above, penetration tests and semi-empirical correlations are used while investigating the behavior of sands.

Boulanger and Idriss (2004) claim that important points for the behavior and engineering properties of clays are:

- In general, the compressibility of clays is high because of the void ratio or density is related to effective consolidation stress and stress history.
- For clays, there is unique relationship between void ratio and confining pressure history.

- Thin-tube sampling methods have less possibility of disturbance for clays because the permeability of clays is generally low and clays remain undrained during sampling.
- For determination of monotonic and cyclic undrained strengths of clays, laboratory tests can be performed.
- The most significant step for the determination of the strength of clayey deposits, is the determination of pre-consolidation stress by performing consolidation test or using the knowledge of the historical loadings.
- CPT correlations give reliable prediction about undrained shear strength of clayey soil deposits.
- SPT correlations give rough prediction about undrained shear strength of clayey soil deposits.
- Because of the reasons given above, laboratory testing and in-situ testing methods are used while investigating the behavior of clays.

As well as determination of strength and stress-strain parameters of soils and stability analyses under static loading conditions, research of the behavior of soils under cyclic loading is one of the important problems in geotechnical engineering.

Coarse grained and fine grained soils behave differently under cyclic loadings. Erken et al. (2004b) state that, providing saturated sandy soils are loose, they are exposed to large deformations by increasing pore pressures under earthquake loadings. However, the dynamic behavior of silty soils is related to plasticity index. In low plasticity silts, excess pore pressures are generated under earthquake loadings; then deformations and strength loss are observed. The dynamic behavior of clays depends on consistency. As the water content approaches to liquid limit, deformations under earthquake loadings significantly increase, but change in pore water pressure is limited.

According to El Hosri (1984), in silty soils, more pore pressure is generated compared to sandy soils. Generation of pore pressure is more rapid in silty-clayey soil deposits, compared to sandy soils in the beginning of dynamic loading.

When investigating dynamic behavior of soils, laboratory and in-situ tests are used. Cyclic triaxial test, cyclic direct simple shear test and cyclic torsional shear test can be performed in laboratory. In the field, SPT, CPT, geophysical tests and seismic dilatometer can be performed. Earthquake loadings and generated stresses in the field can be modeled in laboratory with test equipments. Also, dynamic properties of soils can be determined by using in-situ tests. The suitable option is a combined test programme consisting of both laboratory tests on undisturbed samples and in-situ tests.

2.3 Soil Liquefaction

Soil liquefaction is the most important reason for hazards during earthquake loadings. The destructive effects of liquefaction are seen first in Alaska and Niigata earthquakes in 1964. These earthquakes caused slope failures, foundation failures and floatation of buried structures. After these earthquakes, mechanism of liquefaction started to be researched. Towhata (2008) gives information about the history of liquefaction researches in Table 2.1.

Table 2.1 : Historical change of topics in liquefaction studies (Towhata, 2008).

Topics	Years	Remarks
Mechanism of liquefaction	1960s	Niigata and Alaska earthquakes in 1964
Assessment of liquefaction potential	1970s-1980s	Minimum SPT-N, Factor of safety, Low liquefaction potential of gravel and fine silt Ground subsidence after liquefaction
Prevention of liquefaction	1970s-now	Soil improvement (compaction, gravel drain, grouting mitigation under existing structures etc.) Even gravels and cohesionless silt liquefy
Consequence of liquefaction	1983-2000	Permanent displacement; cause and prediction of displacement
Mitigation of permanent displacement	1995-now	Reliability of lifeline/river dike, Use of underground wall, Protection of existing structures
Real-time earthquake engineering	1990s-now	Quick detection of liquefaction (within one hour and starting emergency action as quickly as possible)

2.3.1 Definition of liquefaction and its mechanism

In loose sandy soils with saturated by water, liquefaction may occur during earthquake. Under earthquake loadings, pore water pressure increases as a result of wave propagation. As seismic shaking occurs rapidly, the cohesionless soil is loaded undrained conditions. According to equation (2.1), effective stress decreases with time, because pore water pressure increases.

$$\sigma = \sigma' - u \qquad \textbf{(2.1)}$$

Since effective stress of soil decreases, shear modulus decreases. Shear strength of sand also decreases, as effective stress and internal friction angle (tanϕ) decrease. As a result, sand becomes softer with time (Towhata, 2008; Kramer, 1996; Day, 2012).

Hence the pore water pressure increase, the water starts to move upwards to the surface. The sand and water start to spout out to surface, if soil becomes weak enough and there are openings in surrounding ground. Hamada (2014) shows the mechanism of sand boiling in Figure 2.1.

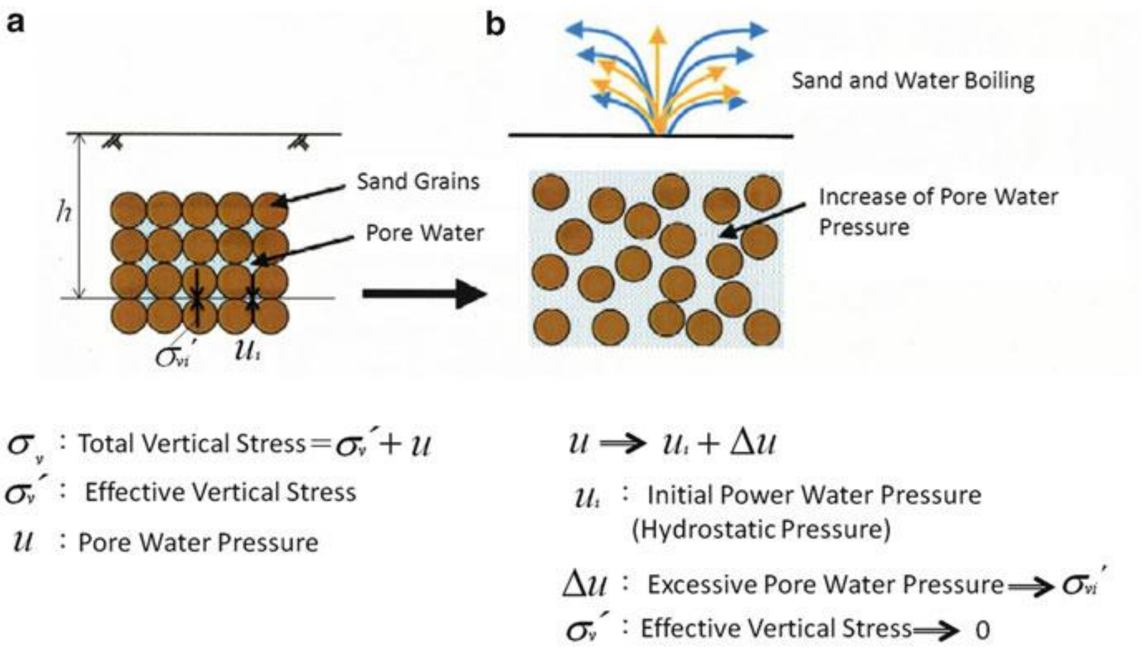

Figure 2.1 : Mechanism of soil liquefaction (Hamada, 2014).

Under extreme conditions, the effective stress of soil may decrease to zero. There is no stress transfer between soil particles, because of zero effective stress. Soil particles start to float in water and soil is like mud water, suspension in water. In this case, there is no shear modulus or shear strength. As a result large deformations take place even under small stresses (Towhata, 2008). In Figure 2.2, as an example, a tilted building because of liquefaction, can be seen from 1999 Kocaeli earthquake in Tığcılar (Erken et al., 2004a).

Figure 2.2 : A tilted building due to liquefaction (Erken et al., 2004).

2.3.2 Factors triggering liquefaction

Many factors like earthquake characteristics, site conditions or geological conditions affect liquefaction susceptibility of soil. These factors affect the behavior of soil during liquefaction. The factors triggering liquefaction is given by Day (2012);

- **Intensity and duration of earthquake:** Liquefaction potential rises if earthquake intensity, acceleration and duration of earthquake increase.
- **Ground water at site:** Unsaturated soils above ground water table do not liquefy.

- **Soil type:** Cohesionless soils and non-plastic silty soils are susceptible to liquefaction.
- **Relative density (D_r):** Loose soils are more susceptible to liquefaction than dense soils.
- **Grain size distribution:** Uniformly graded, non-plastic soils have more tendency to liquefaction than well graded soils.
- **Conditions of placement:** Loose and segregated soils such as soil deposits in lakes, rivers or ocean, have more potential to liquefy.
- **Drainage:** In permeable soils, if drainage of water is easy, excess pore pressure can dissipate quickly and liquefaction may not occur.
- **Confining pressures:** In greater confining pressures, liquefaction potential of soil is lower.
- **Particle shape:** Rounded shaped soil particles can densify easily compared angular shaped soil particles. So, rounded particles have more tendency to liquefaction.
- **Aging and cementation conditions:** Newly deposited soils have more liquefaction potential compared to older soil deposits.
- **Loading history of soil:** Liquefaction resistance of soil rises with over consolidation ratio (OCR) of soil and also lateral earth pressure at rest (K_0) increases liquefaction resistance.
- **Structural Loads:** Building loads can increase the potential of liquefaction. Additional shear stresses are generated because of structural loads, and this increases the liquefaction potential of soil.

2.4 Liquefaction Potential of Soils

In evaluation of liquefaction potential of soils, the first step is the determination of liquefiable soil layers. Mostly, cohesionless soils have tendency to liquefy. Liquefaction usually occurs in saturated loose sands or silts. The liquefaction potential of low-plasticity silts and non-plastic silts should be evaluated carefully, because this type of soils usually have low permeability and dissipation of excess pore pressure takes more time.

Tsuchida (1970) performed sieve analyses on alluvial and diluvial soils that have liquefied during earthquakes. He summarized the test results and developed a range in grain size curves as liquefiable and not liquefiable as shown in Figure 2.3.

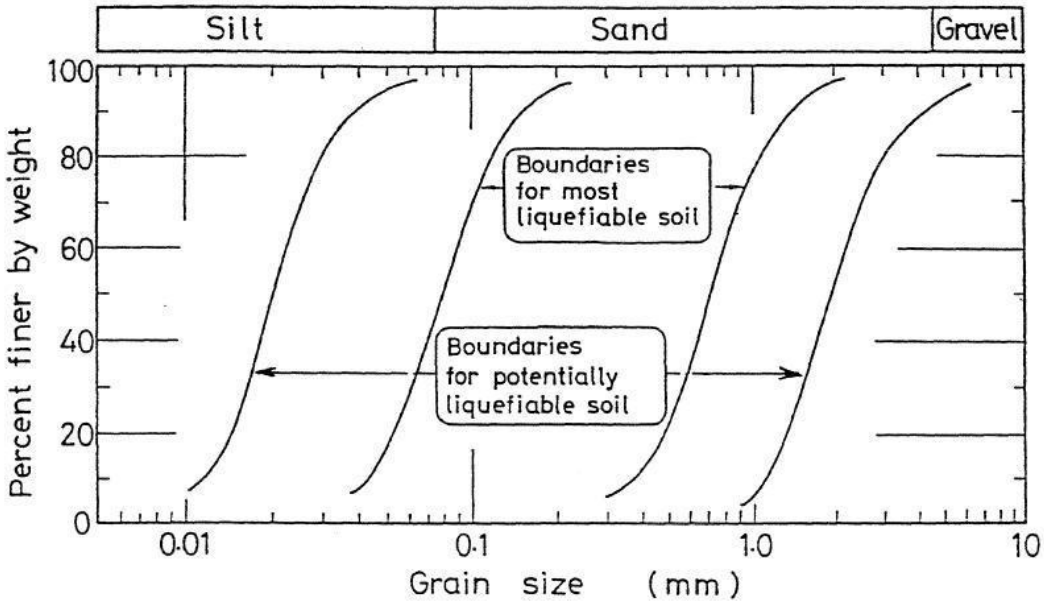

Figure 2.3 : Liquefiable and not liquefiable ranges in grain size (Tsuchida, 1970).

From the researches of Wang (1979), Seed et al. (1983) developed criteria to evaluate liquefaction susceptibility of clayey soils. According to Chinese criteria, soils are susceptible to liquefaction if they have the following characteristics:

- Clay content (defined as % finer than 0.005 mm) < 15%
- Liquid limit < 35
- Water content > 0.9 x liquid limit

Clay content and liquid limit are key parameters that can affect liquefaction behavior during earthquakes, but water content is not a key parameter because it is related to environmental conditions and errors occur during sampling.

Andrews and Martin (2000) re-evaluated the case histories from the researches of Wang (1979) and adjusted to U.S. standards (clay size defined as finer than 0.002). Their findings are given in Table 2.2.

Table 2.2 : Liquefaction susceptibility of silty soils (Andrews and Martin, 2000).

	Liquid Limit <32	Liquid Limit ≥ 32
Clay Content < 10	Susceptible to liquefaction	Further Studies Required (Considering plastic non-clay sized grains)
Clay Content ≥ 10	Further Studies Required (Considering non-plastic clay sized grains)	Not susceptible to liquefaction

According to Andrews and Martin (2000), soils which have clay content less than 10% and their liquid limit is less than 32, are susceptible to liquefaction. Soil which have clay content more than 10% and their liquid limit is more than 32 are not susceptible to liquefaction. Soils between these criteria should be tested in laboratory for evaluating the potential of liquefaction.

Seed et al. (2003) stated that if fines content is sufficient, fine particles separate coarser particles and control the behavior. In Figure 2.4, liquefiable range of soils is shown. Soils in Zone A are susceptible to “classic” (cyclically-induced) liquefaction. Soils in Zone B may liquefy or soften during earthquake and should be tested considering water content. Soils in Zone C (not in Zone A or Zone B) are not susceptible to classic type of liquefaction, but should also be controlled against liquefaction.

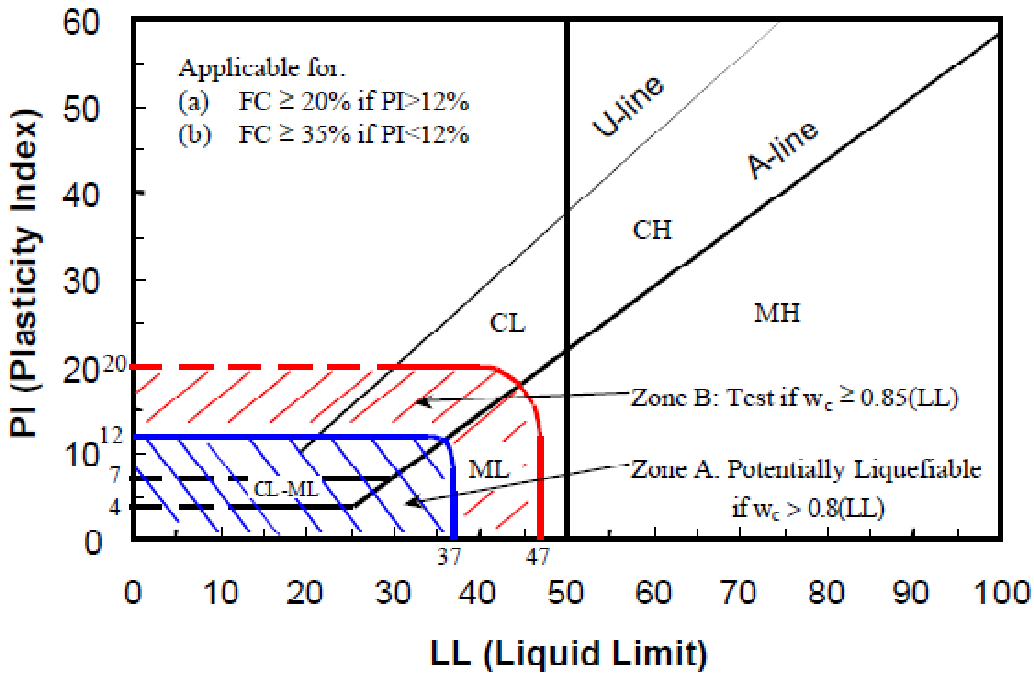

Figure 2.4 : Liquefiable soil types based on Seed et al. research (Seed et al., 2003).

2.5 Liquefaction Induced Displacements

Liquefaction causes different types of failures. Type of failure differentiates with environmental conditions and geometry. New York Transportation Department (2015) grouped liquefaction induced displacements into four:

- Flow failures
- Lateral Spreading
- Ground oscillation
- Loss of bearing capacity

Flow failure is defined by Youd (1973) as a state which unlimited flow of soil occurs. When liquefaction occurs, if the soil is unrestrained and mobilizes, large soil masses may move long distances in the formation of liquefied flows or whole blocks travelling in liquefied flows. Soil continues to flow until driving shear forces decreases (due to reduction of slope). When driving shear force equals to viscous shear resistance of flowing material, flow ceases. Flow failures usually occur in slopes which is inclined 5 percent or greater (New York Transportation Department, 2015).

Pacoima Dam is an example to flow failure. On February 9, 1971 San Fernando earthquake, has magnitude M_w 6.6, caused flow failure of dam (Jennings and Housner, 1971). Another example is Hebgen Lake earthquake. On August 17, 1959 an earthquake Mw 7.3, caused a flow failure in Montana. A flow in canyon created a temporary lake (Day, 2012). Failures are shown in Figures 2.5 and 2.6.

Figure 2.5 : Flow failure on Pacoima Dam (Day, 2012).

Figure 2.6 : Flow failure in Montana during Hebgen Lake Earthquake (Day, 2012).

Lateral spreading is the lateral displacement of soils or blocks at surface due to liquefaction of underlying soils. Unlimited flow is not seen as sediments are too dense; however limited flow may be seen. Lateral spreads usually occur on slopes as flat as 3 degrees (Youd, 1973; New York Transportation Department, 2015).

Lateral spreading affect relatively large areas and has different damages on different structure types. Lateral spreading can damage developed and residential areas, slopes, retaining structures, piles, bridge abutments, ports and harbors, buried pipelines and other lifelines.

Buildings which are constructed on slopes are affected directly from lateral spreading. Movements on slope cause damage to foundation of building. In 2011 Tohoku earthquake, structures on slopes severely damaged in Sendai City. In Figure 2.7, a damaged building on slope is shown (Hamada, 2014).

Figure 2.7 : Structural damage due to slope failure (Hamada, 2014).

Retaining walls can be damaged due to lateral spreading. Liquefaction on backfill causes wall movement. In 1999 Chi-Chi earthquake, a damaged retaining wall supporting highway embankment on slope, is given in Figure 2.8 (Huang, 2011).

Lateral spreading affects pile foundations. Laterally movement of foundation soil cause pile damages. In 1995 Hyogoken-Nambu earthquake pile damages were seen due to extensive liquefaction. At the top and bottom of piles, damages were observed. Damaged piles are shown in Figure 2.9 (Tokimatsu, 2009).

Figure 2.8 : Retaining wall damage due to slope failure (Huang, 2011).

Figure 2.9 : Pile damage due to lateral spreading (Tokimatsu, 2009).

In port structures, quay walls are affected by lateral spreading. Due to the liquefaction in reclaimed backfill soil, walls moves upward. In 1983, Akita Port was struck by Nihonkai-Chubu earthquake. Quay walls damaged due to generated pressure in backfill. It caused an increase in bending moment resulting wall crack. The damaged port and cross section is given in Figure 2.10 and 2.11 (PIANC, 2001).

Figure 2.10 : Quay wall damage in Akita Port during 1983 Nihonkai-Chubu earthquake (PIANC, 2001).

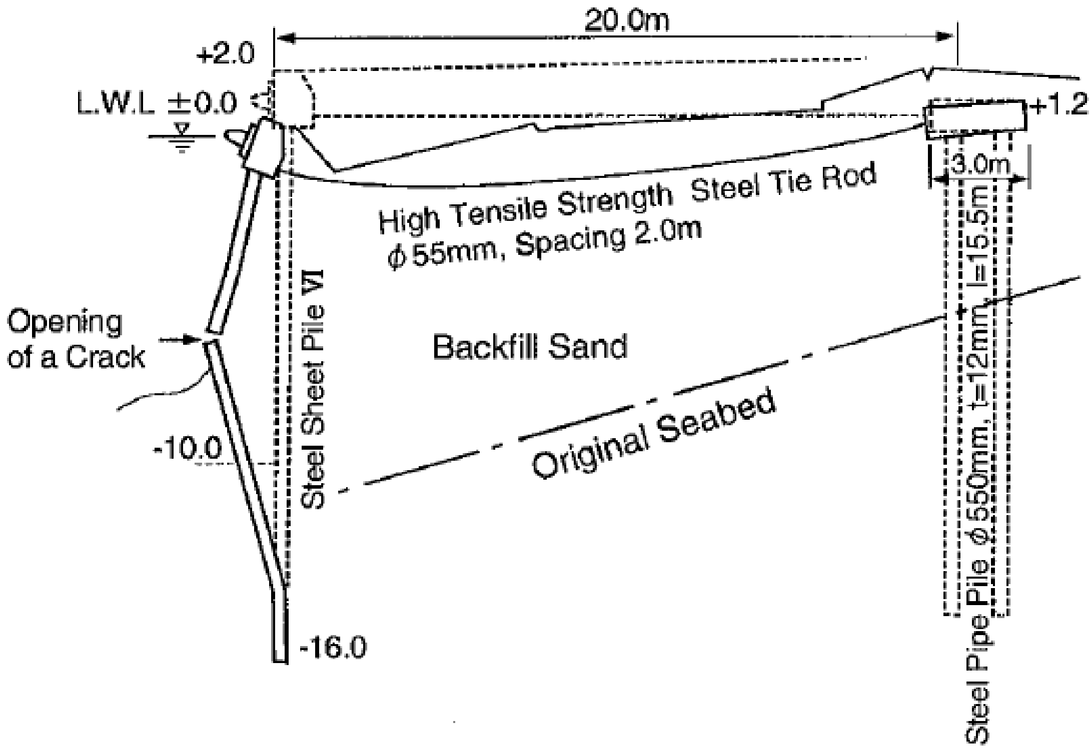

Figure 2.11 : Cross section of damaged quay wall in Akita Port (PIANC, 2001).

Ground oscillation is movement of soil deposit in surface to back and forth due to the liquefaction beneath a flat ground. The soil surface at surface generally cracks and becomes moving blocks. As blocks move, fissures develop between blocks, open and close during earthquake. Amplification of low-frequency seismic motions when transmitted into a liquefied soil deposit causes ground oscillation. Generally, permanent deformations are small. Mechanism of ground oscillation is shown in Figure 2.12 (Kramer, 1996; Youd, 1984).

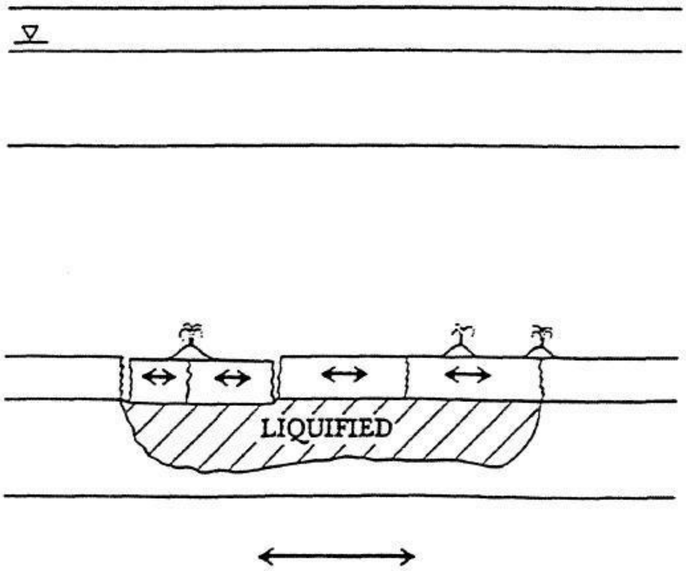

Figure 2.12 : Ground Oscillation before and after earthquake (Youd, 1984).

Sand boils are associated with liquefaction and follow ground oscillations. When liquefaction occurs, excess pore pressures are generated. Excess pore pressures cause upward flow of water between soil particles to channels or cracks. During the flow, sand particles may be carried to the surface. Sand boils are related to the magnitude of excess pore pressure, thickness of soil layers, permeability and fissuring (Kramer, 1996). Sand boils show points in site where excess pore pressure generated during earthquake. Sand boils generated during the 1993 Hokkaido-Nansei-oki earthquake at Hakodate Port, is shown in Figure 2.13.

Figure 2.13 : Sand boils at Hakodate Port during 1993 Hokkaido-Nansei-Oki Earthquake (PIANC, 2001).

Bearing capacity losses are observed when liquefaction occurs beneath foundation soil. As effective stress decreases during and after liquefaction, bearing capacity also decreases. Important settlements occur beneath foundation (Towhata, 2008).

Another effect of liquefaction is change of ground motion. Soil stiffness decreases during earthquake due to generation of excess pore pressure. At the beginning of the earthquake soils are relatively stiffer but they may become softer at the end of earthquake. As a consequence, the amplitude and frequency content of the surface motion change significantly during earthquake. If stiffness and strength decrease so low, high frequency components of bedrock motion can not be transferred to surface. In Figure 2.14, an example to this effect is given. After 7 seconds, frequency content and acceleration amplitude start to change (Kramer, 1996).

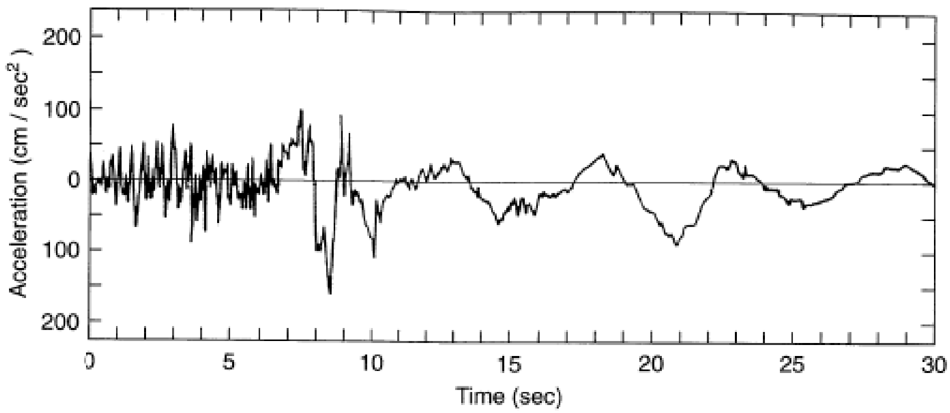

Figure 2.14 : Accelerogram from a liquefied site in 1964 Niigata earthquake (Kramer, 1996).

National Research Center (1985) listed types of structural instabilities and most often affected structures due to liquefaction. The list is given in Table 2.3.

Table 2.3 : Types of liquefaction induced instabilities (Housner, 1985).

Structures Most Often Affected	Types of Structural Instability
Buried and surface structures	Loss of foundation bearing capacity
Structures built on or at the base of a slope	Slope instability slides
Dam embankments and foundations	Slope instability slides
Bridge piers Railway lines Highways Utility lines	Movement of liquefied soil adjacent to topographic depressions
Structures, especially those with slabs on grade Utility lines Highways Railways	Lateral spreading on horizontal ground
Buried tanks Utility poles	Excess structural buoyancy caused by high subsurface pore pressure
Structures built on grade	Formation of sink holes from sand blows
Retaining walls Port structures	Increase of lateral stress in liquefied soil

2.6 Liquefaction Behavior of Soils

As liquefaction occurs in the field, soil stratum starts to soften and cyclic deformations develop. In loose soils, loss of shear strength may be seen and that may lead to large deformations. In denser soils, transient softening and increased shear strains may occur due to liquefaction, however, dilation tendency during shear inhibits major strength loss and large deformations. Cyclic mobility or cyclic liquefaction may be seen following liquefaction of denser soils (Youd et al., 2001).

Liquefaction may lead to flow liquefaction or cyclic mobility. Robertson et al. (2004) proposed a flow chart for the evaluation of liquefaction which is given in Figure 2.15. According to chart, liquefaction behavior of soil may be determined after material characterization. Depending on behavior, flow liquefaction, cyclic mobility or cyclic liquefaction may occur. These terms is explained below.

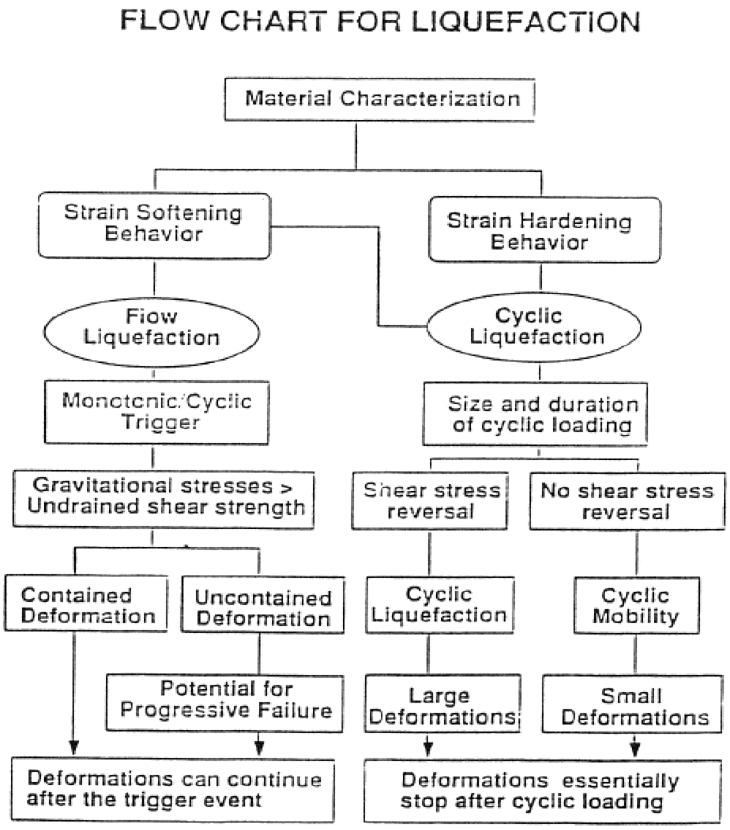

Figure 2.15 : Flow chart for evaluation of liquefaction (Robertson et al., 1994).

2.6.1 Flow liquefaction

Flow liquefaction is seen when the static shear stress is greater than the shear strength of the soil on liquefaction condition. The cyclic stresses turn the soil into unstable state which shear strength of the soil decreases sufficiently and static stresses produce flow failure. Characteristics of flow liquefaction failures are sudden nature, their speed and large distance which liquefied materials moved (Kramer, 1996). Robertson et al. (2004) gives further information about flow liquefaction:

- Flow liquefaction requires softening behavior under undrained loading which results constant shear stress and effective stress (for instance ultimate steady or critical state).
- Flow liquefaction requires greater in-situ shear stress than undrained residual stress or steady state shear strength.
- Either monotonic loading or cyclic loading triggers flow liquefaction.
- Flow liquefaction may be seen in saturated, very loose granular deposits, very sensitive clays and loose loess deposits.

2.6.2 Cyclic mobility

When cyclic mobility occurs, large permanent deformations can be also produced during earthquake shaking. Different from the flow liquefaction, cyclic mobility is seen when the static shear stress is less than the shear strength of the soil which is liquefied state. Cyclic mobility failures occur incrementally during the earthquake. In cyclic mobility, static and cyclic shear stresses cause the deformations, which is different from flow liquefaction. These deformations are called as lateral spreading, can be seen on slopes or waterfront areas. Lateral spreading can cause serious damage, if there is any structure (Kramer, 1996). Robertson et al. (2004) gives further information about cyclic mobility:

- Cyclic mobility requires undrained loading where shear stress is always greater than zero.
- Zero effective stress does not occur.

- Generated deformations due to cyclic loading will stabilize.
- Cyclic mobility can be seen in clays but deformations depend on rate effects (creeps).

2.6.3 Cyclic liquefaction

Cyclic liquefaction is a special case, which is subset of cyclic mobility. As there are no static horizontal shear stresses to drive lateral deformations, liquefaction produces large movements, ground oscillation, but there are little lateral displacements. Upward flow of water when excess pore water pressure dissipates causes level ground liquefaction failure. Loose to medium soils are susceptible to this type of liquefaction, but it can be seen in dense soils, if loading conditions are strong, duration is sufficient and field conditions are convenient. The characteristics of level-ground liquefaction failure are large vertical settlements and development of sand boils (Kramer, 1996). Robertson et al. (2004) gives further information about cyclic liquefaction:

- Cyclic liquefaction requires undrained cyclic loading in which zero stress or shear stress reversal can develop.
- Sufficient undrained cyclic loading is required to allow effective confining stress to decrease approximately zero.
- There is no shear stress at zero effective confining stress. If shear stress is applied, pore water pressures decrease and a very initial stress may lead to large deformations.
- Deformations due to zero effective stress can be large, but at the end of the cyclic loading deformations will stabilize as long as there are pore water pressure effects are not large.
- Cyclic liquefaction can be seen in all sands as long as size and duration of cyclic loading is sufficient. For denser sands cyclic loading characteristics also must be sufficient and zero effective stress may not be reached.
- Cyclic liquefaction can be seen in clays however, deformations are usually small at zero effective stress because of internal cohesion. Also deformations depend on rate effects (creeps).

Flow liquefaction is seen much less frequently than cyclic mobility, the damages of flow liquefaction are more severe. Cyclic mobility also could be seen under a much broader range of soil and site conditions than flow liquefaction; the range of its effects is insignificant to highly damaging (Kramer, 1996).

2.7 Residual Strength of Liquefied Soils

Strength of liquefied soils is not absolutely zero and during sliding downhill due to earthquake non-zero strength is mobilized in a soil deposit. After earthquake, stability of soil deposit should be checked. In order to check the stability, residual strength of soil deposit is required. Estimation of residual strength of a soil deposit is usually a difficult task with a acceptable degree of accuracy (Ishihara, 1996).

Idriss and Boulanger (2007) proposed a SPT-CPT based relationship to estimate residual shear strength of liquefied non-plastic soils. Case history analyses are reviewed, laboratory tests are performed and findings regarding void redistribution mechanisms are considered within the scope of their researches. Residual shear strength relationship graphs are given in Figure 2.16 and 2.17.

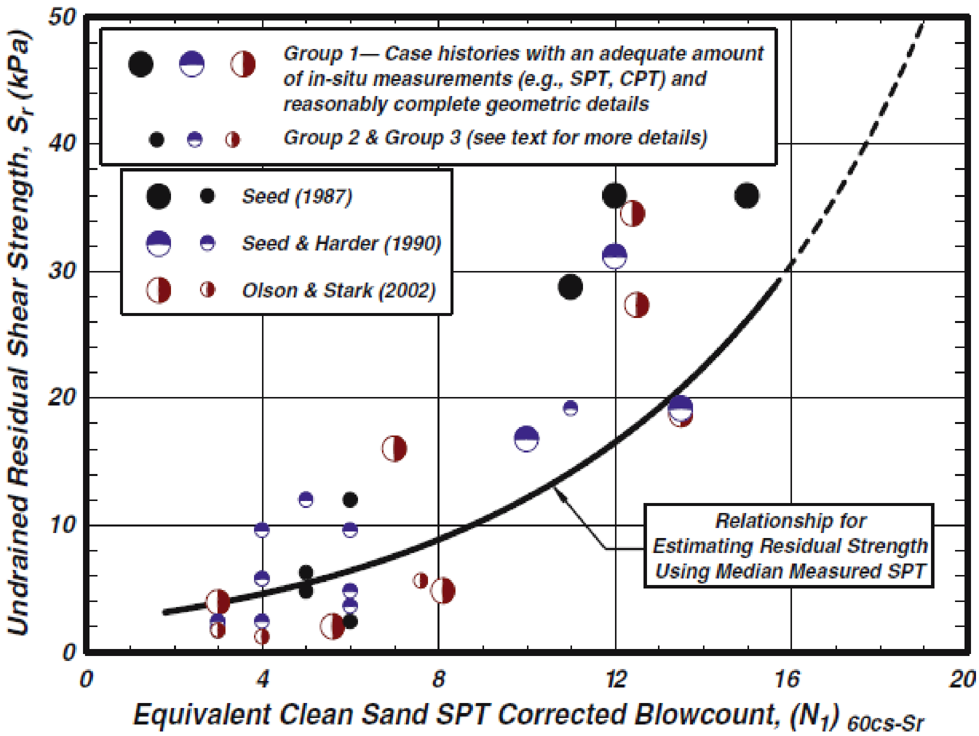

Figure 2.16 : Residual shear strength of liquefied sand versus corrected SPT blow count based on case histories (Idriss and Boulanger, 2007).

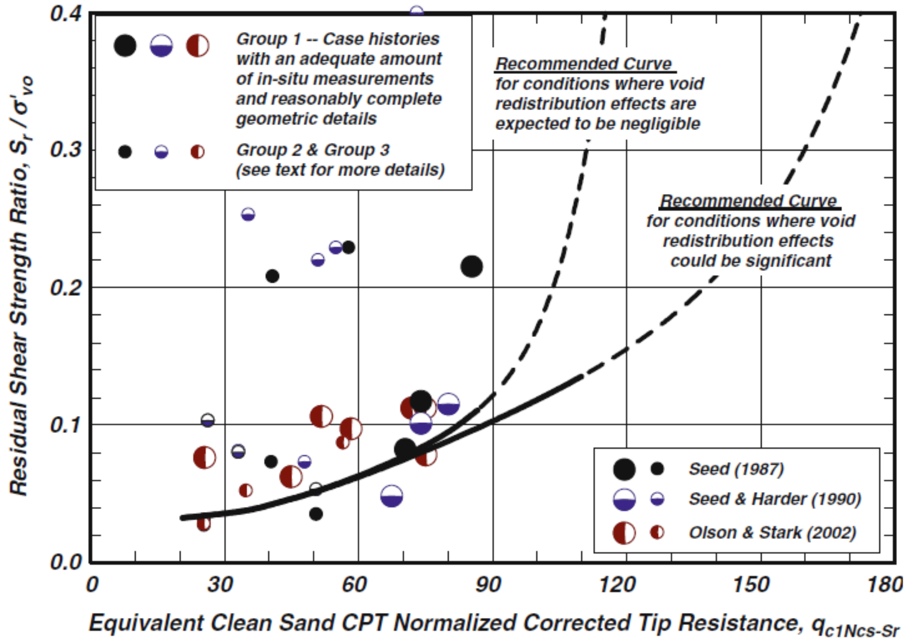

Figure 2.17 : Residual shear strength ratio versus normalized CPT tip resistance (Idriss and Boulanger, 2007).

2.8 Evaluation of Liquefaction Potential

Liquefaction potential of soils can be determined by both performing laboratory experiments and in-situ tests in the field. Laboratory tests have some disadvantages such as sample disturbance and limited representation of field conditions, comparing to field tests. Because of these reasons, laboratory tests, field tests and empirical methods are used together. Standard Penetration Test (SPT) and Cone Penetration Test (CPT) are commonly used in liquefaction analysis.

Seed et al. (1983) proposed a method to determine liquefaction resistance of soils and defined liquefaction inducing cyclic stress ratio as a function of N value in SPT. To evaluate the liquefaction resistance of soils two parameters have to be calculated:

1) The seismic demand on soil layer, which is calculated in terms of Cyclic Stress Ratio (CSR),

2) The resistance capacity of the soil to liquefaction, which is expressed in terms of Cyclic Resistance Ratio (CRR).

Seed and Idriss (1971) developed a formulation to calculate the cyclic resistance ratio of soils. The formula follows as;

$$CSR = (\tau_{av}/\sigma'_{vo}) = 0.65(a_{max}/g)(\sigma_{vo}/\sigma'_{vo})r_d \quad \textbf{(2.2)}$$

Where a_{max} is the peak horizontal acceleration at the ground surface generated by the earthquake g is the acceleration of gravity; σ_{vo} and σ'_{vo} are total and effective vertical stresses, respectively; and r_d is stress reduction coefficient. r_d is calculated by using these formulas;

$$r_d = 1.0 - 0.00765z \qquad \text{for } z \leq 9.15 \text{ m} \quad \textbf{(2.3)}$$

$$r_d = 1.174 - 0.0267z \qquad \text{for } 9.15 \text{ m} < z \leq 23 \text{ m} \quad \textbf{(2.4)}$$

Where, z is depth below ground surface (m).

Cyclic Resistance Ratio can be determined either performing laboratory test on undisturbed samples or using in-situ tests. Seed et al. (1985) proposed a chart to determine cyclic resistance ratio in terms of SPT blow count and shown in Figure 2.18. SPT blow counts in the chart are normalized for 100 kPa overburden pressure and corrected for 60% energy ratio. Curves are plotted for fines content of 35%, 15% and 5%. These curves are valid for 7.5 magnitude earthquakes. Scaling factors can be used for different earthquake magnitudes.

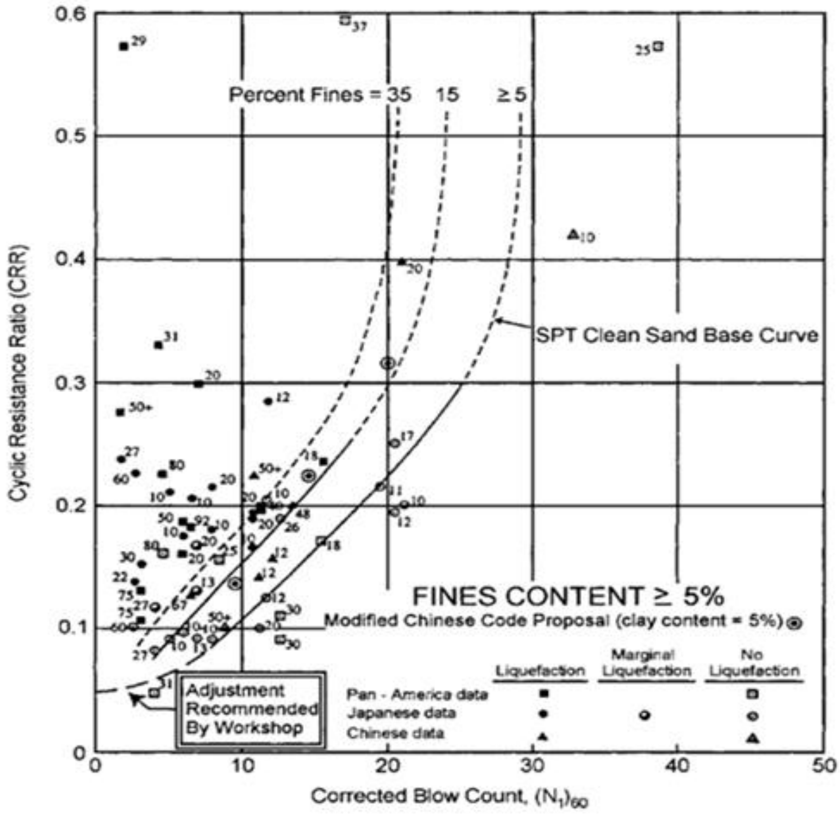

Figure 2.18 : SPT clean sand base curve for Magnitude 7.5 earthquakes (Seed et al., 1985).

Corrected $N_{1,60}$ values can be calculated as follows;

$$N_{1,60} = N_{30} * C_N * C_E * C_B * C_R * C_S \tag{2.5}$$

Where, N_{30} is SPT blow count, C_N is effective stress correction factor, C_E is energy correction factor, C_B is borehole diameter correction factor, C_R is rod length correction factor and C_S is correction for sampler with or without liners.

Liao and Whitman (1986) proposed calculation method for effective stress correction factor, C_N, as follows;

$$C_N = \sqrt{\frac{1}{\sigma'_{VO}}} \leq 1.7 \tag{2.6}$$

Robertson and Wride (1998) give corrections for different variables and presented in Table 2.4.

Table 2.4 : Corrections to SPT (Robertson and Wride, 1998).

Factor	Equipment variable	Term	Correction
Overburden pressure	—	C_N	$(P_a/\sigma'_{vo})^{0.5}$
Overburden pressure	—	C_N	$C_N \leq 1.7$
Energy ratio	Donut hammer	C_E	0.5–1.0
Energy ratio	Safety hammer	C_E	0.7–1.2
Energy ratio	Automatic-trip Donut-type hammer	C_E	0.8–1.3
Borehole diameter	65–115 mm	C_B	1.0
Borehole diameter	150 mm	C_B	1.05
Borehole diameter	200 mm	C_B	1.15
Rod length	<3 m	C_R	0.75
Rod length	3–4 m	C_R	0.8
Rod length	4–6 m	C_R	0.85
Rod length	6–10 m	C_R	0.95
Rod length	10–30 m	C_R	1.0
Sampling method	Standard sampler	C_S	1.0
Sampling method	Sampler without liners	C_S	1.1–1.3

CPT based methods are developed as converting CPT tip resistances to equal SPT blow counts. Robertson and Wride (1988) developed a CPT based liquefaction analysis method. Similar to SPT based method, CPT tip resistance is used to determine cyclic resistance ratio and the chart used for determining CRR is given in Figure 2.19. CRR is plotted as a function of dimensionless, corrected and normalized tip resistance, q_{c1N}. The chart can be used for 7.5 magnitude earthquakes and for the sands fines content lesser than 5%.

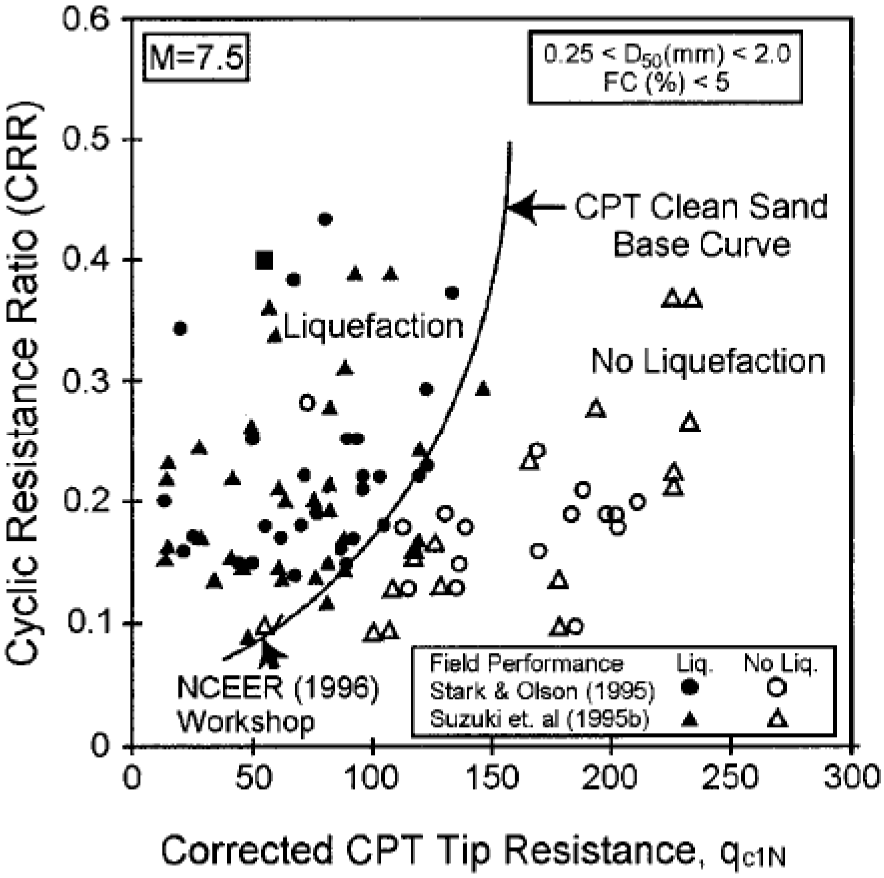

Figure 2.19 : CPT clean sand base curve for Magnitude 7.5 earthquakes (Robertson and Wride, 1998).

In the CPT procedure, tip resistances are normalized by using formulas;

$$q_{c1N} = C_Q(q_c/P_a) \tag{2.7}$$

$$C_Q = (P_a/\sigma'_{vo})^n \tag{2.8}$$

Where, C_Q is normalizing factor for cone penetration resistance, P_a is 1 atm of pressure in the same units for σ'_{vo}; n is exponent varies for soil type and q_c is field cone penetration resistance measured at the tip.

2.9 Conclusions

Liquefaction is strength loss of a soil during undrained loading due to rapid excess pore pressure generation. Pore water pressure generation decreases the effective stress of soil. As a result of effective stress decrease, the strength and rigidity of soil decreases. Due to liquefaction, lateral spreading, flow failures, ground subsidence may be seen and airports, roads, railways, buried pipelines and bridges may be damaged.

Material characteristics determine liquefaction behavior of soils. Loose soils tend to flow liquefaction, provided geometrical conditions are suitable. Also cyclic mobility or cyclic liquefaction may be observed. Dense soils may not liquefy during earthquake loading, however, if loading conditions are sufficient, they may soften due to excess pore pressure. Liquefaction potential of sandy soils can be determined by using developed methods based on in-situ tests such as SPT and CPT.

Residual strength of liquefied soil is important to determine stability of soil and predict possible deformations. Residual strength of liquefied soil can be determined either performing laboratory experiments on undisturbed soil specimens or performing in-situ penetration tests and correlations.

3. LITERATURE REVIEW

3.1 Introduction

Lateral spreading and its effects to engineering structures are given in this chapter. Mechanism of liquefaction induced lateral spreading, liquefaction induced quay wall damages, lateral spreading displacement prediction methods, quay wall displacement methods and liquefaction induced settlement prediction methods are presented. Also, brief information about 1995 Kobe earthquake is given in this chapter.

3.2 Lateral Spreading and its Effects to Engineering Structures

The definition of liquefaction-induced lateral spreading is lateral displacement of gently sloping ground because of pore water pressure generation or liquefaction in an underlying granular soil deposit (Rauch, 1997). The definition is shown in Figure 3.1 schematically.

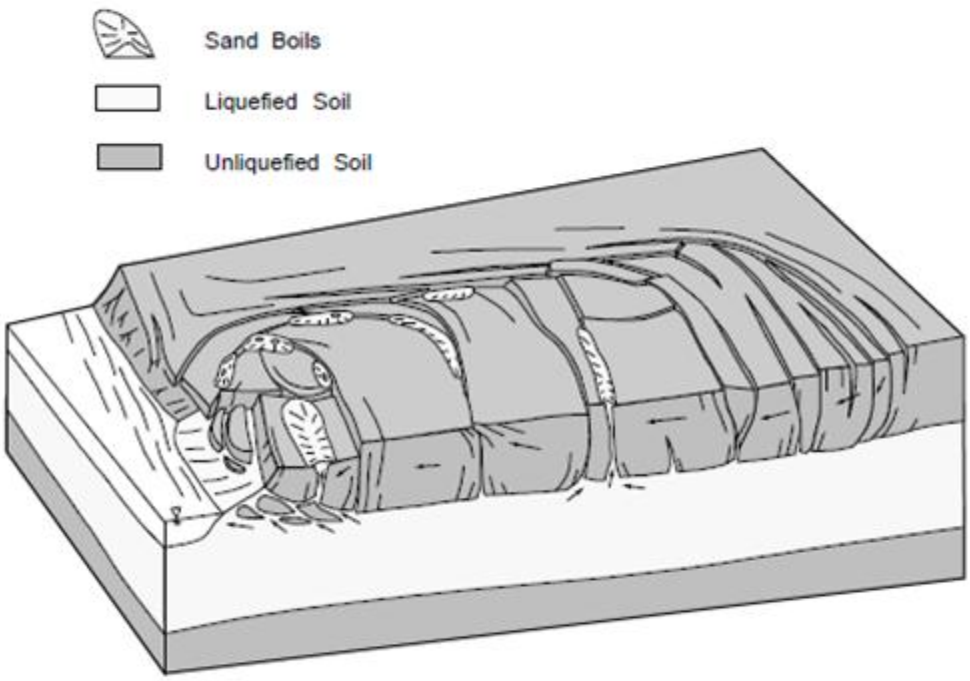

Figure 3.1 : Schematical depiction of lateral spreading due to soil liquefaction (Rauch, 1997).

Hamada (2014) classifies liquefaction induced lateral displacements into two groups as ground displacement due to inclination of ground surface and ground surface displacement due to quay wall movement. In the first group, the ground surface moves down slope as the ground surface was gently inclined. In the second group, the ground behind quay wall moves towards the sea due to liquefaction.

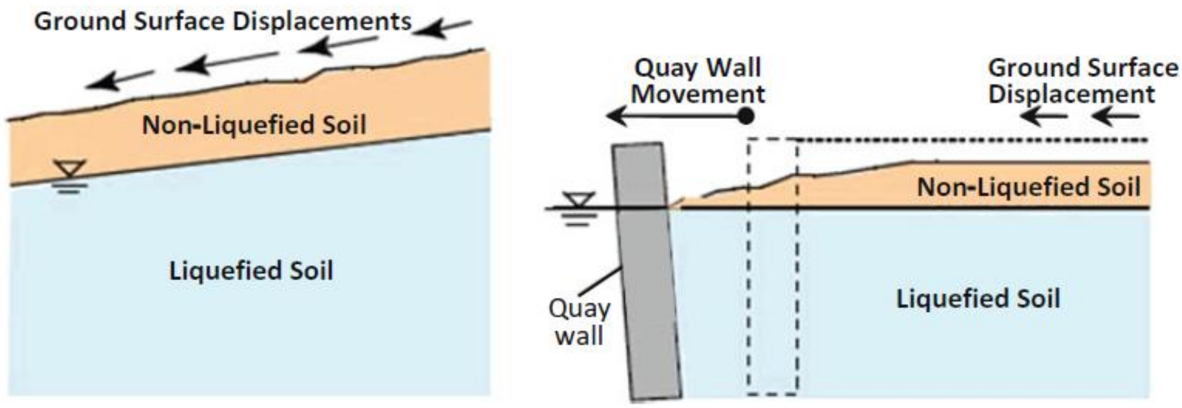

Figure 3.2 : Two types of liquefaction induced ground displacements (Hamada, 2014).

Hamada (2014) states that there are three hypotheses for the mechanism of lateral ground displacements. According to the first hypothesis, ground displacement occurs due to large decrease of soil stiffness. The second hypothesis explains that ground displacements develop due to liquid behavior of liquefied soil. The third hypothesis clarifies that ground moves on a water film that that locates between permeable and impermeable soil layers, afterwards liquefaction. In the first hypothesis, it is required to determine large decrease in soil stiffness because of liquefaction, but difficult part is to estimate soil stiffness reduction. According to second hypothesis, liquefied soil properties must be defined as liquid, but experiments show that liquefied soils behaves as pseudo-plastic fluid. The third hypothesis is not able to explain all cases of ground displacements as, ground displacement occurs not a specific elevation but along the entire depth.

Quay walls may be damaged during earthquakes due to liquefaction of loose saturated soil deposits behind walls. Seaward displacements, tilting and settlements may occur during and after earthquake. In Figure 3.3 deformations of quay wall on firm and loose foundation is shown.

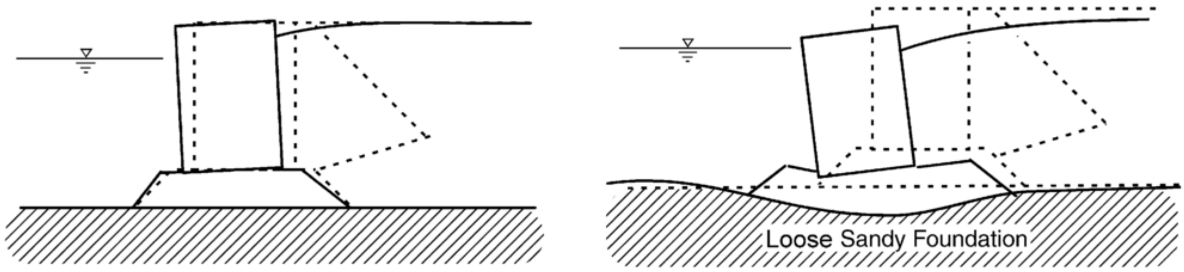

(a) (b)

Figure 3.3 : Deformations on firm (a) and loose (b) foundation (PIANC, 2001).

In 1964 Niigata Earthquake, harbor structures were severely damaged. Hayashi et al. (1966) states that 92.4% of water front structures were damaged out of 16500 m total length. The cause of damage was liquefaction of sand. Cross-sections of two berths (A-C) before and after earthquake are presented in Figure 3.4.

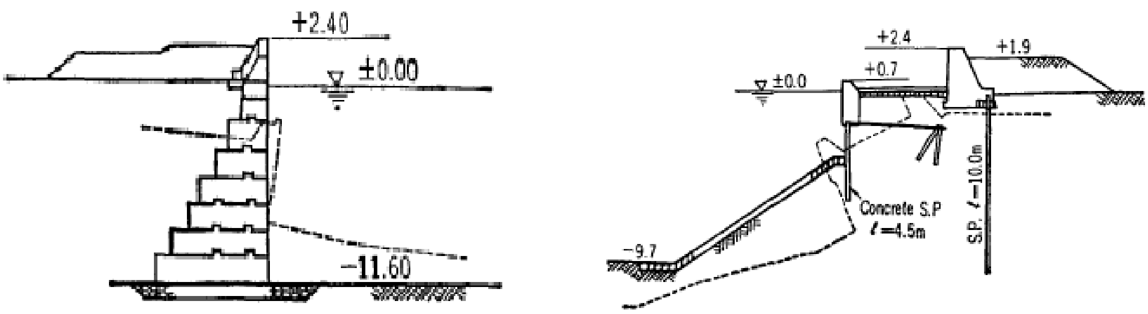

Figure 3.4 : Cross-sections of walls at Rinko Wharves after earthquake (Hayashi et al, 1966).

In 1986 Kalamata Earthquake, block type quay walls moved around 15 cm and rotated 4-5 degrees towards sea and is shown in Figure 3.5 (Pitilakis and Moutsakis, 1989). Settlements on backfill were varying around 20 cm to 0 cm at the distance of 30 m to 40 m. The quay wall was founded on silty sand and gravelly sand. SPT-N values are around 20 and Vs varies around 200 m/s. Backfill material was quite loose and SPT-N values are lesser than 20 and Vs has a mean value 150 m/s.

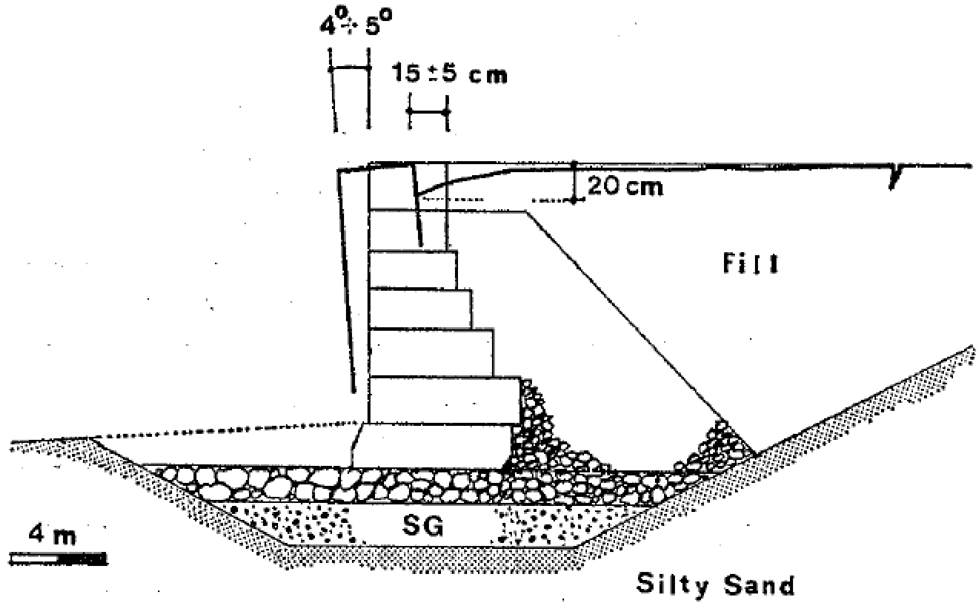

Figure 3.5 : Cross-section of wall before and after earthquake (Pitilakis and Moutsakis, 1989).

In 1999 Chi-Chi Earthquake, caisson type quay walls moved 1 m in average towards sea as loosely filled sand behind wall liquefied due to strong shaking (Chen and Huang, 2000). Settlements were around 70 cm relative to caissons. Soil conditions behind wall were quite loose; SPT-N values varied from 5 to 14. Plan view and lateral displacement are given in Figure 3.6.

Figure 3.6 : Plan view and lateral displacements in Taichung Harbor (Chen and Huang, 2000).

In 1999 Kocaeli earthquake, extensive damage were observed in port facilities and coastal structures. All artificial filled coastal areas moved into sea (Yüksel et al., 2002). Block type concrete quay walls at Derince Port moved 0.5 m towards sea and observed settlements in backfill were 0.5-0.8 m.

3.3 Lateral Spreading Prediction Methods

Lateral spreading displacements due to soil liquefaction during earthquakes needs to be predicted. Analytical, empirical and physical methods have been developed to predict displacements due to lateral spreading. Empirical methods are simpler and less complex, compared to other models. In addition, empirical methods are based on displacements and various geometrical and soil parameters.

3.3.1 Liquefaction severity index (LSI)

Youd and Perkins (1987) developed a simple empirical method to predict displacements due to liquefaction induced lateral spreading. Youd and Perkins defined a new parameter as liquefaction severity index (LSI) to characterize the severity of liquefaction effects at a specific location. LSI parameter is calculated by dividing the maximum ground displacement to 25 (i.e. inches). LSI ranges between 0 and 100 and displacements can not be greater than 2.5 m.

Based on analysis of earthquakes occurred Alaska and United States, Youd and Perkins formulated an equation related to earthquake magnitude and distance from the source.

$$\log LSI = -3.49 - 1.86 * \log R + 0.98 * M_w \quad \textbf{(3.1)}$$

R is horizontal distance from the seismic energy source in km and M_w is earthquake moment magnitude. The relationship between earthquake moment magnitude and horizontal distance from seismic energy source is given in Figure 3.7. LSI increases with M_w and decreases with R.

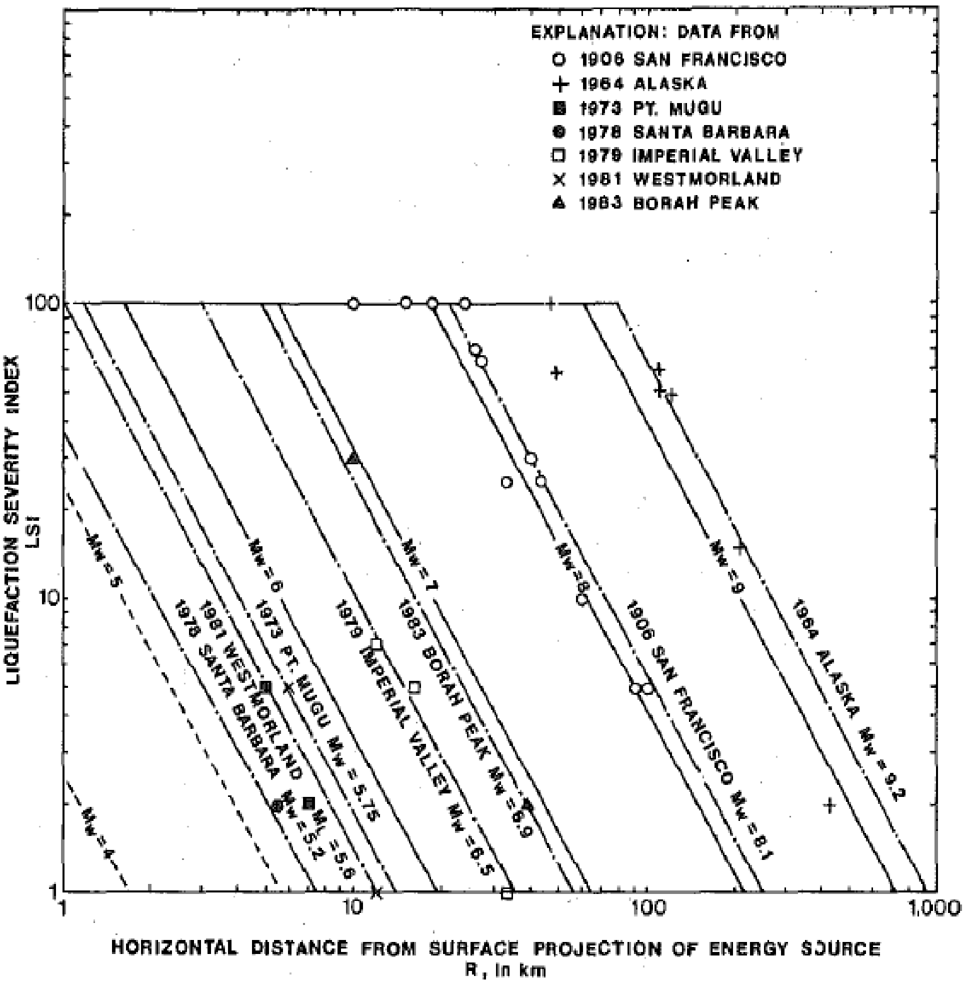

Figure 3.7 : Liquefaction Severity Index for different magnitudes and distance (Youd and Perkins, 1987).

LSI method is a useful method for liquefaction hazard mapping, yet special field conditions are not modeled. In special cases this method is not reliable.

3.3.2 Hamada's empirical method

Hamada formulated an equation based on correlation analysis between measured displacements and various factors such as surface gradient and liquefiable soil thickness (1994). The data used in analyses were taken from the 1983 Central Japan Sea earthquake and 1964 Niigata earthquake.

$$D = 0.75 * \sqrt{H} * \sqrt[3]{\theta} \qquad \textbf{(3.2)}$$

D is horizontal ground displacement on the surface (m), H is thickness of liquefiable soil (m) and θ is larger gradient value between ground surface and lower boundary plane of liquefied soil (%).

A comparison between observed displacements and estimated displacements by formula is given in Figure 3.8. The estimated values are distributed between twice and half of observed values. The scattering is acceptable because of liquid behavior of soil.

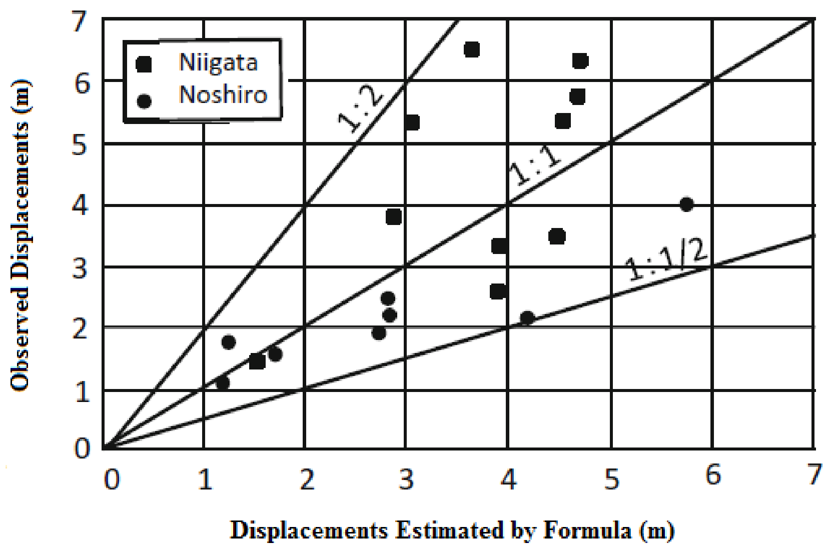

Figure 3.8 : Ground surface displacements by observation and formula (Hamada, 2014).

3.3.3 EPOLLS method

Rauch (1997) developed an empirical model, called EPOLLS (Empirical Prediction of Liquefaction-induced Lateral Spreading), to predict ground surface displacements due to liquefaction induced lateral spreading. The EPOLLS model was developed by multiple linear regression analysis of 71 lateral spreading case studies. EPOLLS model is applicable to lateral spreads that result from soil liquefaction in slopes or large retaining walls.

EPOLLS has three different models for different levels of site information. The names of these models are the Regional-EPOLLS (R-EPOLLS), the Site-EPOLLS (S-EPOLLS) and the Geotechnical-EPOLLS (G-EPOLLS).

R-EPOLLS is designed for seismic hazard surveys of geographic regions. R-EPOLLS requires four parameters: earthquake moment magnitude, peak horizontal acceleration, distance to fault rupture and duration of strong shaking. Horizontal displacement is calculated by:

$$D = (D_R - 2.21)^2 + 0.149 \quad \textbf{(3.3)}$$

$$D_R = \left(613 * M_w - 19.9 * R_f - 2420A_{max} - 11.4T_d\right)/1000 \quad \textbf{(3.4)}$$

Here, D is average horizontal displacement (m); R_f is distance to fault rupture and duration of strong shaking (km), M_w is earthquake moment magnitude, A_{max} is peak horizontal acceleration (g), T_d is duration of strong shaking (sec).

S-EPOLLS is more detailed model comparing to R-EPOLLS and S-EPOLLS give improved predictions in site specific studies. In addition to R-EPOLLS parameters, topographical and geometrical parameters are required. Horizontal displacement is calculated by:

$$D = (D_R + D_S - 2.44)^2 + 0.111 \quad \textbf{(3.5)}$$

$$D_S = \left(0.523 * L_{slide} + 42.3 * S_{top} + 31.3 * H_{face}\right)/1000 \quad \textbf{(3.6)}$$

Here, L_{slide} is length of sliding area (m), S_{top} is slope of ground surface (%), H_{face} is height of free face (m).

G-EPOLLS requires additional data from site explorations in addition to R-EPOLLS and S-EPOLLS components. Thickness of liquefiable layer and factor of safety against liquefaction are added in geotechnical model. Horizontal displacement is calculated by:

$$D = (D_R + D_S + D_G - 2.49)^2 + 0.124 \quad \textbf{(3.7)}$$

$$D_G = \left(50.6 * Z_{FSmin} - 86.1 * Z_{liq}\right)/1000 \quad \textbf{(3.8)}$$

Here, Z_{FSmin} is depth of minimum factor of safety against liquefaction (m), Z_{liq} is depth to top of liquefied soil (m).

3.3.4 MLR (Multiple Linear Regression) method

Bartlett and Youd (1992a, 1992b, 1995) developed an empirical model for prediction of lateral spreading. They formulated an equation by using 467 horizontal displacement vectors collected from lateral spreads in earthquakes in Japan, Western United States. Soil parameters are determined from 267 soil borings.

Bartlett and Youd developed two model equations, firstly a free face model for lateral spreading toward a steep vertical face and secondly ground slope model for lateral spreading without a free face. These equations were formulated using multiple linear regression analysis and later revised by Youd et al. (2002). The equations follow as:

For free face;

$$\log(D_H) = -16.713 + 1.532 * M - 1.406 * \log R^* - 0.012 * R + 0.592 * \log W + 0.540 * \log T_{15} + 3.413 * \log(100 - F_{15}) - 0.795 * \log(D50_{15} - 0.1mm) \qquad \textbf{(3.9)}$$

For sloping ground;

$$\log D_H = -16.213 + 1.532 * M - 1.406 * \log R^* - 0.012 * R + 0.338 * \log S + 0.540 * \log T_{15} + 3.413 * \log(100 - F_{15}) - 0.795 * \log(D50_{15} + 0.1mm) \qquad \textbf{(3.10)}$$

Here; D_H is horizontal displacement (m), Mw is the moment magnitude of the earthquake, R is the nearest horizontal distance to fault (km), T_{15} is the thickness (m) of saturated cohesionless soils where $N_{1,60}$ is lesser than 15 (soils deeper than 20 m or has more than 15% clay content are excluded), F_{15} is the average fines content in T_{15} and $D50_{15}$ is the average D50 grain size in T_{15} (mm).

R term is revised as R^* because in earthquakes R<0.5 km formula over predicts displacements. R^* is calculated as:

$$R_0 = 10^{(0.89M - 5.64)} \qquad \textbf{(3.11)}$$

$$R^* = R_0 + R \qquad \textbf{(3.12)}$$

In sloping ground equation, S is the gradient of the ground surface (%). It is defined as change in elevation over horizontal distance for long slopes. For the free face equation, W is the free face ratio (%). It is defined as height of the face divided by horizontal distance to face toe.

3.4 Quay Wall Seismic Displacement Prediction Methods

Quay walls subjected to earthquake loading will vibrate with backfill soil and may move from the original position. The level of movement and degree of damage due to earthquake should be predicted. Available methods for displacement based analysis of retaining walls during earthquake loadings are based on the work of Newmark (1965). Newmark developed a procedure to evaluate the deformation of an embankment dam subjected to an earthquake. His method is based on the analogy with a sliding block-on-a-plane. Also, empirical methods have been developed to predict displacements due to earthquake loadings. These methods will be presented in this chapter.

3.4.1 Franklin-Chang (1977) method

Franklin and Chang (1977) applied Newmark's sliding blocks theory and integrated 169 strong motion data from 27 different earthquakes and 10 synthetic accelograms. For each record, displacements are calculated using Newmark's method. Franklin and Chang developed functional relationship between the standardized displacements and the critical acceleration by using analyzed records and calculated displacements and it is given in Figure3.9. When the critical acceleration ratio is known, displacements can be estimated.

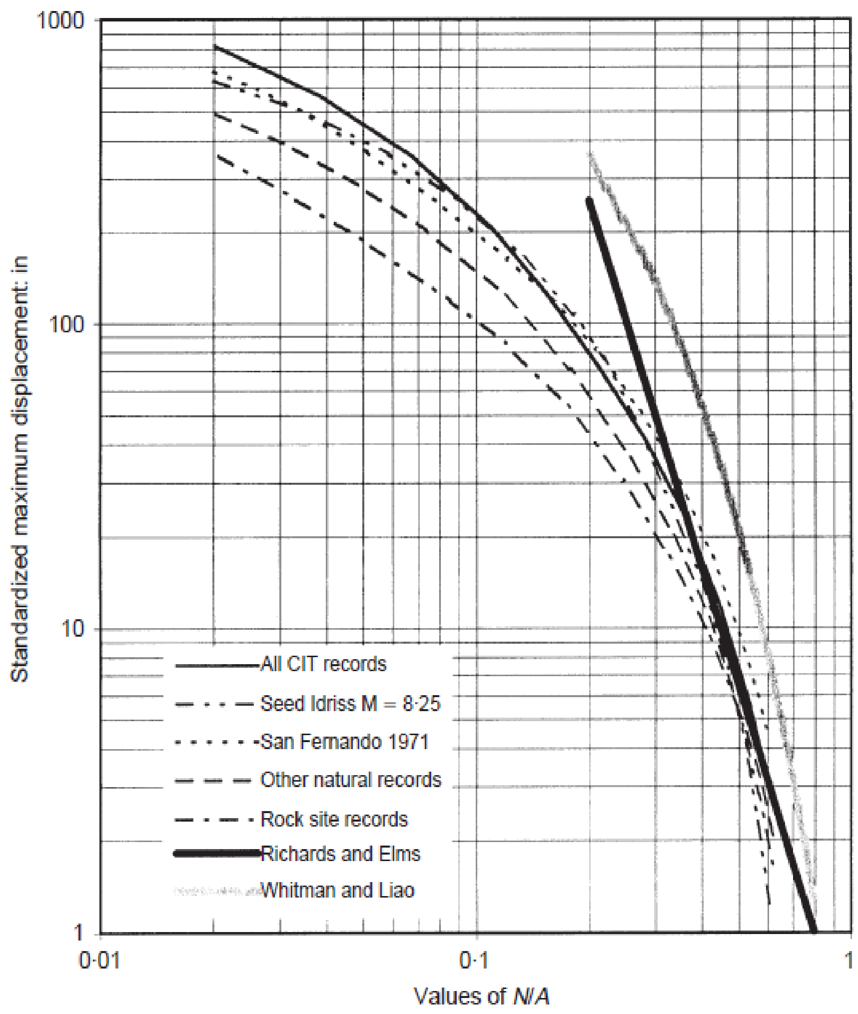

Figure 3.9 : Standardized maximum displacement and critical acceleration ratio relationship (Franklin and Chang, 1977).

3.4.2 Richards-Elms (1979) method

Richards and Elms (1979) develop a calculation method for seismic displacements of gravity type retaining walls. The proposed method is developed by modifying Newmark's Sliding Block method. Dynamic earth pressure coefficient and dynamic earth pressure acting on wall are calculated by using Mononobe-Okabe (M-O) method.

$$K_{AE} = \frac{cos^2(\phi-\theta-\psi)}{\cos\psi\, cos^2\theta \cos(\delta+\theta+\psi)\left[1+\sqrt{\frac{\sin(\delta+\phi)\sin(\phi-\beta-\psi)}{\cos(\delta+\theta+\psi)\cos(\beta-\theta)}}\right]^2} \qquad \textbf{(3.13)}$$

Where, K_{AE} is dynamic earth pressure coefficient, ϕ is internal friction angle of soil, θ is rotation angle of wall, ψ equals to $\tan^{-1}(a_{max}/g)$, δ is friction angle between soil and wall and β is wall slope angle. By using dynamic earth pressure coefficient, the force acting on wall is calculated.

$$P_{AE} = \frac{1}{2} K_{AE}\gamma H^2(1-k_v) \qquad \textbf{(3.14)}$$

Where, P_{AE} is dynamic earth pressure acting on wall, γ is unit weight of soil, H is height of the wall and k_v is vertical earthquake acceleration coefficient.

Then, yield acceleration is calculated for the retaining wall and soil system.

$$a_y = \left[\tan\phi_b - \frac{P_{AE}\cos(\delta+\theta)-P_{AE}\sin(\delta+\theta)}{W}\right] \qquad \textbf{(3.15)}$$

Where, a_y is yield acceleration, ϕ_b is the friction angle between wall and its base and W is the weight of the wall.

According to proposed method, permanent wall displacement is calculated by formula.

$$d_{perm} = \frac{v_{max}^2\, a_{max}^3}{a_y^4} \qquad \textbf{(3.16)}$$

Where, d_{perm} is permanent displacement of the wall, v_{max} is peak ground velocity, a_{max} is the peak ground acceleration and a_y is the yield acceleration for wall and soil system.

3.4.3 Whitman-Liao (1985) method

Whitman and Liao (1985) developed a method based on Newmark's Sliding Block method (1965) for seismic displacements of retaining walls. Whitman and Liao performed a regression analysis on standardized displacement data and proposed a different formula to estimate seismic displacement. Similar to Richards-Elms method, earth pressures acting on wall calculated by using Mononobe-Okabe method. The formula as follows:

$$d_{perm} = \frac{37 v_{max}^2}{a_{max}} exp\left(\frac{-9.4 a_y}{a_{max}}\right) \quad \textbf{(3.17)}$$

3.4.4 Iai et al. (1997) method

Iai et al. (1997) developed a method to evaluate liquefaction induced seismic displacements of quay walls. Following equation was proposed for the prediction of the horizontal displacement at the top of quay walls:

$$\Delta = \frac{F_d}{100} H_w \quad \textbf{(3.18)}$$

Where, Δ is horizontal displacement at the top of the wall (m), H_w is height of quay wall (m), and F_d is displacement ratio of quay wall. Displacement rates for different wall types, ground motions and soil conditions are given in Table 3.1.

Table 3.1 : Displacement rate of quay wall due to liquefaction (Iai et al.,1997).

Type of Quay Wall	**Ground Motion**	**Soil Condition**		**Displacement Ratio Fd (%)**
Gravity type	Level 1	Loose sand behind quay wall		5-10
		Loose sand behind quay wall and foundation ground		10-20
	Level 2	Loose sand behind quay wall		10-20
		Loose sand behind quay wall and foundation ground		20-40
Sheet piles type	Level 1	Loose sand behind quay wall	Firm ground around anchorage	5-15
			Loose sand around anchorage	15-25
		Loose sand behind quay wall, around anchorage and foundation ground		25-50
	Level 2	Loose sand behind quay wall	Firm ground around anchorage	15-20
			Loose sand around anchorage	25-40
		Loose sand behind quay wall, around anchorage and foundation ground		50-75

Seismic horizontal displacements behind the wall decrease when the distance from the wall increase. For this case, following formula is given:

$$D/\Delta = \exp(-3.35x/L) \quad \textbf{(3.19)}$$

Where, D is ground displacement behind wall (m), x is distance between quay wall and application point (m) and L is the distance from ground deformation is caused (m), assumed as 100 m in practice.

3.4.5 Iai et al. (1999) method

Iai et al. (1999) did effective stress analyses to find major parameters which controls seismic performance of gravity quay walls. After analyses, a simplified method was developed to evaluate the displacement of a quay wall. During the analyses, computer code FLIP is used.

Wall geometry, thickness of soil deposit below the wall, liquefaction resistance of backfill and subsoil are key parameters for seismic performance of a quay wall. A typical cross section which is used in analyses is given in Figure 3.10. Authors assumed that thickness of backfill (D2) was the same as the wall height (H) for simplicity in analyses. Soil parameters used in analyses were determined by SPT-N values. Another assumption was made by authors that backfill soil were the same as foundation soil for simplicity and they were represented by equivalent SPT-N value.

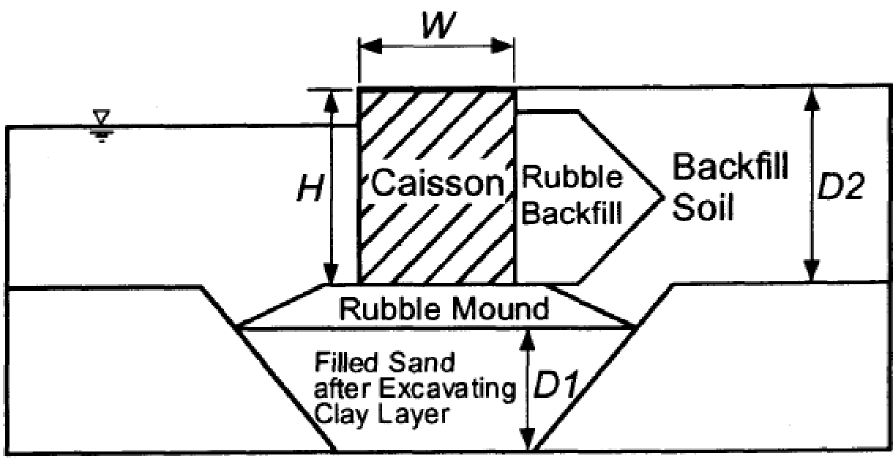

Figure 3.10 : Typical cross section of a quay wall used in analyses (Iai et al.,1999).

According to Iai et al., major parameters that control the seismic performance of a quay wall during earthquake are width to height ratio (W/H), input excitation level, equivalent SPT-N value and thickness of soil below the wall.

Authors developed a simplified method to evaluate for seismic displacements of a quay wall, after parametric study. The new method can be seen in Figure 3.11. The seismic displacement of wall is determined with parameters that control seismic displacement of wall in the order of sensitivity to the wall displacement. The seismic displacement of wall is determined with the effects of input excitation level, equivalent SPT-N value and wall geometry.

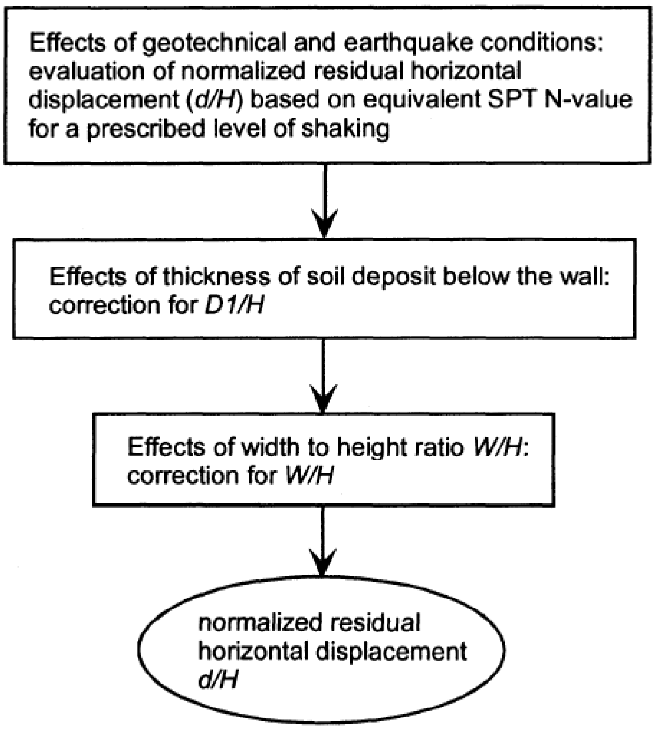

Figure 3.11 : Flow chart of developed method to evaluate displacement (Ichii et al.,2002).

3.4.6 Wang et al. (2011) method

Wang et al. (2011) analyzed caisson quay wall displacements by using multi shear mechanism plasticity model. Finite element code FLIP was used in analysis. Index of extent liquefaction was defined to represent the effects of excess pore water pressure under different loading conditions. According to authors, physical properties of the system, such as thickness of soil deposits, wall geometry and characteristics of earthquake loading controls the seismic displacement of caisson quay wall. In Figure 3.12., a cross section of analyzed quay wall system is shown.

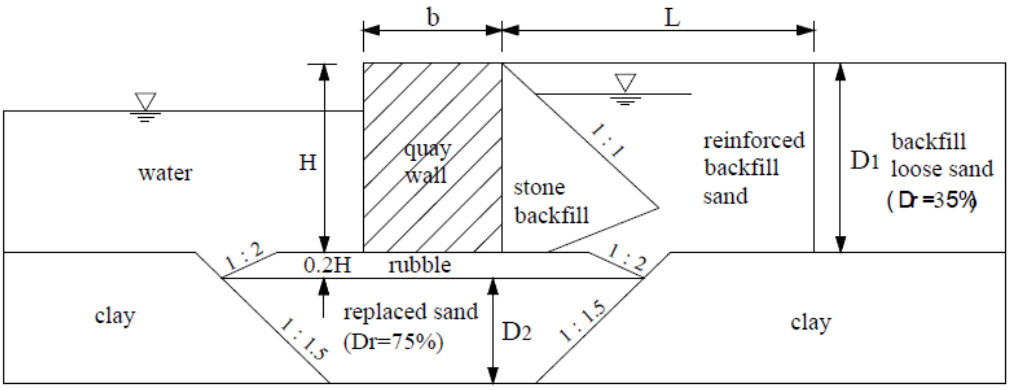

Figure 3.12 : Cross section of a analyzed quay wall (Wang et al.,2011).

The extent of liquefaction (E_l) is introduced to define the effects of the changes of excess pore water pressure in soils. Authors proposed a method to predict the seismic residual displacement, by using E_l. E_l is used to determine the seismic displacement of quay wall and the relation between displacement and E_l is shown in Figure 3.13.

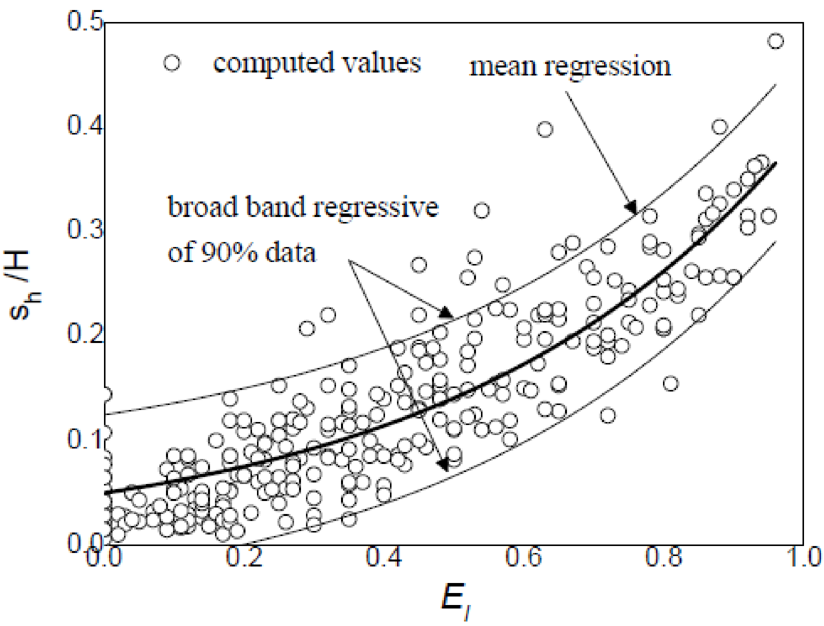

Figure 3.13 : Relationship between residual seismic displacement and extent of liquefaction (Wang et al.,2011).

The extent of liquefaction affects the residual displacement directly and should be determined carefully. After analyses, 1g shaking table tests were performed and reliability of prediction methods was validated.

3.5 Settlement Prediction Methods

As soils liquefy due to excess pore pressure generation, not only lateral displacements are observed but also ground surface settlements occur. The amount of settlements may be predicted by using empirical methods.

Tokimatsu and Seed (1987) proposed a method to estimate settlements due to earthquake shaking. The authors developed a chart to predict ground surface settlements of saturated clean sands. The chart is given in Figure 3.14. CSR is the cyclic stress ratio of soil and $(N_1)_{60}$ is corrected SPT value of soil according to 60% energy ratio. By using these parameters volumetric strain is determined.

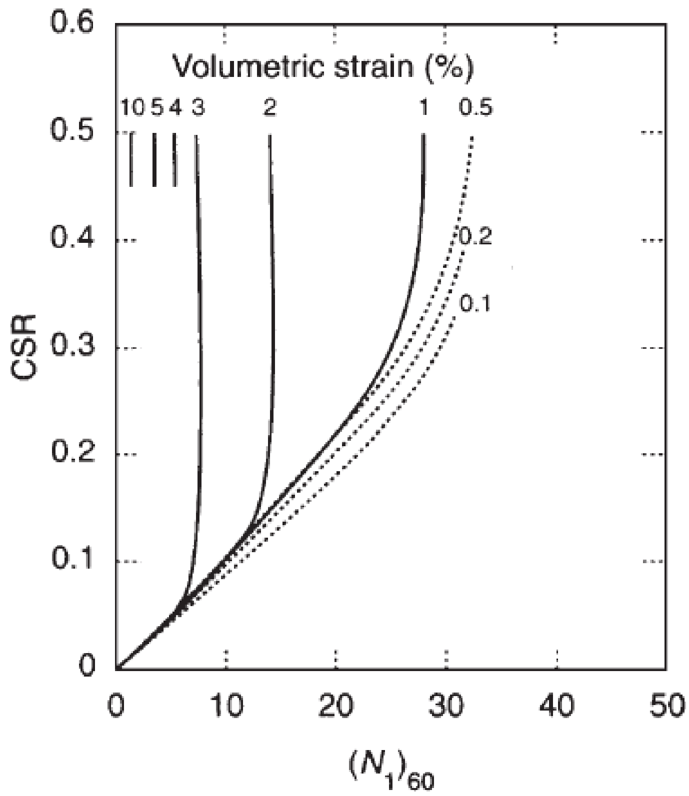

Figure 3.14 : Chart for settlement estimation of clean saturated sands (Tokimatsu and Seed, 1987).

In first step cyclic stress ratio is calculated, then adjusted to 7.5 magnitude earthquake by using magnitude scaling factors. After that step, SPT-N values are corrected and energy corrections made. Then, volumetric strain is obtained via using CSR and $(N_1)_{60}$. Volumetric strain value is multiplied by layer thickness.

Ishihara and Yoshimine (1992) also developed a chart by using dynamic simple shear tests to predict liquefaction induced settlements. In the chart which is given in Figure 3.15, FS_L

represents factor of safety against liquefaction and ε_v is post-liquefaction volumetric strain. Factor of safety against liquefaction is calculated and D_r is determined. Later either corrected cone penetration resistance q_{c1} or corrected standard penetration test $(N_1)_{70}$ value is determined. By using these parameters volumetric strain ratio is obtained from graph. Then volumetric strain is multiplied by thickness of layer to calculate settlement.

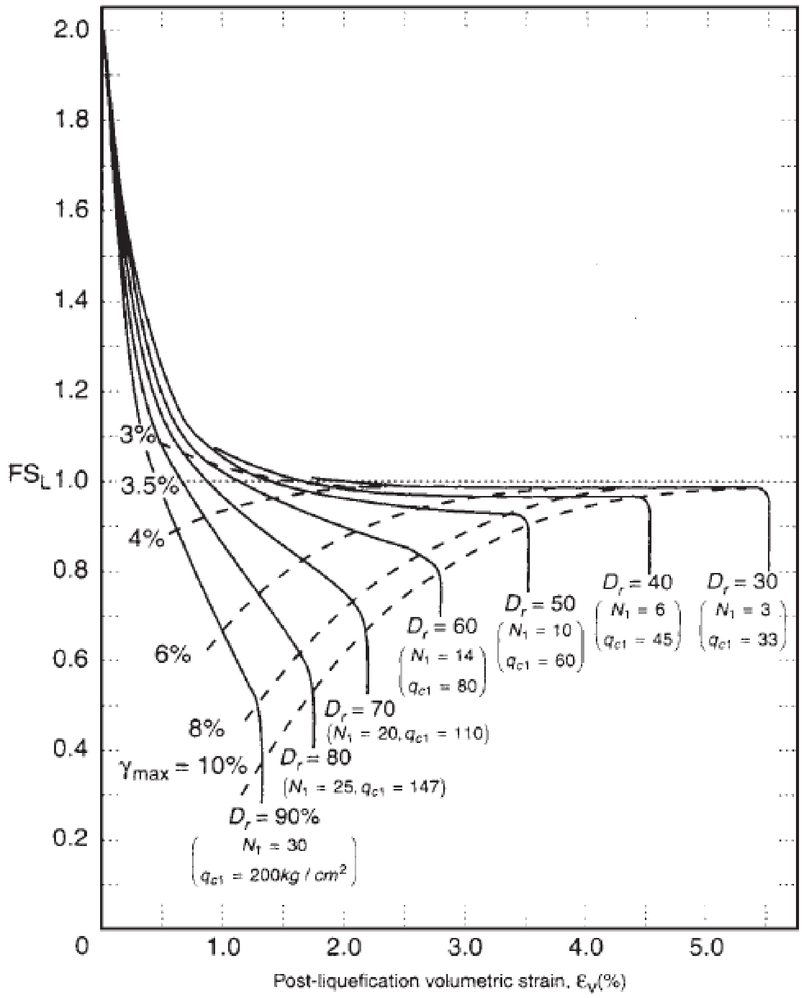

Figure 3.15 : Ground surface settlement estimation chart for clean saturated sands (Ishihara and Yoshimine, 1992).

3.6 1995 Kobe Earthquake

On the January 17, 1995, Kobe Earthquake, which is one of the most powerful earthquakes in Japanese history, hit Japan. The magnitude of the earthquake was 7.2 on the Richter scale. Awaji Island and the other provinces of the Hanshin region were struck by the earthquake. Major cities, including Kobe, Ashiya and Nishinomiya damaged in large scale. The intensity level of earthquake was VII in Kobe and Nishinomiya on Japanese Intensity Scale. The death and missing toll was more than 5,000 people and more than 83,000 houses were destroyed (Japanese Society of Civil Engineers, 1995).

3.6.1 Kobe city and Kobe port

Kobe City has been founded on alluvial and diluvial deposits in the south of Rokko mountain range. The earthquake damaged an area about 3 km in width and 30 km long. This area could be classified as alluvial and diluvial deposits in the south of Rokko Mountain and reclaimed islands in ports (Japanese Society of Civil Engineers, 1995).

Kobe Port which handles more than 20% of the country's foreign trade, consists of a coast line about 12 km in width and 6 km long, and two artificial islands in the south of Kobe city. The plan of the port is given in Figure 3.16. Port Island and Rokko Island were constructed by using reclamation methods. The construction of Port Island and Rokko Island began in 1966 and 1972, respectively (Inagaki et al., 1996).

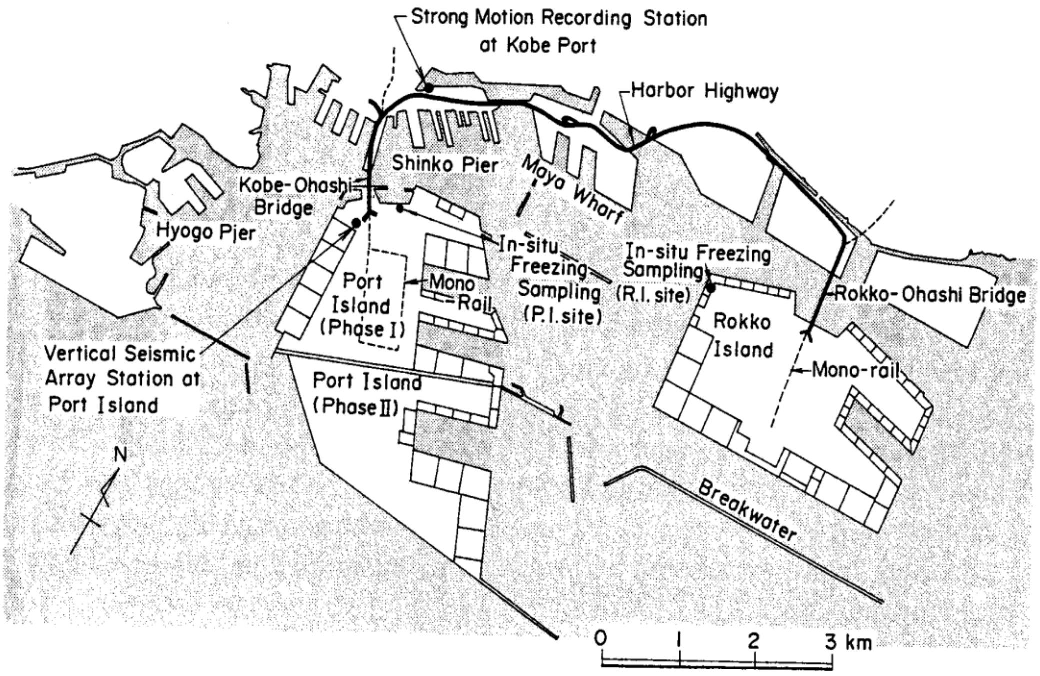

Figure 3.16 : Plan of Kobe Port (Inagaki et al., 1996).

3.6.2 Construction of artificial islands

Rokko Mountains were excavated for the landfill. The soil was transported from mountains and placed in-situ where water level ranges from 12 m to 15 m. The landfill soil was granite-based soil and its particle size changes widely from gravel to silt. Particle size distribution of landfill is given in Figure 3.17. The soil consists of about 30% gravel, 50% sand and 20% silt (Japanese Society of Civil Engineers, 1995). The SPT-N values of the reclaimed Masado soil changes 5 to 10 mostly, and the N values of alluvial clay changes 0 to 1. According to the Inagaki, after the earthquake SPT-N values measured again in the site. The results of his works show that after the earthquake, N values ranges 5 to 10 and there were not large differences in SPT-N values between before and after earthquake (1996).

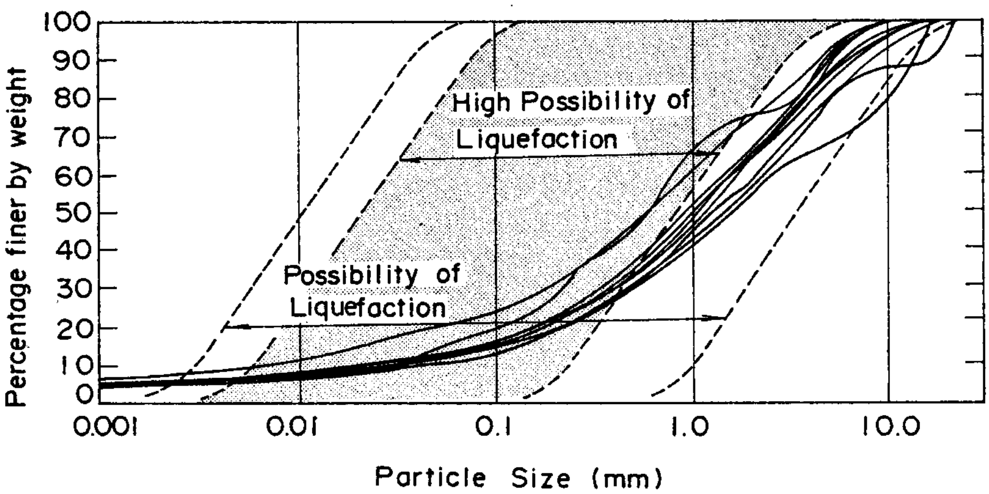

Figure 3.17 : Grain size distribution curves of Masado soil (Inagaki et al., 1996).

In order to maintain the stability of quay walls, bearing capacity of foundation soil must be sufficient. As alluvial clay in Kobe Port does not have sufficient bearing capacity, soil improvement techniques were applied to fulfill the required bearing capacity. The clay layer beneath quay wall was removed and replaced with sand (Inagaki et al., 1996). Cross section of quay walls in Rokko Island is given in Figure 3.18.

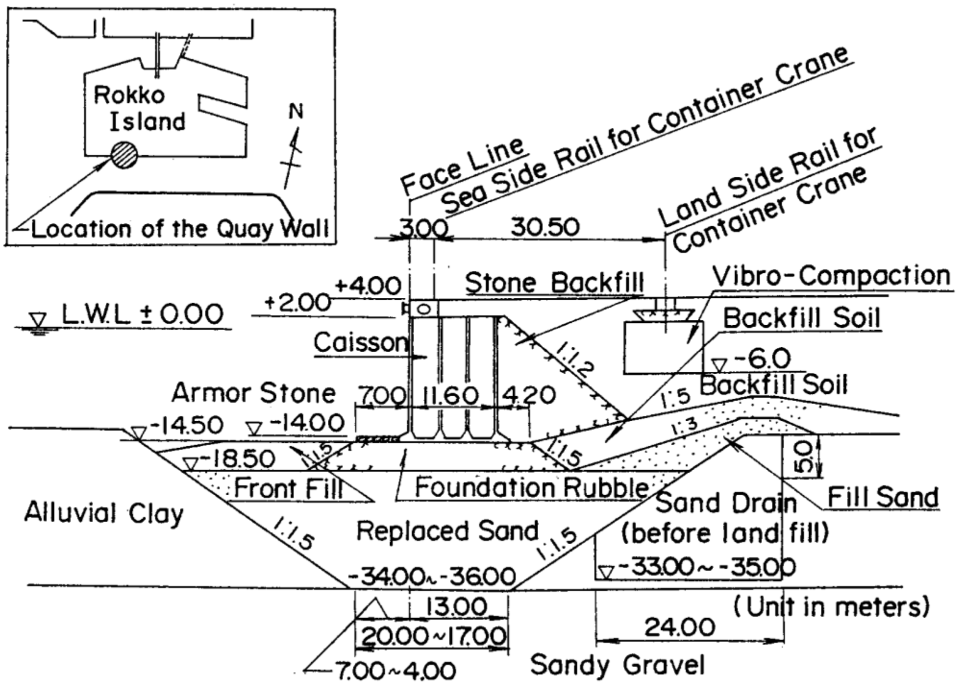

Figure 3.18 : Cross section of quay wall in Rokko Island (Inagaki et al., 1996).

3.6.3 Quay wall damages

Kobe Port has 186 quay walls and about 90% of these walls were caisson type walls. Quay walls displaced seaward about maximum 5 m and about 3 m average, inclined 4 degrees in the direction of sea (Inagaki et al., 1996). Moreover, liquefaction occurred in reclaimed coastal areas and artificial islands. The map of liquefied areas is given in Figure 3.19. Effects of liquefaction were observed as: settlement in level-ground, damage in port walls as a result of horizontal movement, damage to the embedded lifeline and damage to the bridge piers on coastal areas (Japanese Society of Civil Engineers, 1995).

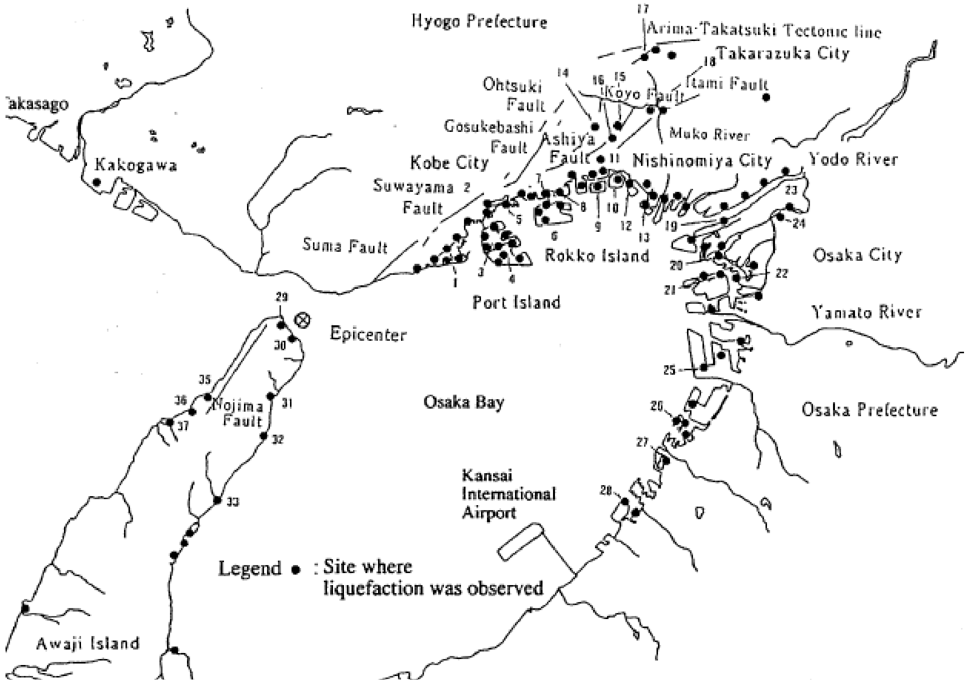

Figure 3.19 : Distribution of liquefied places (Shibata et al., 1996).

The heaviest liquefaction damage was observed on Port Island and Rokko Island. As a consequence of liquefaction, settlements occurred on the entire island, but buildings damaged less. Most of the buildings on the islands were supported with piles (Japanese Society of Civil Engineers, 1995). The areas where soil improvements were made and liquefaction occurred in artificial islands are given in Figure 3.20.

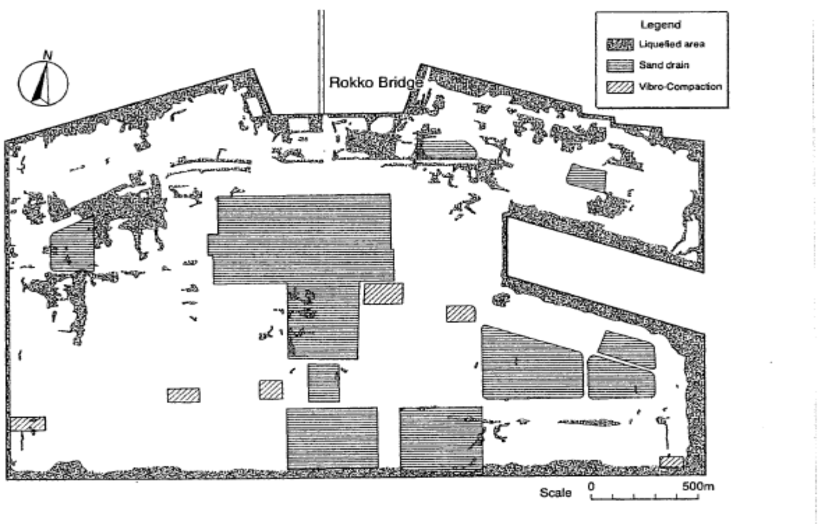

Figure 3.20 : Distribution of liquefied areas at Rokko Island (Shibata et al., 1996).

While the earthquake motion is in excess of seismic limiting condition of quay wall, the wall moves seawards and settlements observed behind the wall. In 1995 Kobe Earthquake, peak ground acceleration was 0.54 g in horizontal direction and limiting conditions were exceeded. Quay walls in Port Island and Rokko Island were designed with seismic coefficients of 0.10 and 0.15, respectively (Inagaki et al., 1996).

Quay walls in Port Island moved towards to sea about 3 m, settled about 1 m and tilted about 3 degrees average. Quay walls in Rokko Island moved towards to sea about 4 to 5 m, settled about 2 m and tilted about 4 to 5 degrees average. The soils behind the wall settled, but there were no collapse or overturning in quay walls. Displacements of quay walls were measured and given in Figure 3.21.

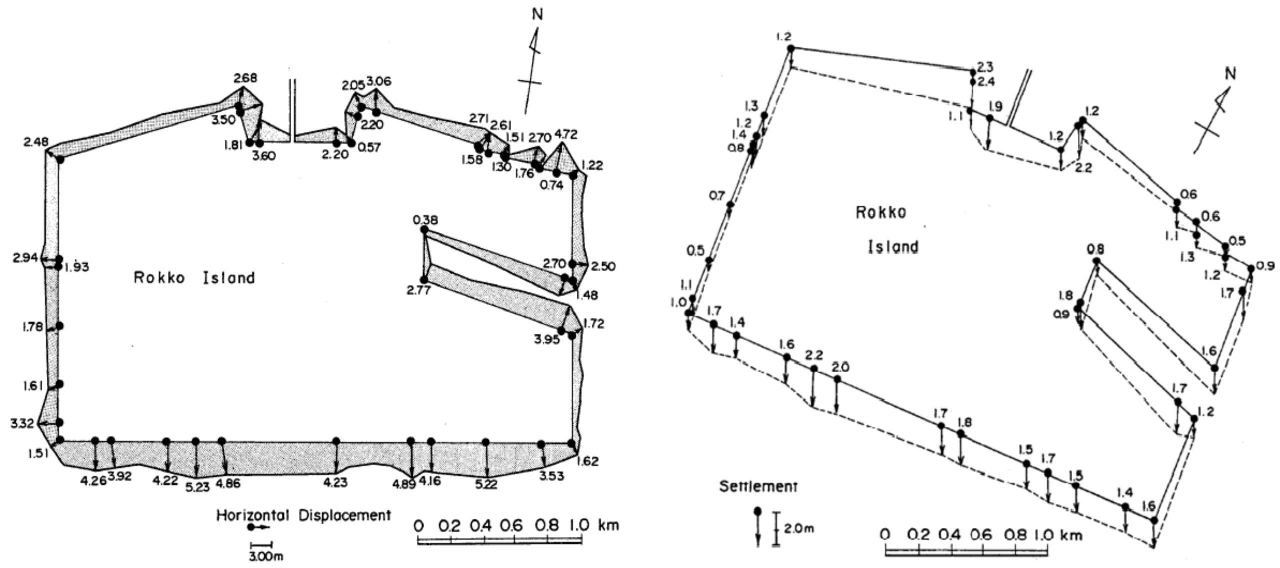

Figure 3.21 : Horizontal and vertical displacements after eq. Rokko Island (Inagaki et al., 1996)

High seismic resistant quay walls in Maya Wharf, which had seismic coefficient of 0.25, was not damaged seriously. There was nearly no damage to caisson type quay walls, except small settlements and displacements in the order of tens of centimeters. The caisson which was designed with higher coefficient performed well against earthquake.

3.7 Conclusions

Liquefaction induced lateral spreading is the main cause of catastrophic damages in disastrous earthquakes. For that reason, mechanism of liquefaction and lateral spreading should be understood clearly and their impacts on engineering structures analyzed carefully during and after earthquake.

Lateral spreading causes large deformations on slopes and retaining structures. Several researchers have developed different methods to predict liquefaction induced lateral spreading, seismic quay wall displacements and settlements. These methods can be used to estimate potential damages on existing structures and can also be used on design process.

4. FINITE ELEMENT METHOD

4.1 Introduction

Finite element method, selection of material model and input parameters are given in this chapter. Brief information about finite element programme and selection of model parameters is given.

4.2 Constitutive Soil Models

Soil behaviour may be modeled at different degree of accuracy. Many constitutive models are developed to characterize and interpret soil behaviour accurately. On the other hand, complex soil models require more soil parameter selection (Brinkgreve, 2005). In addition, every constitutive model requires different parameters and every model has limitations. It is very significant to choose the appropriate constitutive soil model.

There are some constitutive models available in the Plaxis 2D:

- Linear Elastic Model (LE)
- Mohr-Coulomb Model (MC)
- Hardening Soil Model (HS)
- Hardening Soil Model with small strains (HSsmall)
- Soft Soil Model (SS)
- Soft Soil Creep Model (SSC)
- Modified Cam-Clay Model (MCC) (Plaxis Material Models Manual, 2012).

4.2.1 Linear elastic model (LE)

The Linear Elastic Model is built on Hooke's law of elasticity. Only two basic parameters are involved: Young's Modulus (E) and Poisson's Ratio (ν). The LE model is not applicable to soils because of non-linear and irreversible behaviour. It is applicable for modelling of stiff volumes in soils, like concrete walls or rock formations (Plaxis Material Models Manual, 2012).

4.2.2 Mohr-Coulomb model (MC)

Mohr-Coulomb model requires five input parameters and the behaviour is linear elastic and perfectly plastic. In addition to elasticity parameters, Young's Modulus and Poisson's Ratio, internal friction angle (φ) and cohesion (c) are required for soil plasticity and the dilatancy angle (ψ) is also needed (Plaxis Material Models Manual, 2012).

Mohr-Coulomb model gives good results for stress states in elastic region. Furthermore, MC model requires well known parameters, E and ν, to define stiffness. These parameters are easy to obtain from different laboratory tests.

Mohr-Coulomb model involves very limited number of aspects that soils behaves in reality. MC model does not include stress-dependency, stress path dependency, strain dependency of stiffness or anisotropic stiffness (Plaxis Material Models Manual, 2012). In addition, MC model includes only perfectly plastic deformations.

4.2.3 Hardening Soil model (HS)

In simulation of soil behaviour, Hardening Soil Model is an advanced model. Limiting stress states are defined by internal friction angle (φ), cohesion (c) and dilatancy angle (ψ), similar to the Mohr-Coulomb model. In contrast to MC model, three new input parameters are defined to model soil stiffness more accurately. These parameters are: the triaxial loading stiffness (E_{50}), the triaxial unloading stiffness (E_{ur}), and the oedemeter loading stiffness (E_{oed}) (Plaxis Material Models Manual, 2012).

Differently from MC model, stress dependency of stiffness moduli is taken into account in Hardening Soil model. All stiffnesses increase with pressure. As well as stiffnesses, Hardening soil model also accounts for pre-consolidation (Plaxis Material Models Manual, 2012). This parameter is significant for deformation problems.

Despite being an advanced model, hardening soil does not include softening due to dilatancy and de-bonding effects. Also, hysteretic and cyclic loading and cyclic mobility are not taken into account. Furthermore, large stiffness at small strains and reduced stiffness at engineering strain levels are not separated in the model (Plaxis Material Models Manual, 2012).

4.2.4 Hardening Soil model with small-strain stiffness (HSsmall)

The Hardening Soil model with small strain-stiffness is a modified version of the Hardening Soil model. Increased stiffness of soils at small strains is taken into account. At low strain levels, soil behaviour is different and most soils behave stiffer. This behaviour of soils is defined in HSsmall model with two new parameters: small strain shear modulus (G_0^{ref}) and strain level at which the shear modulus reduces to 70% of the small strain shear modulus ($\gamma_{0.7}$) (Plaxis Material Models Manual, 2012).

HSsmall model has two major advantages compared to HS model. Firstly, HSsmall model calculates displacements more reliably than HS model. Secondly, in dynamic applications, HSsmall model accounts for hysteretic material damping (Plaxis Material Models Manual, 2012).

4.3 Selection of Soil Model and Parameters

As it is mentioned before, mechanical soil behavior can be modeled at different accuracy degrees. The simplest stress-strain relationship to model soil behavior is linear elastic model, but it makes rough calculations in some aspects of modeling soil behavior. Furthermore, to model different features of soil behavior, many constitutive soil models have been developed. Nevertheless, selection of a more complex soil model to model behavior more accurately requires selection of more model parameters. This situation leads to insufficient data to select model parameters.

Brinkgreve (2005) states that some model parameters are not easy to obtain although they have a clear physical meaning. In some geotechnical applications, model parameters can not be obtained directly due to limited soil data available. Under this circumstances, some parameters should be estimated and require further evaluation in view of the application.

Soil parameters are selected by using the results of laboratory tests such as oedemeter test, triaxial tests and direct or simple shear tests. Also, in-situ test results can be used for parameters selection. For instance, Standard penetration tests (SPT), Cone Penetration Test (CPT), Menard Pressuremeter Test (PMT) are field tests which provide useful data. In addition, to obtain some soil parameters, correlations such as classification tests or general soil tests can be used. Moreover, tables and norms are useful sources to obtain some soil parameters.

4.4 Hardening Soil Model with Small-strain Stiffness

The behaviour of soil is assumed elastic in the hardening soil model during unloading and reloading. Nonetheless, elastic strain range in soils is very small. Most soils display higher stiffness at low strain levels. As strain amplitude increases, soil stiffness decreases nonlinearly. In Figure 4.1, reduction of stiffness is shown.

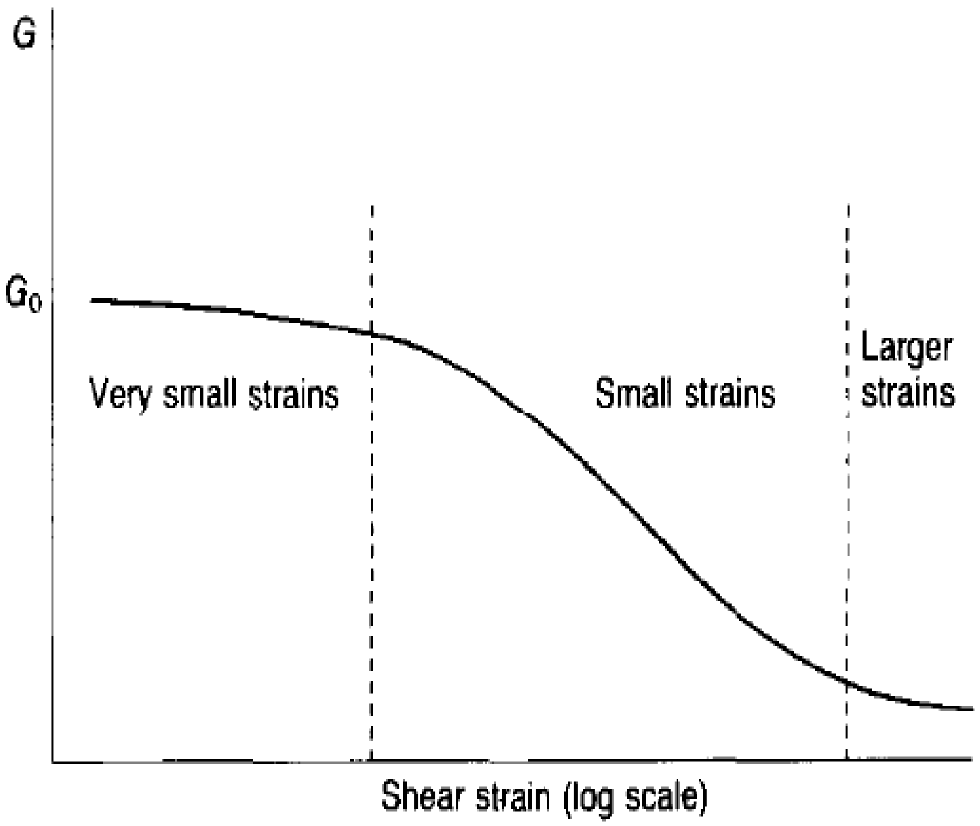

Figure 4.1: Reduction of shear modulus with typical strain ranges (Atkinson & Sallfors, 1991).

4.4.1 Model parameters

The material parameters which are used in HSsmall model are given in Table 4.1.

Table 4.1 : Input parameters of HSsmall model (Plaxis Material Models Manual, 2012).

Symbol	Parameter
φ'	Internal friction angle
c'	Cohesion
ψ	Dilatancy angle
E_{50}^{ref}	Reference secant stiffness from drained triaxial test
E_{oed}^{ref}	Reference tangent stiffness for oedometer primary loading
E_{ur}^{ref}	Reference unloading/reloading stiffness
m	Power for stress-level dependency of stiffness
ν_{ur}	Unloading/reloading Poisson's ratio
G_0^{ref}	Reference small strain shear modulus
$\gamma_{0.7}$	Shear strain magnitude at 0.722G0
K_0	Coefficient of earth pressure at rest
R_f	Failure ratio

Determination of soil parameters are explained in this section. In the determination of model parameters, in-situ test results are used.

4.4.1.1 Internal friction angle

Internal friction angle of soils is determined by performing laboratory tests or in-situ tests. In laboratory, simple shear tests or triaxial tests are performed to determine internal friction angle. In field, penetration tests could be used to determine internal friction angle of cohesionless soils. Hatanaka and Uchida (1996) developed an empirical correlation formula between N1,60 values and internal friction angle. The authors performed a series of drained triaxial tests on undisturbed sand samples for correlations. This formula is represented in (4.1);

$$\varphi' = (20\mathrm{N}_{1,60})^{0.5} \tag{4.1}$$

Where, ϕ is internal friction angle of sand and $\mathrm{N}_{1,60}$ is corrected SPT-N value.

Bowles (1988), based on his works, summarizes the values of ϕ, Dr, corrected SPT values in a table which is presented Table 4.2.

Table 4.2 : Values of ϕ and D_r based on SPT N'_{70} (Bowles, 1988).

Description		Very Loose	Loose	Medium	Dense	Very Dense
Relative Density (D_r) (%)		0-15	15-35	35-65	65-85	85-100
SPT N'_{70}	fine	1-2	3-6	7-15	16-30	?
	medium	2-3	4-7	8-20	21-40	>40
	coarse	3-6	5-9	10-25	26-45	>45
ϕ	fine	26-28	28-30	30-34	33-38	<50
	medium	27-28	30-32	32-36	36-42	
	coarse	28-30	30-34	30-34	40-50	

4.4.1.2 Cohesion

In literature, there are many correlation formulas between standard penetration value and undrained shear strength of clay. Undrained triaxial tests and standard penetration tests on insensitive clays are performed to derive correlations. The general form of correlations follows;

$$q_u = kN_{1,60} \tag{4.2}$$

Where, q_u is undrained shear strength of clay, k is site-dependent constant and $N_{1,60}$ is corrected SPT-N value.

Terzaghi and Peck (1967) proposed a table about consistency of cohesive soils and shown in Table 4.3.

Table 4.3 : Consistency of cohesive soils (Terzaghi and Peck, 1967).

Consistency	SPT-N	q_u (kPa)
Very Soft	<2	<25
Soft	2-4	25-50
Medium	4-8	50-100
Stiff	8-15	100-200
Very Stiff	15-30	200-400
Hard	>30	>400

Cohesion value of soils is determined by using undrained shear strength.

$$c = q_u/2 \tag{4.3}$$

Where; c is cohesion and q_u is undrained shear strength.

4.4.1.3 Dilatancy angle

The dilatancy angle of sands is related to the density and internal friction angle of soil. Generally, dilatancy angle of soil is a smaller value than internal friction angle. For quartz sands dilatancy angle is calculated as;

$$\psi = \phi - 30 \qquad \textbf{(4.4)}$$

Where, ψ is dilatancy angle and ϕ is internal friction angle of soil.

For the soils whose internal friction angle is smaller than 30°, the dilatancy angle is zero (Plaxis Material Models Manual, 2012).

4.4.1.4 Stiffness parameters

There are three different stiffness parameters and five other parameters required to model hyperbolic stress-strain curve. These parameters are;

- Secant stiffness in standard drained triaxial test, E_{50}^{ref}
- Tangent stiffness for primary oedometer loading, E_{oed}^{ref}
- Unloading/reloading stiffness, E_{ur}^{ref}
- Power for stress-level dependency of stiffness, m
- Poisson's ratio for unloading/reloading, ν_{ur}
- Failure ratio, R_f
- Reference stress for stiffness, p^{ref}
- K_0^{NC},K_0value for normal consolidation (coefficient of lateral earth pressure at rest) (Schanz & Vermeer, 1998).

Hyperbolic stress-strain relation between in primary loading for a standard drained triaxial test is given in Figure 4.2.

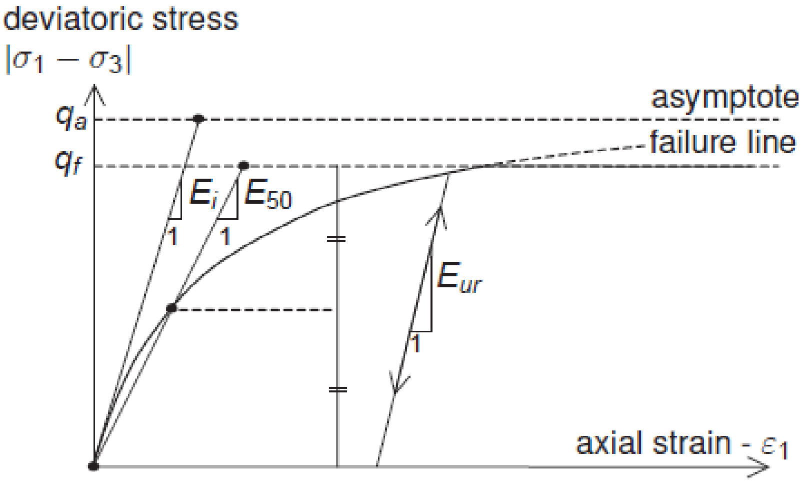

Figure 4.2: Hyperbolic stress-strain relation between in primary loading for a standard drained triaxial test (Plaxis Material Models Manual, 2012).

The secant modulus parameter,E_{50}, is determined by using strain curve at 50% of the ultimate shear strength in triaxial test. Also, E_{50}can be determined by using initial modulus, E_0. Based on the works of Mayne (2007) E_{50}can be obtained by using modulus reduction curves. The curves are shown in Figure 4.3.

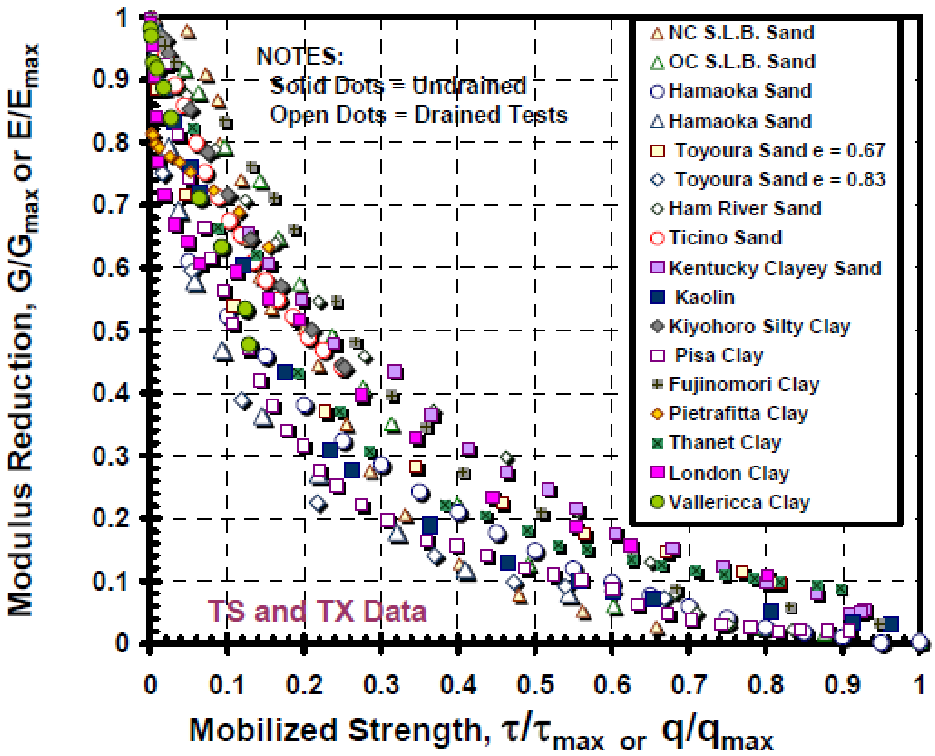

Figure 4.3: Monotonic modulus reduction curves static torsional and triaxial shear data onclays and sands (Mayne, 2007).

The confining stress dependent stiffness modulus for primary loading is calculated by using following equation;

$$E_{50} = E_{50}^{ref} \left(\frac{c\, cos\phi - \sigma_3' sin\phi}{c\, cos\phi - p^{ref} sin\phi} \right)^m \qquad \textbf{(4.5)}$$

Where, E_{50}^{ref} is reference stiffness modulus corresponding to the reference pressure, p^{ref} and m is power for stress-level dependency of stiffness.

Tangent stiffness for primary oedometer loading, E_{oed}^{ref}, is used to model stiffness for compression behaviour. Determination of E_{oed}^{ref} is shown in Figure 4.4. E_{oed}^{ref} is calculated by following equation;

$$E_{oed} = E_{oed}^{ref} \left(\frac{c\, cos\phi - \sigma_3' sin\phi}{c\, cos\phi - p^{ref} sin\phi} \right)^m \qquad \textbf{(4.6)}$$

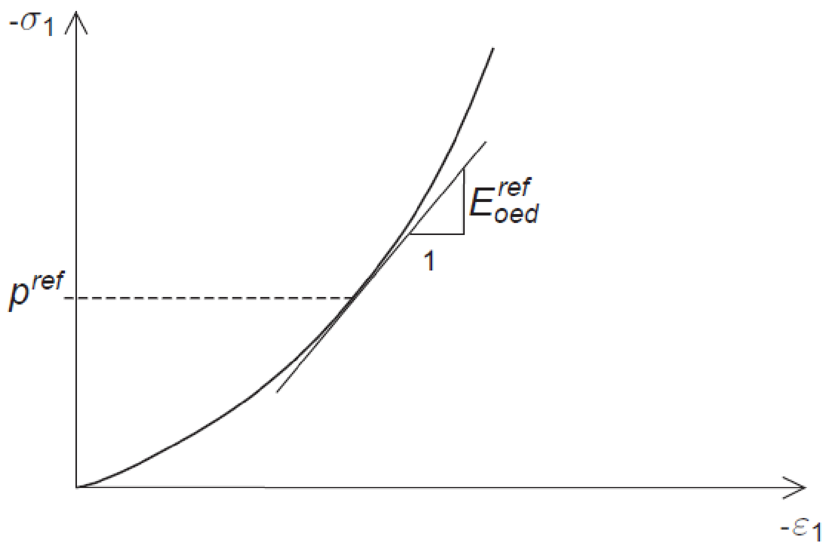

Figure 4.4: Definition of Tangent stiffness for primary oedometer loading, E_{oed}^{ref} (Plaxis Material Models Manual, 2012).

Unloading/reloading stiffness, E_{ur}^{ref} is used for unloading and reloading stress paths and calculated for a reference stress as;

$$E_{ur} = E_{ur}^{ref} \left(\frac{c\, cos\phi - \sigma_3' sin\phi}{c\, cos\phi - p^{ref} sin\phi} \right)^m \qquad \textbf{(4.7)}$$

It is suggested in Plaxis Material Models Manual (2012) that E_{ur}^{ref} can be estimated as;

$$E_{ur}^{ref} = 3E_{50}^{ref} \qquad \textbf{(4.8)}$$

According to Schanz and Vermeer's research (1998) on different sands E_{50}^{ref} can be equal to E_{oed}^{ref}, as it is shown in Figure 4.5.

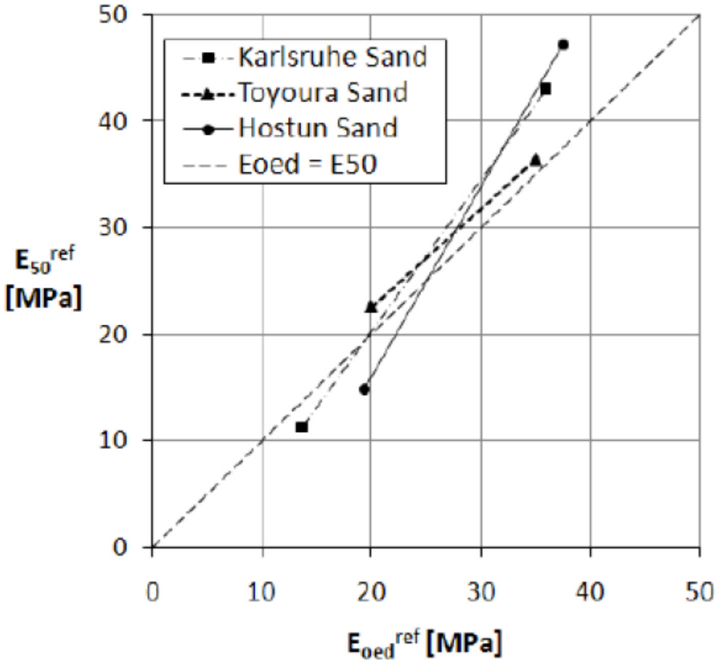

Figure 4.5: Relationship between E_{50}^{ref} and E_{oed}^{ref} (Schanz and Vermeer, 1998).

m defines the stress dependency and used to simulate logarithmic stress dependency of stiffness. According to von Soos (2001), m changes between 0.5 and 1 on different soil types. For the clayey soils it is between 0.9 and 1. Brinkgreve et al. (2007) proposed an empirical formula to determine m value for quartz sands as it follows;

$$m = 0.7 - (RD/320) \quad \textbf{(4.9)}$$

Here, RD is the relative density of sand.

ν_{ur} is the Poisson's ratio for unloading/reloading. It is suggested in Plaxis Material Models Manual to take ν_{ur} between 0.2-0.3 values (2012). R_f is defined as failure ratio and it is the ratio between ultimate deviatoric stress at failure and asymptotic value of shear strength. In Plaxis Material Models Manual, the default value of R_f is 0.9 (2012). K_0^{NC} is lateral earth pressure coefficient at rest for normal consolidation. It is calculated by using Jaky's (1944) formula as it follows:

$$K_0 = 1 - \sin\phi' \quad \textbf{(4.10)}$$

Where, ϕ is the internal friction angle.

4.4.1.5 Small strain stiffness parameters

There are two small strain parameters in HSsmall model: G_0^{ref}, Initial or very small strain shear modulus and $\gamma_{0.7}$ shear strain at which $G_s = 0.722G_0$.

Small strain stiffness is modeled using S shape curves which are obtained from sketching the graph of shear modulus (G) against shear strain (γ) in logarithmic scale. From this graph, small strain shear modulus (G_0) and shear strain ($\gamma_{0.7}$) at which the shear modulus is 70% of G_0 is given and that graph can be seen in Figure 4.6.

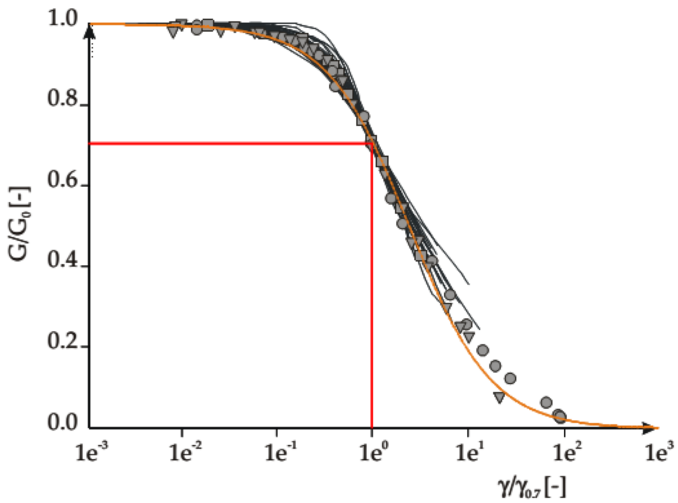

Figure 4.6: S shaped curve for reduction of shear modulus against shear strain (Plaxis Material Models Manual, 2012).

Different charts and correlations are developed by several researchers to estimate stiffness reduction. Vucetic and Dobry (1991) show the effect of plasticity on stiffness in their works which is presented in Figure 4.7. By using chart, shear strain at $0.7G_0$ can be obtained. Also, Seed and Idriss (1970) show the stiffness reduction-shear strain relationship for sandy soils in their works. The graph is presented in Figure 4.8.

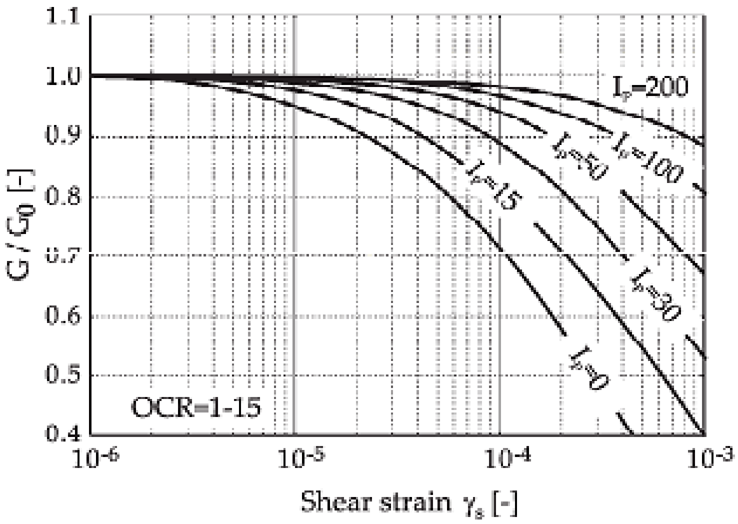

Figure 4.7: Effect of plasticity on stiffness reduction (Vucetic and Dobry, 1991).

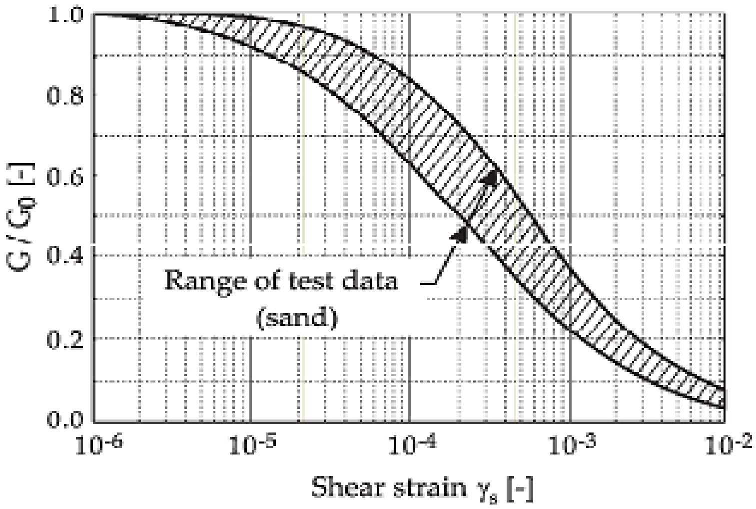

Figure 4.8: Stiffness reduction curve (Seed and Idriss, 1970).

In addition, initial shear modulus can be calculated by using this formula;

$$G_0 = \frac{\gamma}{g} * V_s^2 \qquad \textbf{(4.11)}$$

Where, γ is unit weight of soil (kN/m^3), g is gravitational acceleration (m/s^2) and V_s is shear wave velocity (m/s).

There are some empirical formulas to calculate$\gamma_{0.7}$. Darendeli (2001) proposed correlations based on statistical evaluation of test data for clayey soils. Correlations are given for different plasticity indexes.

IP=0; $$\gamma_{0.7} = 0.00015\sqrt{\frac{p'}{p_{ref}}} \qquad \textbf{(4.12)}$$

IP=30; $$\gamma_{0.7} = 0.00026\sqrt{\frac{p'}{p_{ref}}} \quad \textbf{(4.13)}$$

IP=100; $$\gamma_{0.7} = 0.00055\sqrt{\frac{p'}{p_{ref}}} \quad \textbf{(4.14)}$$

Where, p' is actual stress and p_{ref} is reference stress.

Also, Brinkgreve et al. (2007) proposed a correlation for quartz sands to calculate $\gamma_{0.7}$. The formula follows:

$$\gamma_{0.7} = (2 - RD/100)10^{-4} \quad \textbf{(4.15)}$$

Where, RD is relative density of sand.

4.4.1.6 Determination of shear wave velocity

Shear wave velocity is not a parameter directly used in model, but it is needed for the calculation initial shear modulus (G_0). In the field, shear wave velocity is measured by geophysical methods such as down-hole method, up-hole method, cross-hole method, seismic refraction, PS logging, Spectral Analysis of Surface Waves (SASW) and Multichannel Analysis of Surface Waves (MASW). If shear waves are not directly measured in the field, they can be determined by using empirical correlations for Standard Penetration Test (SPT). The correlation formulas are given below:

Fujimara (1972) $$V_s = 92.1 * N^{0.337} \quad \textbf{(4.16)}$$

Imai et al. (1976) $$V_s = 89,8 * N^{0.341} \quad \textbf{(4.17)}$$

Ohta and Goto (1978) $$V_s = 85.3 * N^{0.348} \quad \textbf{(4.18)}$$

Imai and Tonouchi (1982) $$V_s = 97.0 * N^{0.314} \quad \textbf{(4.19)}$$

İyisan (1996) $$V_s = 51.5 * N^{0.516} \quad \textbf{(4.20)}$$

Kiku et al. (2001) $$V_s = 68.3 * N^{0.292} \quad \textbf{(4.21)}$$

After determination of shear wave velocity, initial shear modulus (G_0) is calculated by using equation 4.11. Then, E_0 can be calculated by;

$$E_0 = 2 * (1 + \nu) * G_0 \quad \textbf{(4.22)}$$

4.5 Dynamic Parameters

Dynamic parameters which affect the dynamic analysis stability and calculations are explained in this chapter.

4.5.1 Finite element model

The 15-node triangular element is used in these analyses. 15-node element provides a fourth order interpolation for displacement and the numerical integration involves 12 stress points. It produces high quality stress results and is very accurate. The average element size (AES) is the average side length of the element was used and it is an average dimension, which is represents mesh thickness (Plaxis Material Models Manual, 2012). Every time a numerical analysis is performed, effect of mesh should be checked. Kuhlmeyer and Lysmer (1973) stated that element size should not be larger than $\lambda/8$, where λ is wave length with maximum frequency. Average element sizes for layers are checked and in this study, the mesh density is chosen medium for analyses.

4.5.2 Absorbent boundaries

When performing a dynamic analysis, special boundary conditions are defined to model semi-infinite media in reality. Absorbent boundaries are used to prevent reflecting waves back from model boundaries (Plaxis Material Models Manual, 2012).

4.5.3 Newmark alpha and beta

Newmark alpha and beta parameters are defined in the iterative procedure group in PLAXIS manual and used for determination of numeric time integration according to the implicit Newmark scheme (Plaxis Material Models Manual, 2012). For performing an unconditionally stable solution, Newmark parameters must fulfill the following conditions;

Newmark $\beta \geq 0.5$ **(4.23)**

Newmark $\alpha \geq 0.25(0.5+\beta)^2$ **(4.24)**

In dynamic analyses $\beta = 0.5$ and $\alpha = 0.25$ were used as an average acceleration scheme are used.

4.5.4 Boundary C_1 and C_2

Boundary C_1 and C_2 coefficients are used for relaxation to improve wave absorption which is done on absorbent boundaries. C_1 is used for correction of the dissipation in the direction normal to the boundary and C_2 does the some in tangential direction. If the waves move only perpendicular to boundaries, use of relaxation is not necessary (C_1=C_2=1). If waves move in arbitrary direction, C_2 should be adjusted to improve absorption on boundaries (Plaxis Material Models Manual, 2012).

As earthquake waves move in arbitrary direction, C_2 is adjusted. C_1=1 and C_2=0.25 are used in analyses.

4.5.5 Dynamic multipliers

When running an analysis, dynamic multipliers are used to activate dynamic loads. Either defining a harmonic load or reading a dynamic load multiplier from a data file is possible. The format of data file can be ASCII or SMC (Strong Motion CD-ROM). Prescribed displacements are used to apply ground motion data or harmonic load (Plaxis Material Models Manual, 2012). Ground motion data can be downloaded from sources such as PEER, USGS or VDC.

4.5.6 Material damping

The vibration amplitude decreases in soil with respect to time. In Plaxis, viscous properties of soil, friction and development of plastic strains, causes material damping to a certain extent but in reality there are more damping observed. For modeling the real damping in soil behavior, Rayleigh parameters are used (Plaxis Material Models Manual, 2012).

Rayleigh α parameter is defined to determine the influence of mass in the damping of the system and Rayleigh β parameter is defined to determine the influence of stiffness in the damping of the system.

$$C = \alpha M + \beta K \tag{4.25}$$

Where, C is damping matrix, M is mass matrix and K is stiffness matrix.

Rayleigh parameters can be calculated as;

$$\alpha = 2\omega_1\omega_2 \frac{\omega_1\xi_2 - \omega_2\xi_1}{\omega_1^2 - \omega_2^2} \tag{4.26}$$

$$\beta = 2\frac{\omega_1\xi_2 - \omega_2\xi_1}{\omega_1^2 - \omega_2^2} \quad \textbf{(4.27)}$$

$$\omega_1 = 2\pi f_1 \quad and \quad \omega_2 = 2\pi f_2 \quad \textbf{(4.28)}$$

Where, ξ represents damping, ω_1 is the first angular frequency and, ω_2 is the second angular frequency, f_1 and f_2 are first and second natural vibration frequency.

f_1 and f_2 are inverse of period (T) and can be determined by;

$$T = \frac{4H}{V_s} \quad \textbf{(4.29)}$$

$$f = \frac{1}{T} \quad \textbf{(4.30)}$$

Here, H is the thickness of soil layers and V_s is the shear wave velocity.

4.5.7 Dynamic substeps

When performing a dynamic analysis, it is important to define proper numbers of time steps. The time steps used in dynamic analysis is constant and calculated as;

$$\delta_t = \frac{\Delta_t}{n.m} \quad \textbf{(4.31)}$$

Where, Δt is duration of dynamic loading (earthquake time interval), n is number of dynamic sub steps and m is number of additional steps.

For each additional time step, PLAXIS calculates the number of substeps necessary to reach the estimated end time with the sufficient accuracy relating to generated mesh and calculated δ_t. The number of additional steps specifies the number of steps which is used in plots in the Output programme of PLAXIS. Higher number of additional steps gives more detail in plots, on the other hand, time of analysis increases.

4.6 Case Study and Results

A quay wall in Rokko Island which was damaged during the 1995 Kobe Earthquake is modeled in PLAXIS. The wall is located at the Northwest of the Rokko Island. The modeled quay wall moved 2.48 m towards sea and settled 1.2 m, according to Inagaki (1996). The cross-section of site and SPT values are given in Figure 4.9.

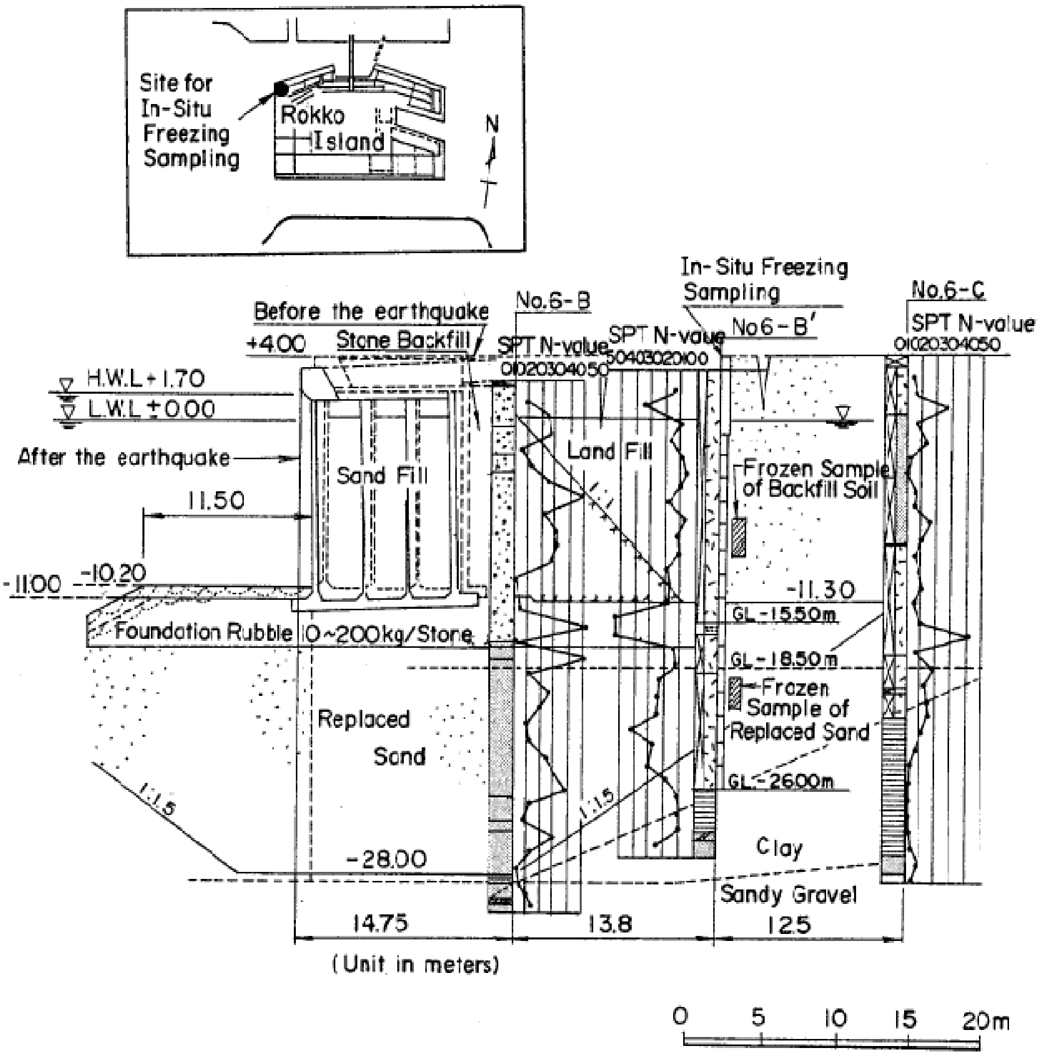

Figure 4.9: Cross-section of quay wall and SPT values (Inagaki, 1996).

The wall was designed with pseudo static method whose seismic coefficient was 0.15. The SPT values vary between 0-2 in alluvial clay, foundation soil was replaced to provide sufficient bearing capacity for the wall. Masado soil was used in artificial fills which were used both backfill and foundation fill. Below the alluvial clay, there is Sandy Gravel layer and measured SPT values of Sandy Gravel are 5, 10, 14 and increases with depth.

The model in used analyses is given in Figure 4.10. Cross-sectional area is 200 m by 48 m. The caisson wall dimensions are 11.5 m in width and 18 m in height. The finite element mesh is given in Figure 4.11.

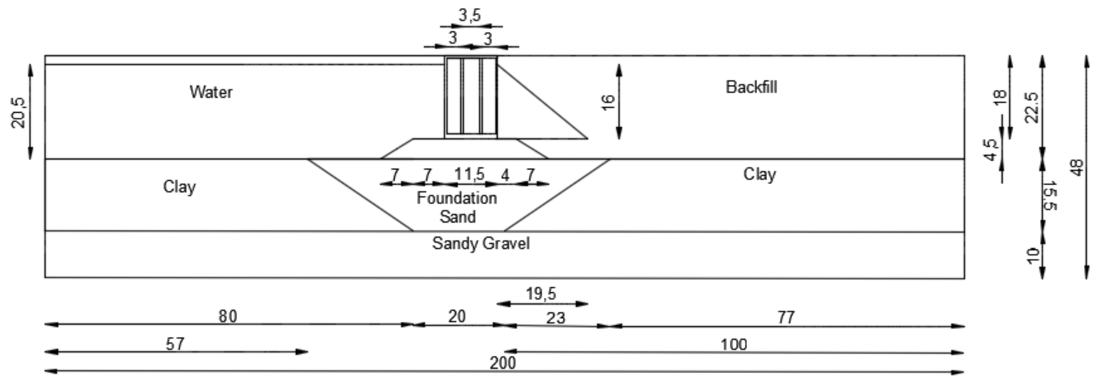

Figure 4.10: Cross-section of analyzed quay wall.

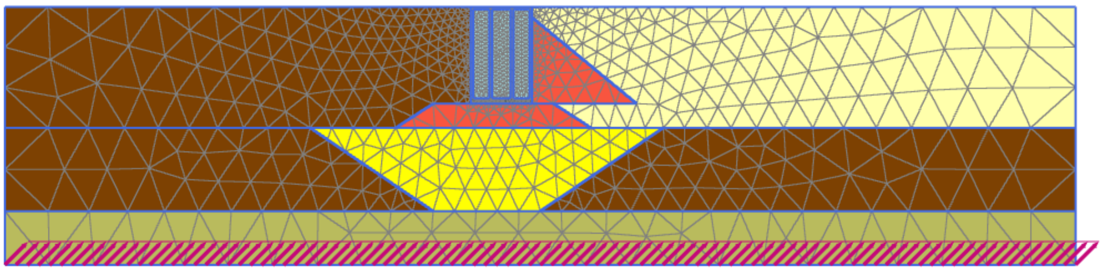

Figure 4.11: Finite element mesh in PLAXIS

The soil model in used analyses is described in Section 4.4. Backfill, foundation soil, clay and sandy gravel layers are modeled with HS small model. Rubble is modeled in Mohr-Coulomb. Caisson fill and concrete is modeled using linear elastic model.

Model parameters are determined using Standard Penetration Test results. Energy correction and overburden pressure correction are done. Then, empirical correlation formulas are used to determine shear wave velocity. 6 different correlation formulas are used including Fujimara (1972), Imai et al. (1976), Ohta and Goto (1978), Imai and Tonouchi (1982), İyisan (1996) and Kiku et al. (2001) which explained in previous chapter. Calculated shear wave velocities of 6-B, 6-B’ and 6-C are presented in Figure 4.12, 4.13 and 4.14.

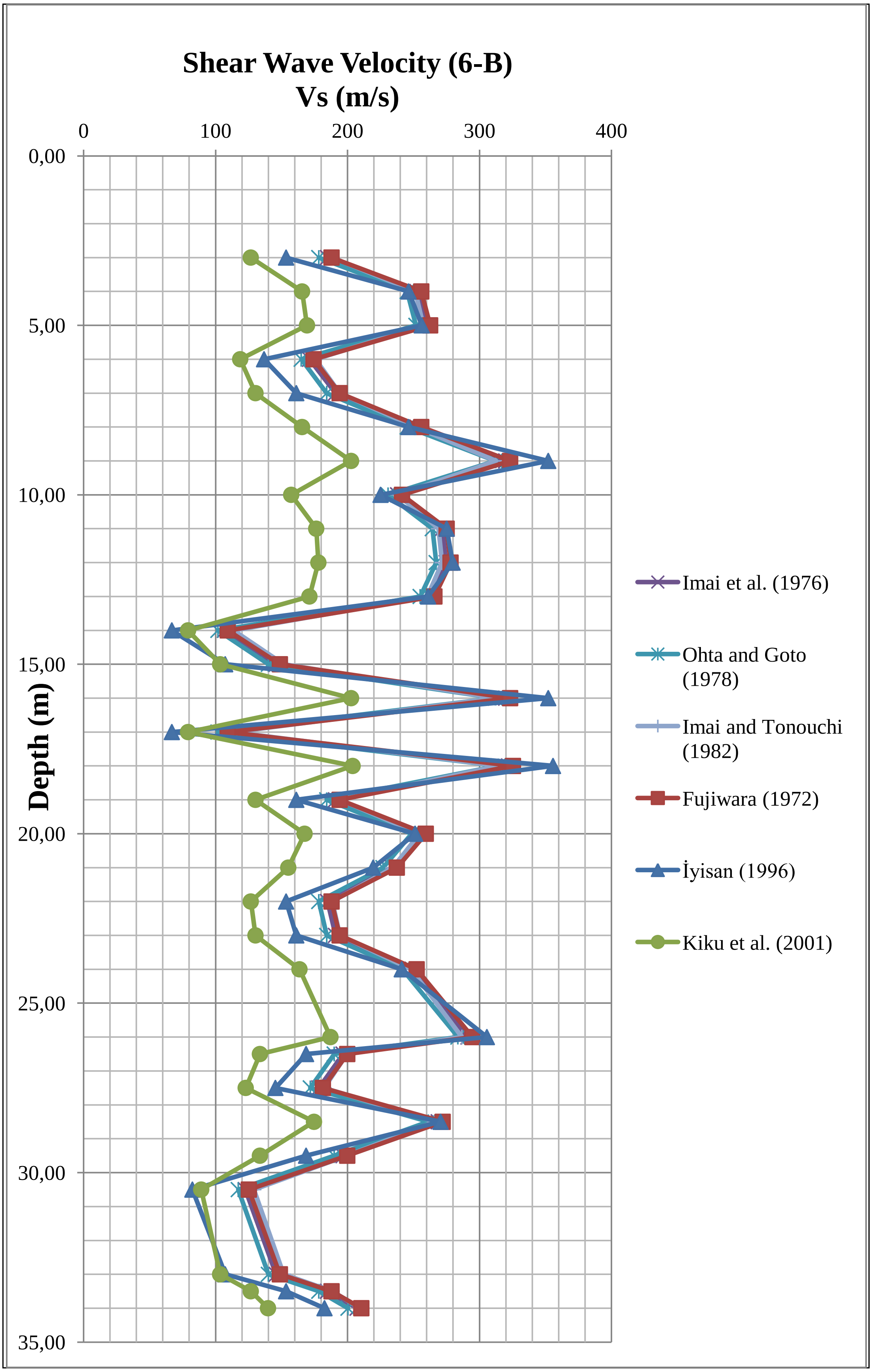

Figure 4.12: Shear wave velocity with depth in 6-B

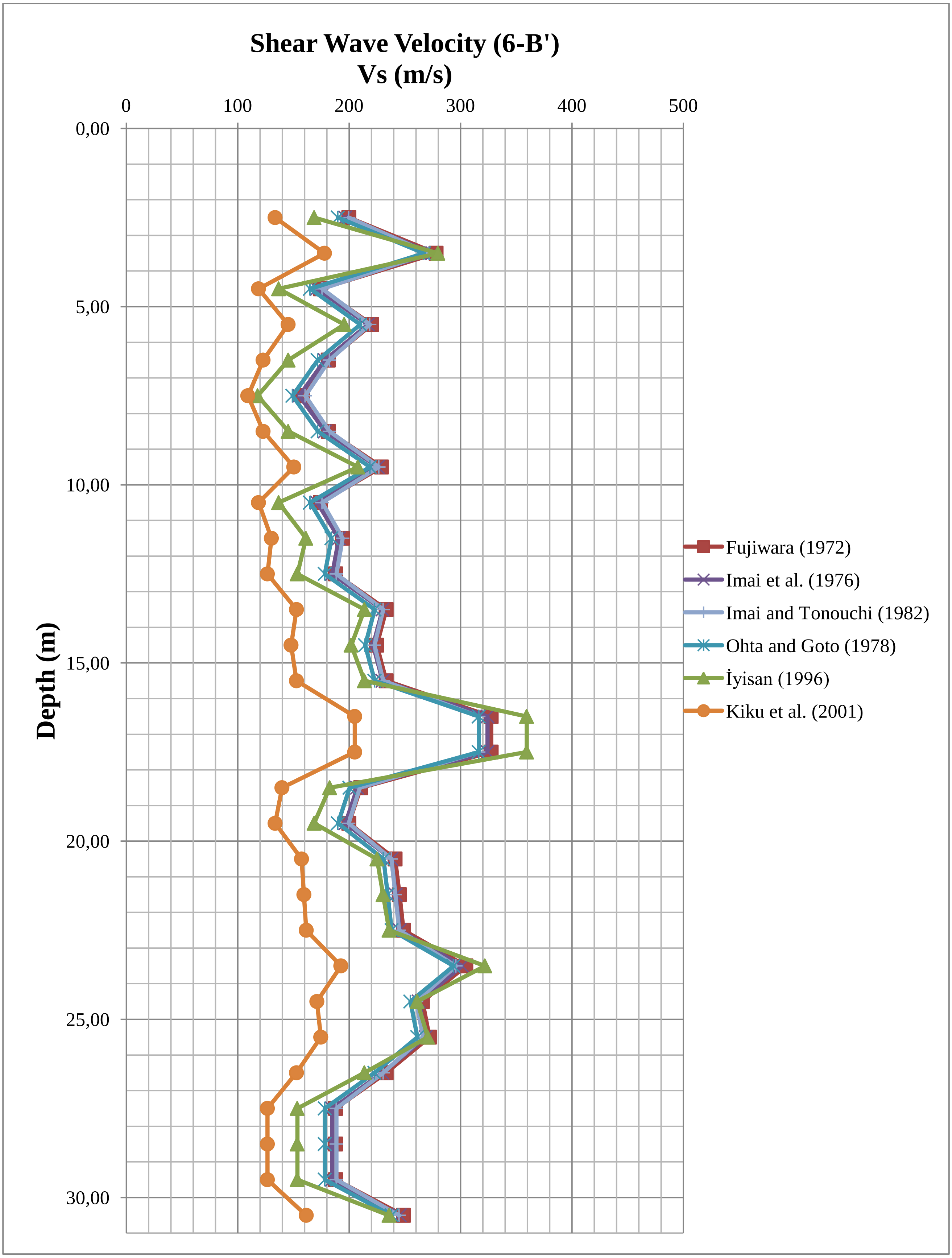

Figure 4.13: Shear wave velocity with depth in 6-B’

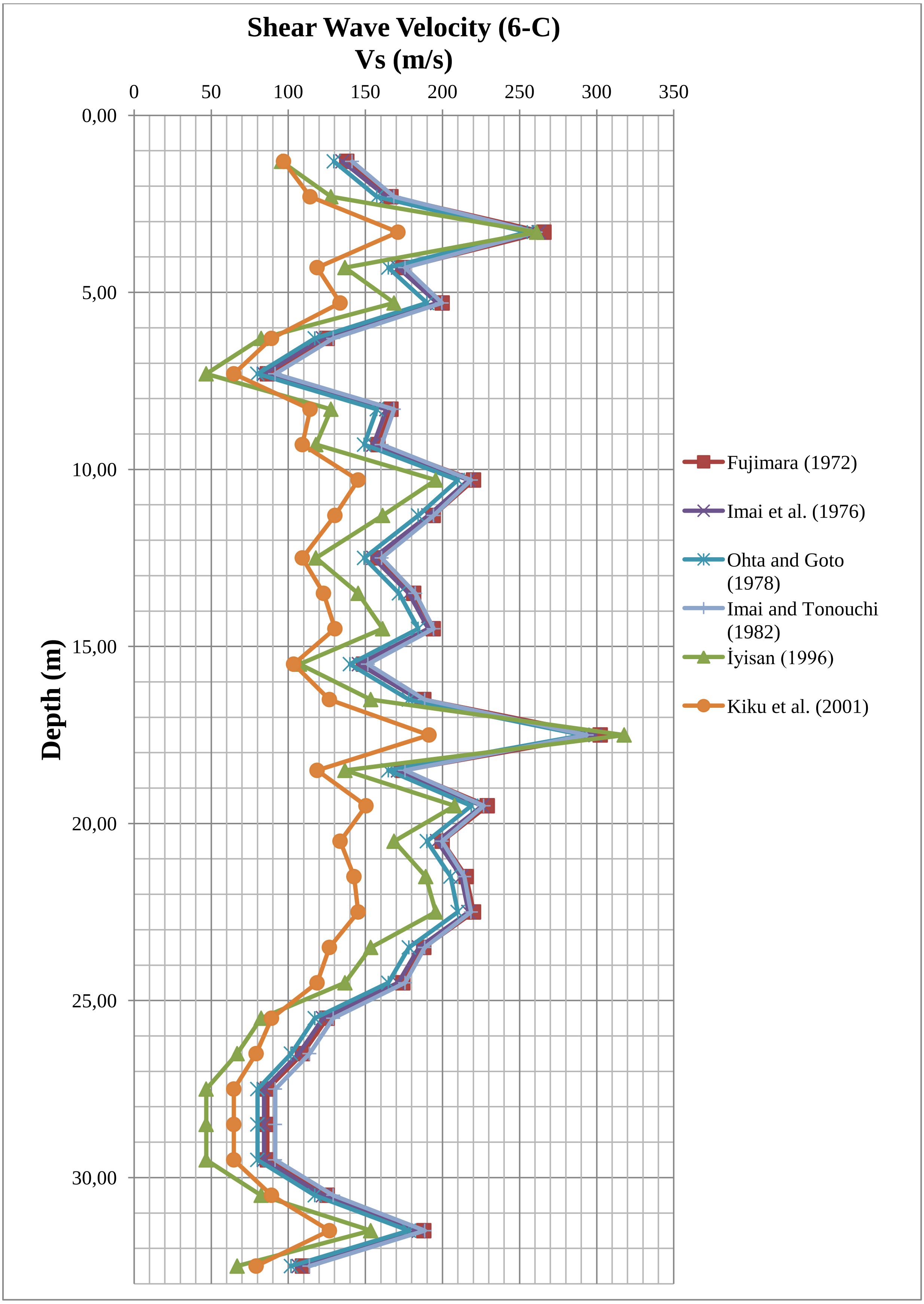

Figure 4.14: Shear wave velocity with depth in 6-C

After determination of shear wave velocity, Rayleigh parameters are calculated for material damping. Firstly, period is calculated by using layer thickness and shear wave velocity. Then, frequency is determined as it is inverse of period. Thereafter, angular frequencies are calculated. Finally, Rayleigh parameters are determined by using angular frequencies. Rayleigh parameters are calculated for 5% damping. Parameters are given in Table 4.4 for every layer.

Table 4.4 : Rayleigh parameters for soil layers.

Layer	Backfill	Foundation Sand	Clay	Sandy Gravel
Thickness (m)	22,5	15,5	15,5	10
Vs (m/s)	200	220	100	180
Period (s)	0,45	0,28	0,62	0,22
Frequency (f_1)	2,22	3,55	1,61	4,50
Frequency (f_2)	10	10	10	10
Angular frequency (ω_1)	13,96	22,30	10,13	28,27
Angular frequency (ω_2)	62,83	62,83	62,83	62,83
Rayleigh α	1,14	1,65	0,87	1,95
Rayleigh β	0,0013	0,0012	0,0014	0,0011

The average element size (AES) is explained in previous chapter. Maximum element size is calculated for every layer according to Kuhlmeyer and Lysmer (1973) and given in Table 4.5. To determine the maximum element size, period and frequency of layers are calculated at first. Then, shear wave velocity is divided to frequency to determine wave length. 1/8 of wave length is maximum element size.

Table 4.5 : Maximum element sizes for soil layers.

Layer	Thickness (m)	Vs (m/s)	Period (s)	Frequency (s^{-1})	Wave length (m)	Maximum element size (m)
Backfill	22,5	200	0,45	2,22	90	11,25
Foundation Sand	15,5	220	0,28	3,55	62	7,75
Clay	15,5	100	0,62	1,61	62	7,75
Sandy Gravel	10	180	0,22	4,50	40	5

HS small model stiffness parameters are determined using shear wave velocities. Using equation (4.11), initial shear modulus (G_0) is calculated. Then, E_0 is calculated with Poisson's ratio. Mayne's (2007) modulus reduction curves are used to determine E_{50}. By using E_{50}, the other stiffness parameters are determined and adjusted for reference stress. To determine strength parameters such as internal friction (ϕ) angle, dilatancy angle (ψ) and cohesion (c) empirical relations between SPT and tables are used. All soil parameters used in analyses are given in Table 4.6. For rubble and caisson fill parameters, properties proposed by Iai et al. (1998) are used. Concrete rubble and caisson fill parameters are given in Table 4.7.

Table 4.6 : Calculated parameters for soil layers.

Material	Backfill	Foundation	Clay	Sandy Gravel
$N_{average}$	12	16	2	10
V_s (m/s)	200	220	100	180
D_r (%)	35	40	-	35
Material Model	HS Small	HS Small	HS Small	HS Small
γ_{unsat} (kN/m^3)	15	16	16	18
γ_{sat} (kN/m^3)	17	18	18	20
φ (°)	33	35	1	33
ψ (°)	3	5	-	3
c (kPa)	-	-	10	-
$\boldsymbol{E_{50}^{ref}}$ (kPa)	20000	23000	10000	30000
$\boldsymbol{E_{oed}^{ref}}$ (kPa)	20000	23000	29500	30000
$\boldsymbol{E_{ur}^{ref}}$ (kPa)	60000	69000	30000	90000
m	0,5	0,5	0,9	0,5
ν_{ur}	0,2	0,2	0,2	0,2
$\boldsymbol{G_{0}^{ref}}$ (kPa)	38000	42000	14000	45000
$\gamma_{0.7}$	0,000165	0,00016	0,002	0,00016

Table 4.7 : Rubble, concrete and caisson fill parameters.

Material	Rubble	Concrete	Caisson Fill
Material Model	Mohr-Coulomb	Linear Elastic	Linear Elastic
γ_{unsat}	17	21	14
γ_{sat}	20	-	-
φ	40	-	-
c (Kpa)	0	-	-
E (Kpa)	432000	32000000	100000
G (Kpa)	180000	14550000	41670
ν	0,2	0,1	0,2

4.6.1.1 Input motion

In dynamic analyses, different earthquake records are used as dynamic multipliers. Firstly, the accelerogram which recorded during 1995 Kobe earthquake at Port Island station used as dynamic multiplier. The earthquake data retrieved from website of Strong-Motion Virtual Data Center. As accelerations in y directions were greater than other directions, y component of earthquake is used in analysis. Filtering and baseline corrections are applied to the record. The accelerogram is given in Figure 4.15.

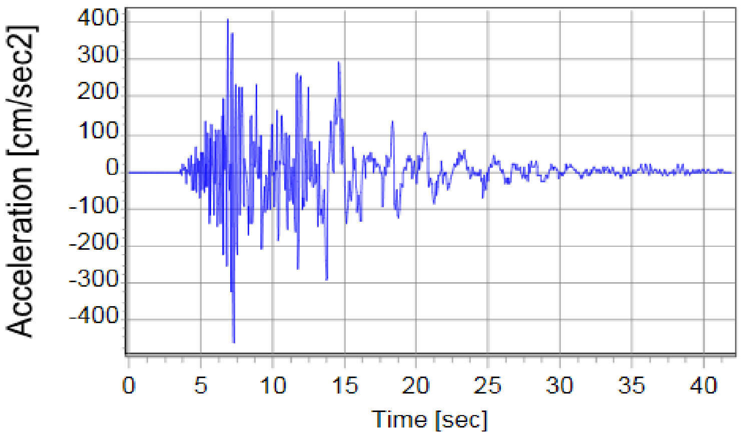

Figure 4.15: 1995 Kobe accelogram in y direction recorded at Port Island Station.

Also, four other earthquake data used as dynamic multipliers. Firstly, record of 1999 Kocaeli (Turkey) earthquake which is recorded in Yarımca Station is used. The accelerogram of Kocaeli is given Figure 4.16. The peak ground acceleration was 343 cm/s^2 and duration of record is 35 seconds. The magnitude of earthquake was 7.4, fault type was strike-slip and depth of earthquake was 15 km.

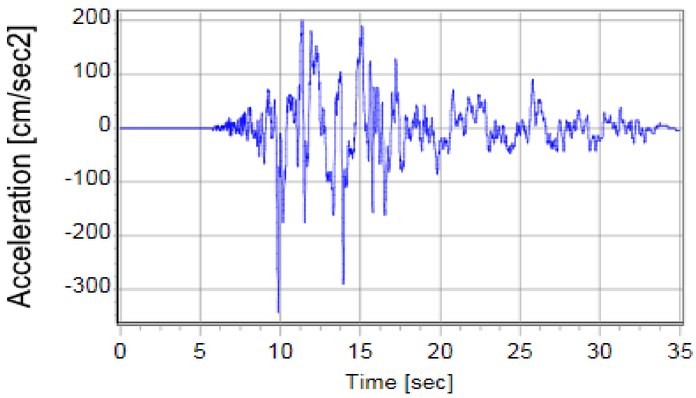

Figure 4.16: 1999 Kocaeli earthquake accelerogram recorded at Yarımca Station.

Secondly, 1999 Chi-Chi (Taiwan) earthquake data which is recorded at TCU045 station is used. The accelerogram of Chi-Chi earthquake is given in Figure 4.17. The peak ground acceleration of record was 359 cm/s^2 and duration of record is 53 seconds. The magnitude of earthquake was 7.6, fault type was reverse-oblique and depth of earthquake was 6.8 km.

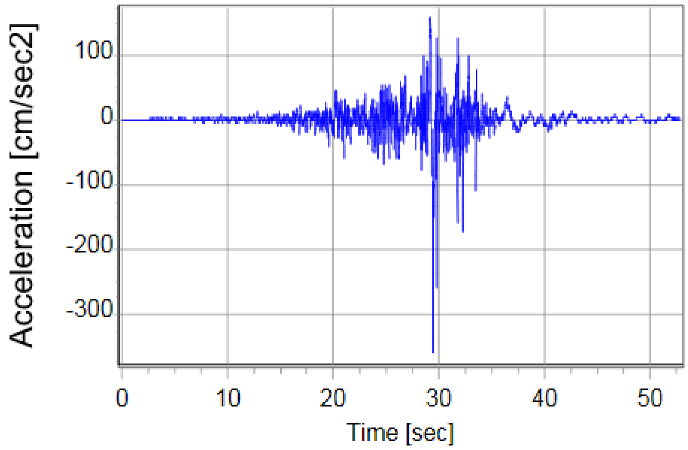

Figure 4.17: 1999 Chi-Chi earthquake accelerogram recorded at TCU045 Station.

Thirdly, 1994 Northridge (USA) earthquake data which is recorded at CDMG 24278 station is used. The accelerogram of Northridge earthquake is given in Figure 4.18. The peak ground acceleration of record was 603 cm/s^2 and duration of record is 40 seconds. The magnitude of earthquake was 6.7, fault type was reverse and depth of earthquake was 17.5 km.

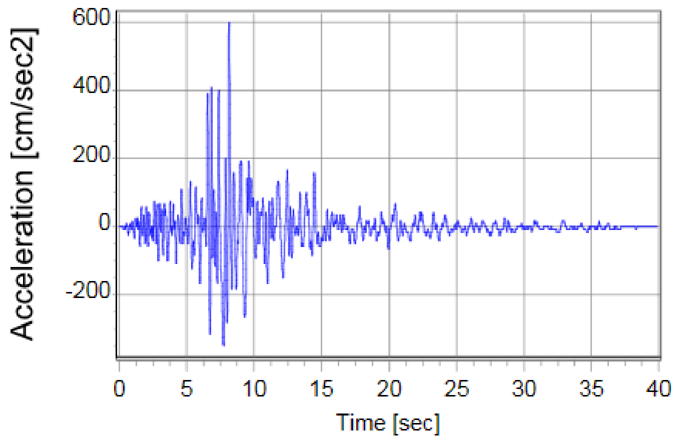

Figure 4.18:1994 Northridge earthquake accelerogram recorded at CDMG 24278 Station.

Fourthly, 1976 Friuli (Italy) earthquake data which is recorded at Tolmezzo station is used. The accelerogram of Friuli earthquake is given in Figure 4.19. The peak ground acceleration of record was 327 cm/s^2 and duration of record is 37 seconds.

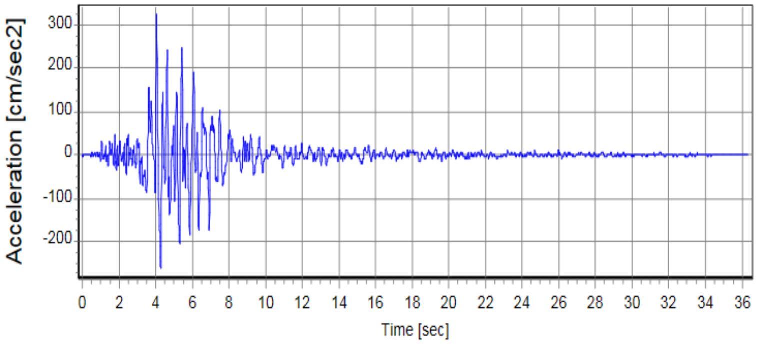

Figure 4.19: 1976 Friuli earthquake accelerogram recorded at Tolmezzo Station.

Data of four earthquakes retrieved from PEER. Filtering and baseline corrections are applied. All applied earthquake records are summarize in Table 4.8.

Table 4.8 : Station, duration and acceleration informations of earthquakes.

Earthquake Name	Year	Station Name	Maximum acceleration (a_{max}) (cm/s^2)	Duration (s)
Kobe	1995	Port Island	463	42
Chi-Chi	1999	TCU 045	359	53
Kocaeli	1999	Yarımca	342	35
Northridge	1994	CDMG 24278	603	40
Friuli	1976	Tolmezzo	326	36

5. ANALYSIS RESULTS

After all inputs are defined in PLAXIS, the dynamic analyses performed for quay wall at Rokko Island. First analysis is performed for Kobe earthquake. The result of analysis is given in Figure 5.1. The horizontal displacement of top of the caisson is 2.43 m and vertical displacement of top of the caisson is 1.54 m. Plot of deformed mesh is given in Figure 5.2.

Plot of deformed stiffness reduction in shadings is presented in Figure 5.3. Also, deformation contours and excess pore pressures are plotted Figure 5.4 and Figure 5.5.

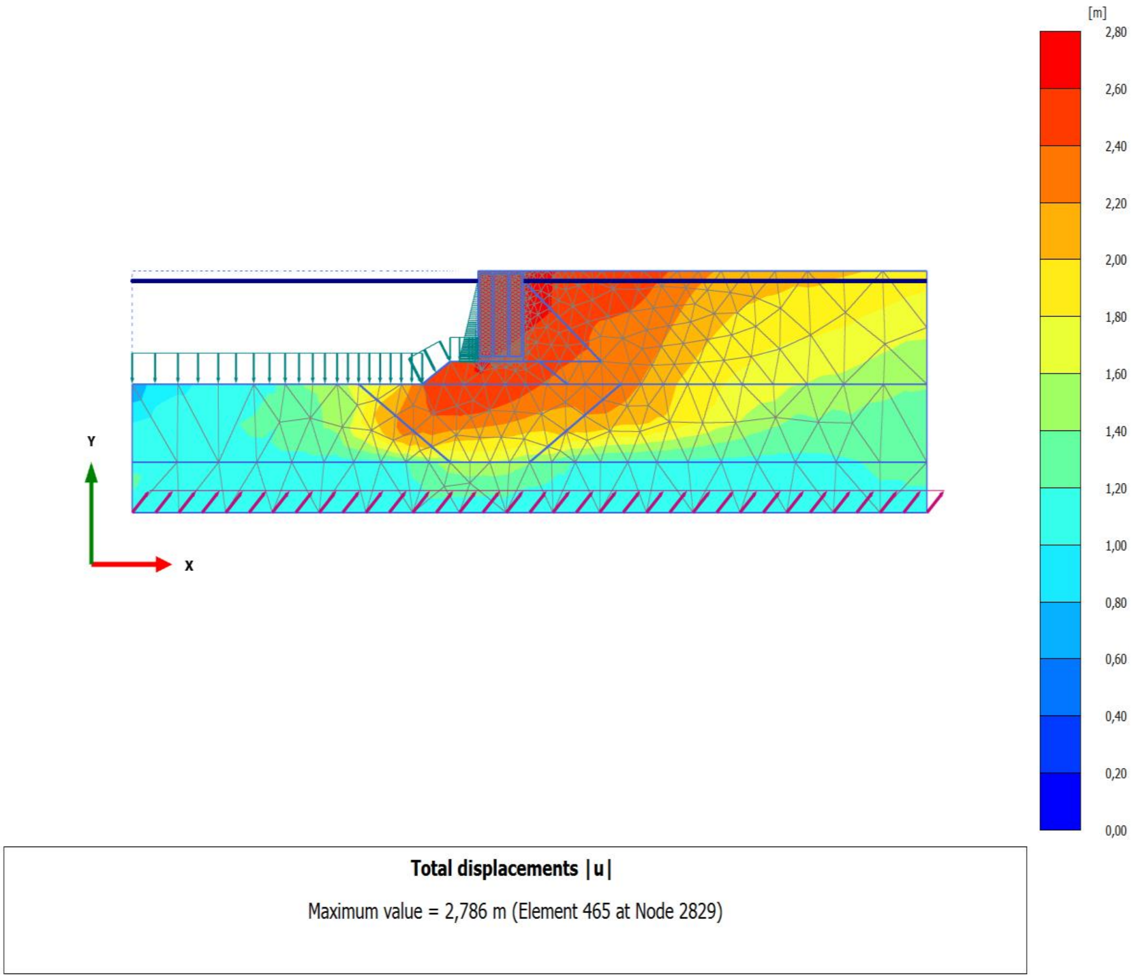

Figure 5.1 : Plot of total displacements for Kobe earthquake (shadings).

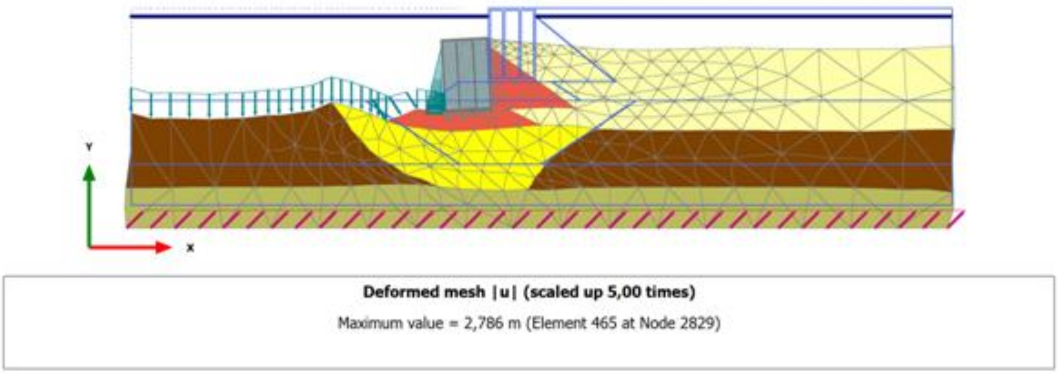

Figure 5.2 : Plot of deformed mesh (scaled 5 times)

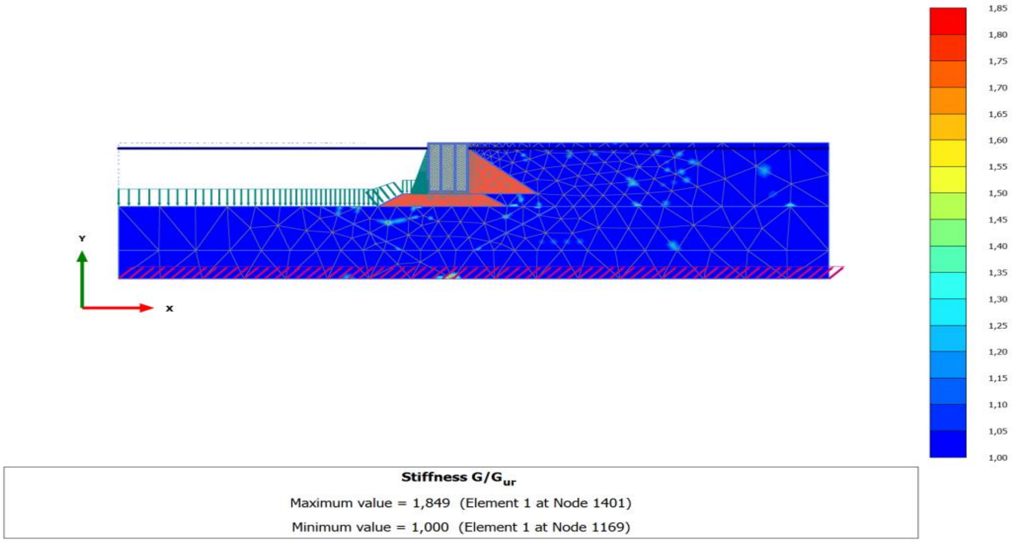

Figure 5.3 : Plot of stiffness reduction in model

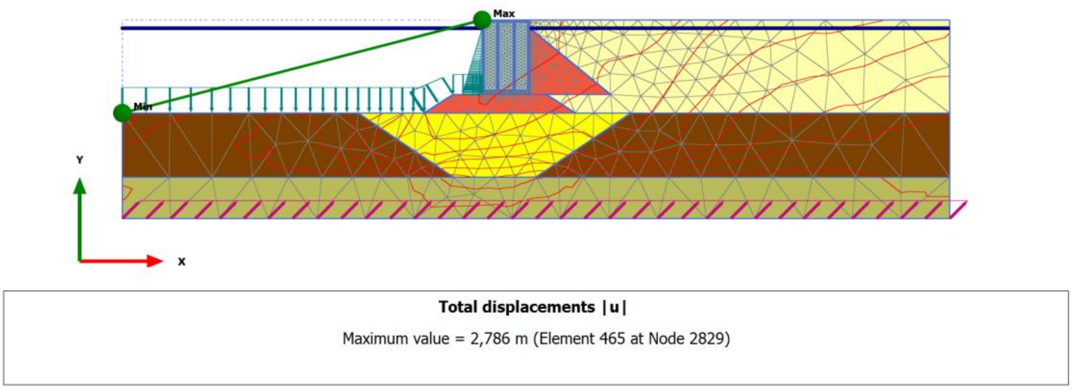

Figure 5.4 : Plot of deformation contours

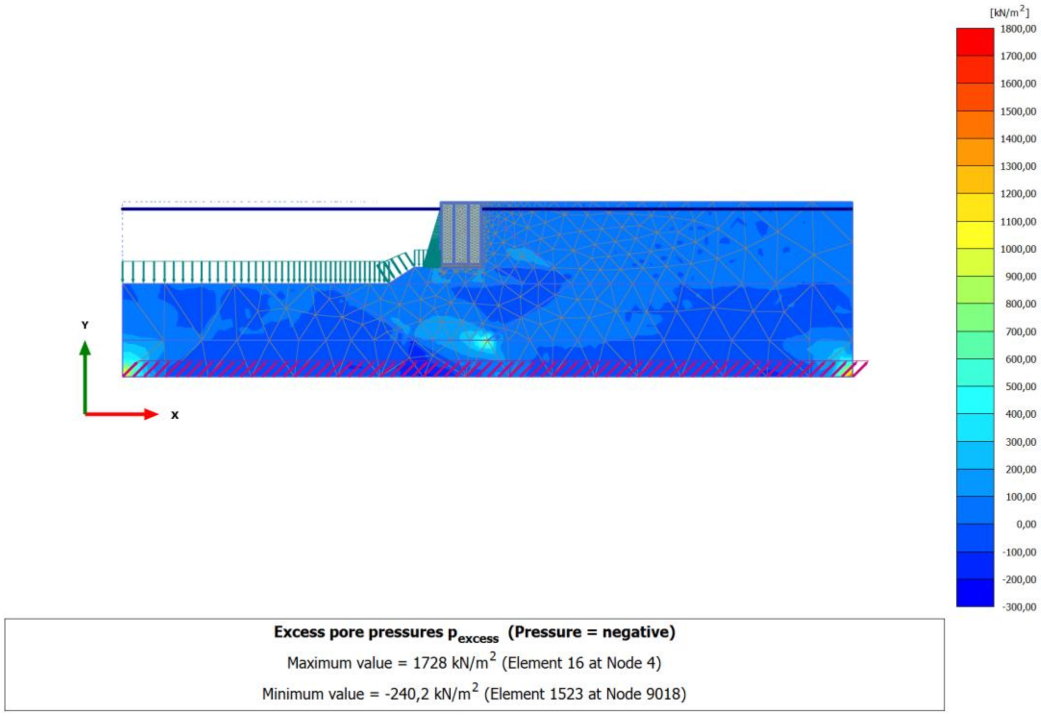

Figure 5.5 : Plot of excess pore pressures

Dynamic analyses are performed for other four earthquakes records. Displacement-time graph for all earthquakes are given in Figure 5.6 for horizontal displacements and in Figure 5.7 vertical displacements. Displacements of top of the caisson for all earthquakes are summarized in Table 5.1. Excess pore pressures and effective stress are given in Appendix A.

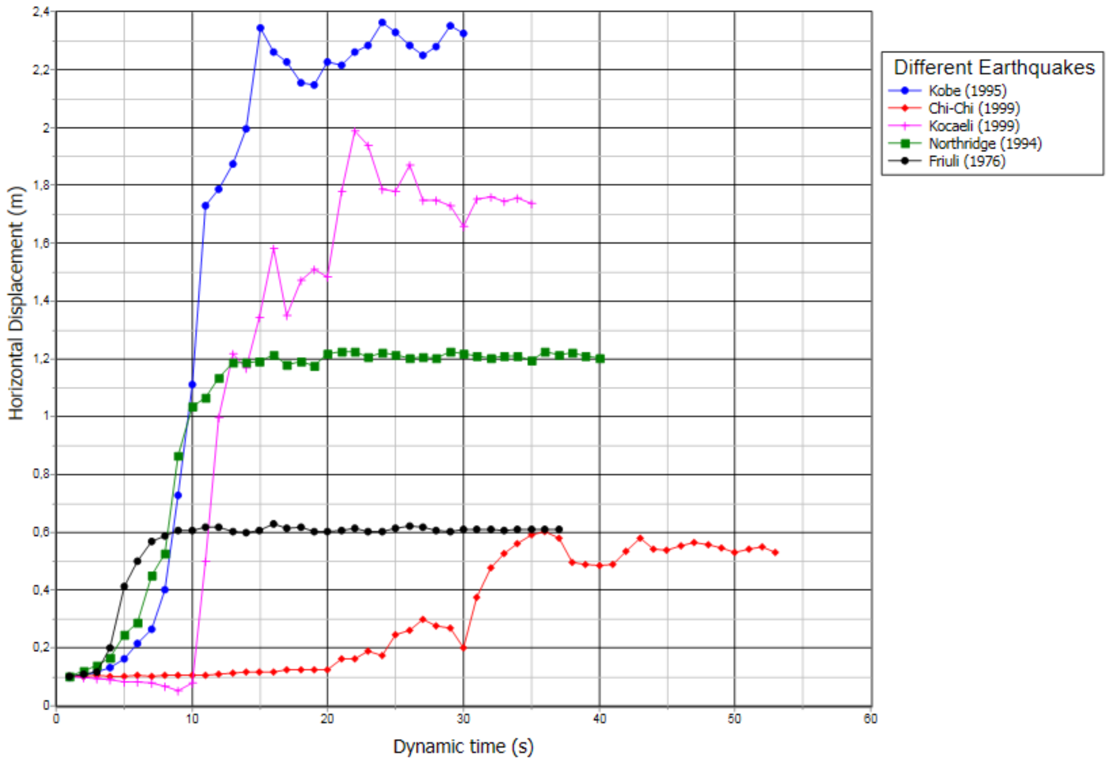

Figure 5.6 : Time-displacement graph in horizontal direction for the point of top of the caisson.

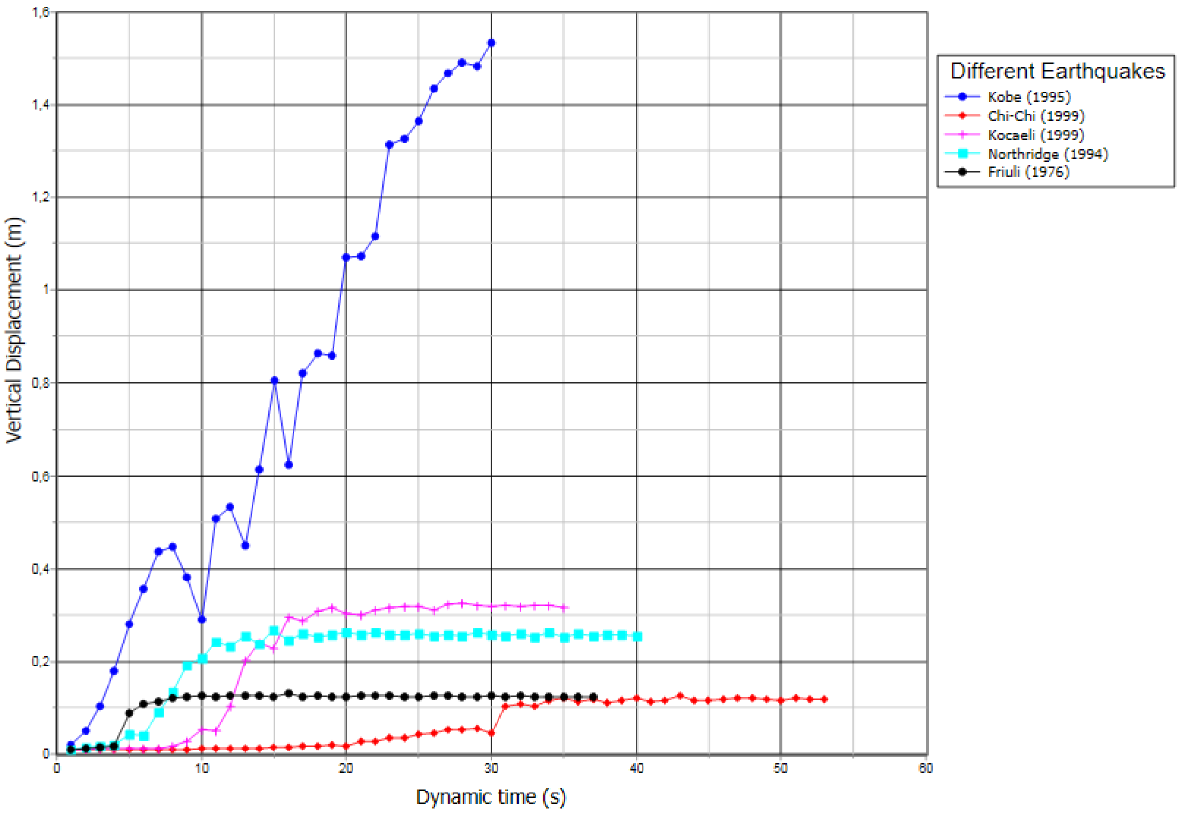

Figure 5.7 : Time-displacement graph in vertical direction for the point of top of the caisson.

Table 5.1 : Displacements at the top point of the caisson for different earthquakes.

Applied Earthquake	Displacement of caisson top (m)	
	ux	uy
Observed Displacement	2,48	1,20
Kobe (1995)	2,33	1,53
Kocaeli (1999)	1,74	0,32
Chi-Chi (1999)	0,53	0,12
Northridge (1994)	1,20	0,26
Friuli (1976)	0,61	0,13

5.1 Soil Densification

After the effect of different earthquakes is analyzed, effect of soil improvement to displacements is analyzed. Different layers are densified for different cases. Two new soil layers are defined as medium sand and dense sand. The relative density of medium sand is 50% and the relative density of dense sand is 70%. Material properties of two soils are given in Table 5.2.

Table 5.2 : Model parameters for medium sand and dense sand.

Material	Dense Sand	Medium Sand
D_r (%)	70	50
Material Model	HS Small	HS Small
γ_{unsat} (kN/m^3)	18	17
γ_{sat} (kN/m^3)	20	20
φ (°)	37	34
ψ (°)	7	4
c (Kpa)	-	-
$\boldsymbol{E_{50}^{ref}}$ (kPa)	42000	30000
$\boldsymbol{E_{oed}^{ref}}$ (kPa)	42000	30000
$\boldsymbol{E_{ur}^{ref}}$ (kPa)	126000	90000
m	0,5	0,5
ν_{ur}	0,2	0,2
$\boldsymbol{G_0^{ref}}$ (kPa)	107600	94000
$\gamma_{0.7}$	0,00013	0,00015

In the first case, backfill soil is densified. The relative density of backfill is increased from 35% to 50%. In the second case, foundation sand is densified. The relative density of foundation sand is improved from 40% to 70%. In the third case, foundation soil is improved partially (D_r=%70) below toe of caisson. Improved part of foundation is given in Figure 5.8. Horizontal and vertical displacements of top of the caisson are given in Table 5.3. Displacement time-graph of caisson in horizontal direction is given in Figure 5.9.

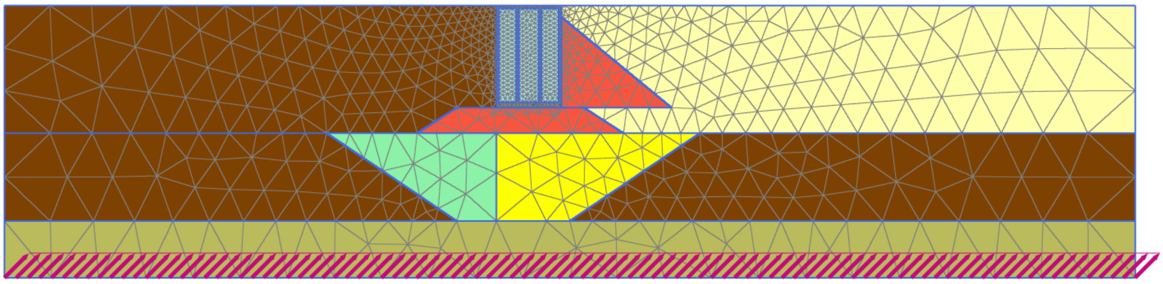

Figure 5.8 : Improved part of foundation soil.

Table 5.3 : Horizontal and vertical displacements at the top of the caisson for different improvement cases.

Densification	Displacement of caisson top (m)	
	u_x	u_y
No densification	2,33	1,53
Backfill densified	1,00	1,28
Foundation densified	1,81	1,47
Foundation densified partially	2,05	1,44

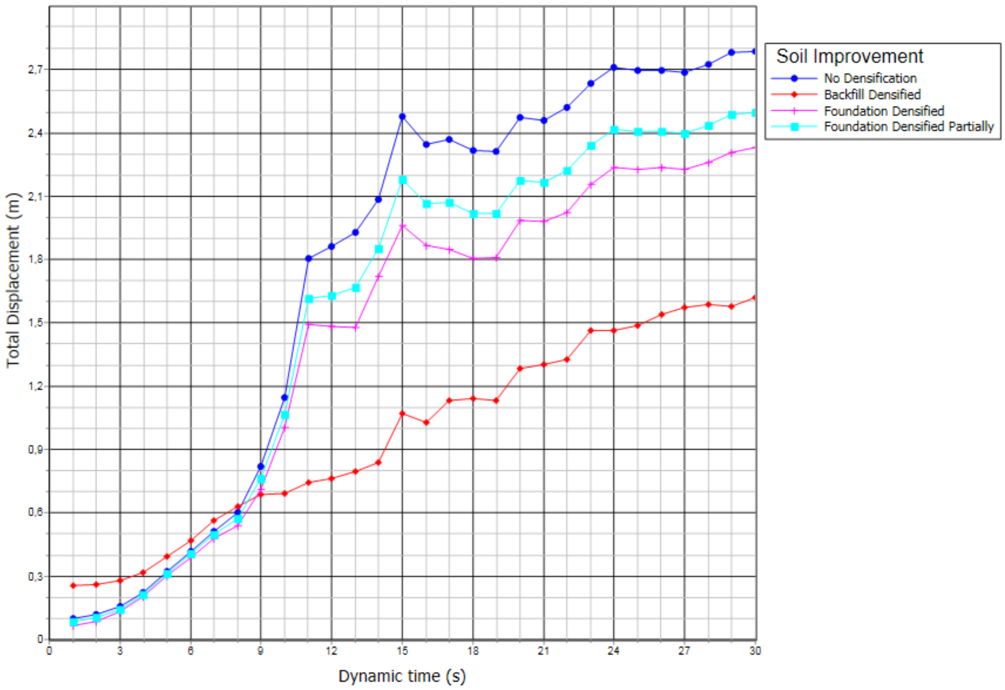

Figure 5.9 : Time-displacement graph in horizontal direction for the point of top of the caisson for different improvement cases.

5.2 Effect of B/H Ratio

Also effect of B/H ratio to displacement is analyzed. Three different B/H ratios are used in analysis. The B/H ratio of quay wall in Rokko Island is 0.66. B/H ratios 0.8 and 1.0 are also analyzed. Horizontal and vertical displacements of top of the caisson are given in Table 5.4. Total displacement time-graph of caisson in is given in Figure 5.10.

Table 5.4 : Horizontal and vertical displacements at the top point of the caisson for different B/H ratios.

B/H ratio	Displacement of caisson top (m)	
	u_x	u_y
0,66	2,33	1,53
0,80	2,35	1,58
1,00	2,27	1,52

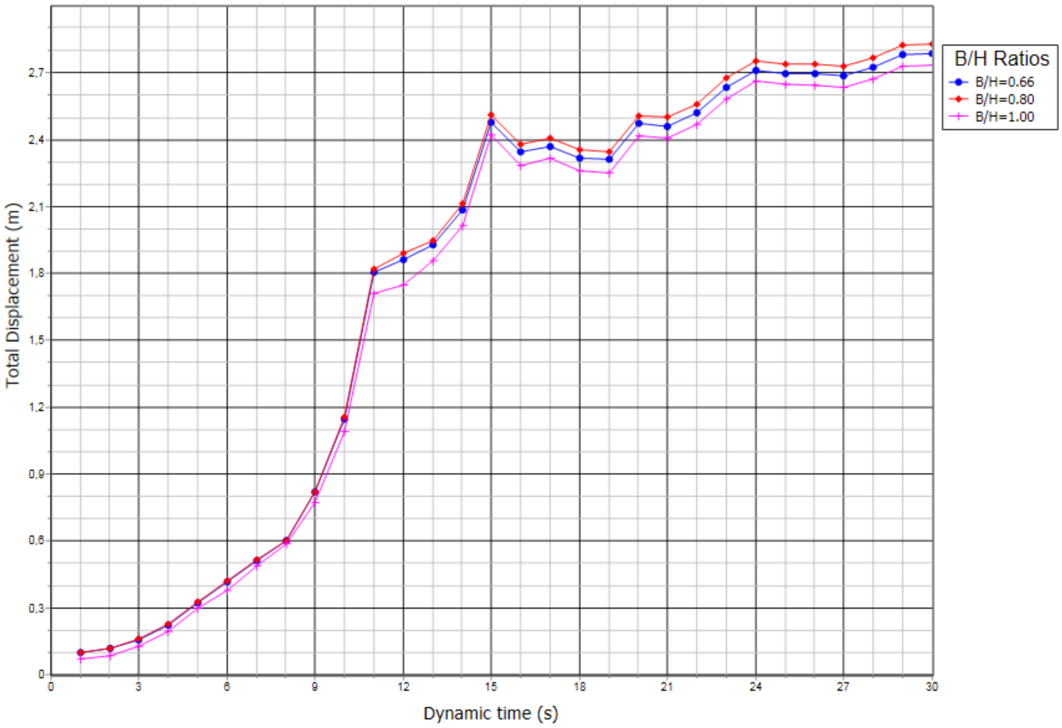

Figure 5.10 : Time-displacement graph in horizontal direction for the point of top of the caisson for different B/H ratios.

5.3 Kushiro Port

Also Kushiro Port is analyzed. On 15 January 1993, Kushiro-oki earthquake hit 13 km off the coast of Kushiro, Hokkaido. The magnitude of earthquake was 7.8 and hypo central depth was 107 km. Kushiro City was shaken with 0.47g peak horizontal acceleration (Hamada, 2014).

Kushiro Port is in southeastern part of Hokkaido Island. Quay walls were constructed on relatively dense seabed deposits from the sand dune and backfilled with dredged sand. The seismic coefficient of quay walls is 0.20. The analyzed quay wall is located at Pier No.2 in West Port. The caisson quay wall moved towards sea 26 cm and settled about 40 cm. The cross-section of wall is given in Figure 5.11 (Sugano, 2009).

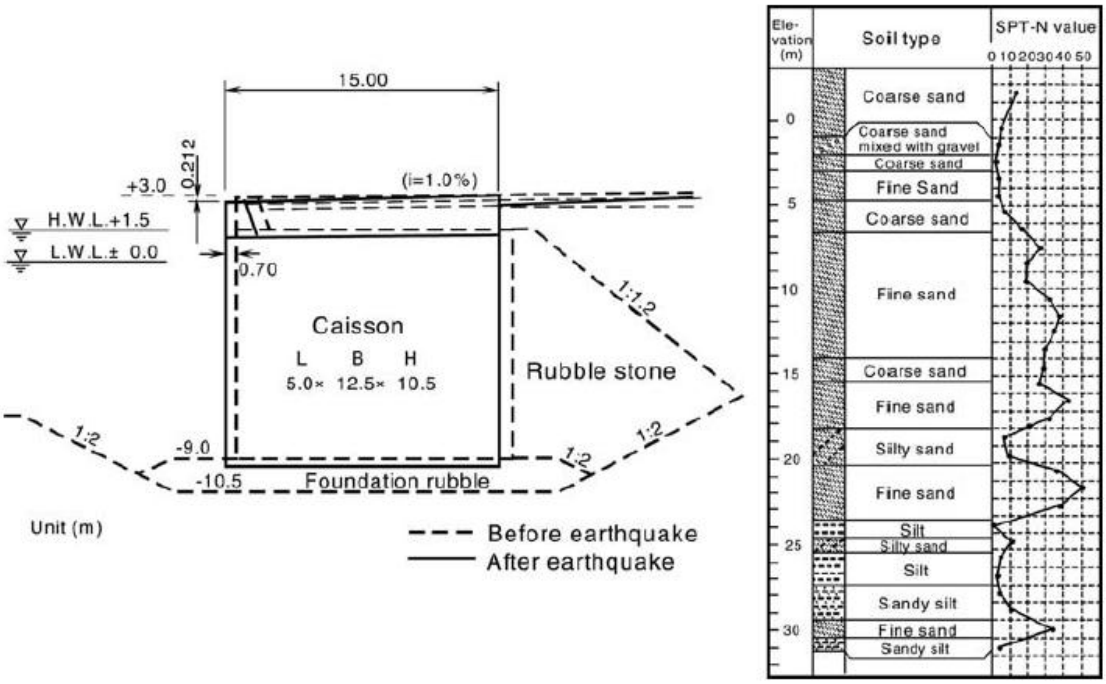

Figure 5.11 : Cross-section of quay wall at Kushiro Port and SPT values (Sugano, 2009).

According to Standard Penetration Test data, soil model is established. Relative density of coarse sand layer is 35% and SPT values of this layer change between 2 and 12, averagely 7. The depth of this layer is 7 m. Below coarse sand, there is first fine sand layer which defined as Fine Sand 1. Relative density of this fine sand is 50% and SPT values change between 20 and 42, averagely 30. The depth of Fine Sand 1 is 11.5 m. Below Fine Sand 1 layer, there is silty sand layer. Silty sand layer is loose and its relative density is 30%. Average SPT value is 9. Silty sand layer is 2 m thick. Beneath silty sand, there is another fine sand layer and it is defined as Fine Sand 2. Fine Sand 2 layer has relative density of 60% and average SPT value of this layer is 41. Depth of Fine Sand 2 layer is 3.5 m. Below Fine Sand 2 layer, there is silt layer. Average SPT value of silt is 5 and layer thickness is 3 m. Beneath silt, there is sandy silt layer. Average SPT value of silt is 11 and depth of layer is 5 m. Cross-section of quay wall and soil model is given Figure 5.12.

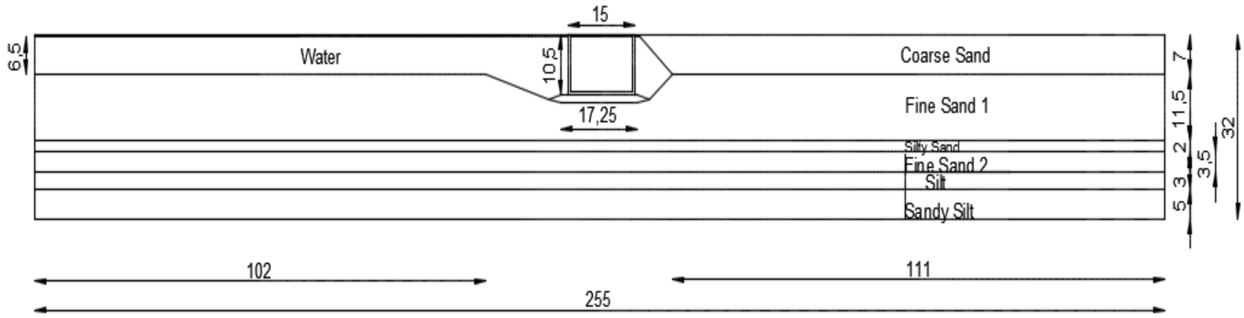

Figure 5.12 : Cross-section of quay wall and soil model.

SPT values are corrected and shear wave velocities are calculated using correlation formulas. Shear wave velocities are used to determine Rayleigh parameters for material damping and to calculate maximum element size for dynamic analysis. Rayleigh parameters for layers are given in Table 5.5 and maximum element sizes for every layer are given in Table 5.6. Finite element mesh is checked for maximum element sizes for every layer. Finite element mesh is given in Figure 5.13.

Table 5.5 : Rayleigh parameters for soil layers.

Layer	Coarse Sand	Fine Sand 1	Silty Sand	Fine Sand 2	Silt	Sandy Silt
Thickness (m)	7	11,5	2	3,5	3	5
Vs (m/s)	164	267	172	297	147	191
Period (s)	0,17	0,17	0,05	0,05	0,08	0,10
Frequency (f_1)	5,86	5,80	21,50	21,21	12,25	9,55
Frequency (f_2)	10	10	10	10	10	10
Angular frequency (ω_1)	36,80	36,47	135,09	133,29	76,97	60,00
Angular frequency (ω_2)	62,83	62,83	62,83	62,83	62,83	62,83
Rayleigh α	2,32	2,31	4,29	4,27	3,46	3,07
Rayleigh β	0,0010	0,0010	0,0005	0,0005	0,0007	0,0008

Table 5.6 : Maximum element sizes for soil layers.

Layer	Thickness (m)	Vs (m/s)	Period (s)	Frequency (s^{-1})	Wave length (m)	Maximum element size (m)
Coarse Sand	7	164	0,171	5,86	28	3,5
Fine Sand 1	11,5	267	0,172	5,81	46	5,75
Silty Sand	2	172	0,047	21,45	8	1
Fine Sand 2	3,5	297	0,047	21,18	14	1,75
Silt	3	147	0,082	12,22	12	1,5
Sandy Silt	5	191	0,105	9,54	20	2,5

Similar to Rokko Island model, stiffness parameters are derived using shear wave velocities. Strength parameters are calculated SPT correlation formulas. All parameters used in analyses are given Table 5.7. Rubble and concrete parameters are taken same with Kobe case which is given in Table 4.7 before.

Table 5.7 : Calculated parameters for soil layers.

Layer	Coarse Sand	Fine Sand 1	Silty Sand	Fine Sand 2	Silt	Sandy Silt
$N_{average}$	7	30	8	41	5	11
V_s (m/s)	164	267	172	297	147	191
D_r (%)	35	50	30	60	-	-
Material Model	HS Small	HS Small	HS Small	HS Small	HS Small	HS Small
γ_{unsat} (kN/m^3)	18	17	17	17	18	18
γ_{sat} (kN/m^3)	20	19	19	19	20	20
φ (°)	32	34	31	35	-	-
ψ (°)	2	4	1	5	-	-
c (Kpa)	-	-	-	-	25	50
E_{50}^{ref} (kPa)	11500	26500	11000	32500	11500	19500
E_{oed}^{ref} (kPa)	11500	26500	11000	32500	11500	19500
E_{ur}^{ref} (kPa)	34500	79500	33000	97500	34500	58500
m	0,5	0,5	0,5	0,5	0,9	0,9
ν_{ur}	0,2	0,2	0,2	0,2	0,2	0,2
G_0^{ref} (kPa)	22000	60000	21000	62750	17550	30000
$\gamma_{0.7}$	0,00017	0,00015	0,00017	0,00014	0,00017	0,00017

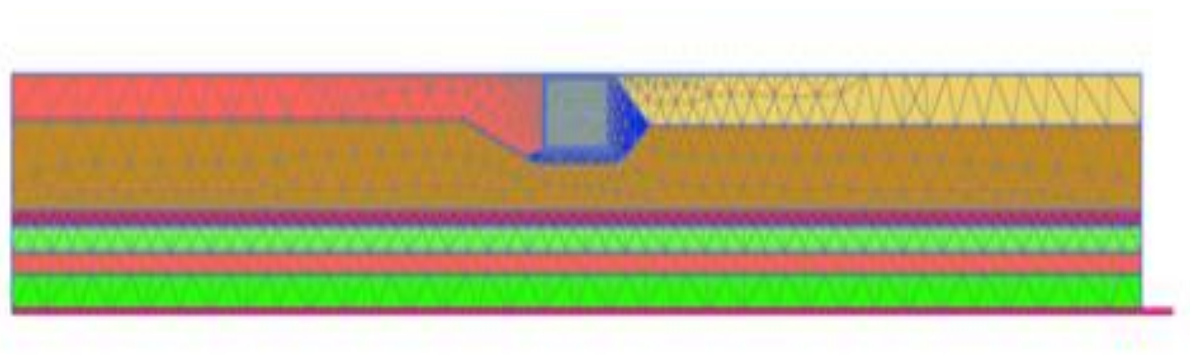

Figure 5.13 : Finite element mesh of Kushiro Port

In analyses of Kushiro Port, the digital data of 1993 Kushiro-oki earthquake can not be retrieved. Friuli (1976), Northridge (1994), Kobe (1995) and Chi-Chi (1999) record which their accelerograms used also Rokko Island case, are used as dynamic multipliers. After all inputs are defined, analyses are performed. Plot of total displacements for Northridge record is given in Figure 5.14. Displacements for three earthquakes are summarized in Table 5.8. Time-displacement graph for the top point of the caisson in horizontal direction and vertical direction are given in Figure 5.15 and 5.16, respectively.

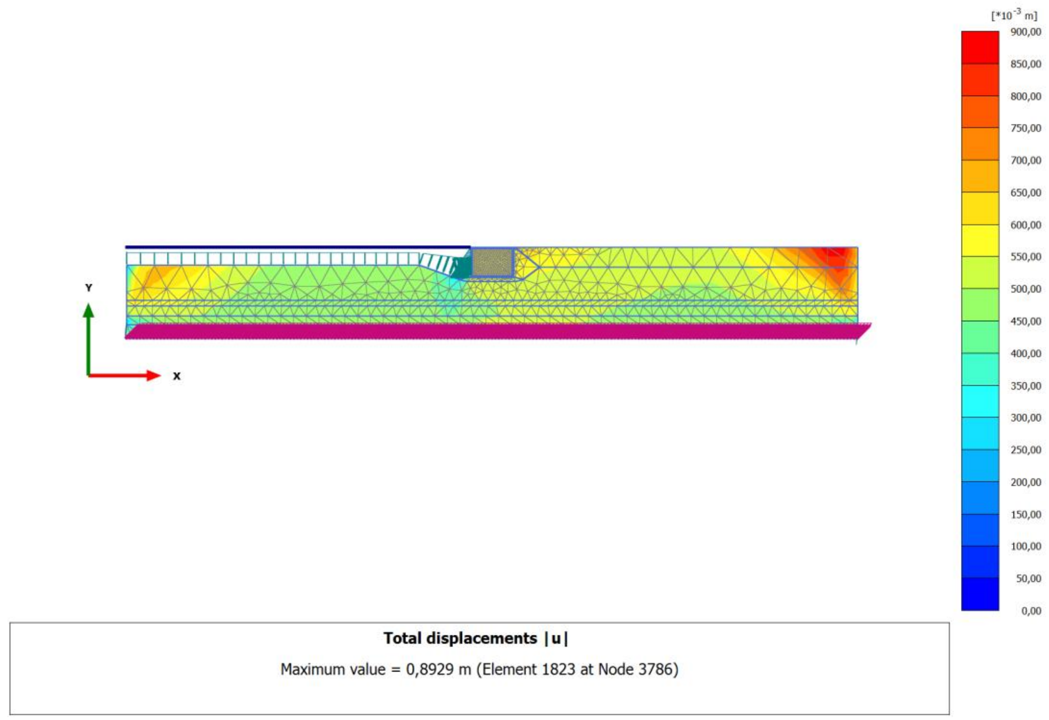

Figure 5.14 : Plot of total displacements for Kobe earthquake (shadings).

Table 5.8 : Displacements at the top point of the caisson for different earthquakes.

Applied Earthquake	Displacement of caisson top (m)	
	u_x	u_y
Observed Displacement	0,26	0,40
Kobe (1995)	0,22	0,51
Chi-Chi (1999)	0,11	0,008
Northridge (1994)	0,14	0,012
Friuli (1976)	0,08	0,001

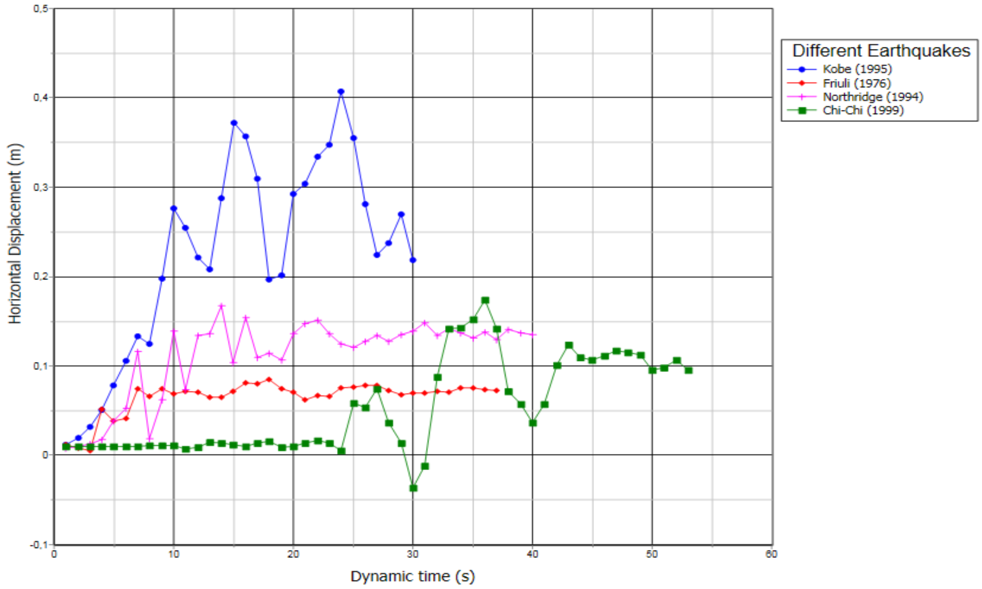

Figure 5.15 : Time-displacement graph in horizontal direction for the point of top of the caisson.

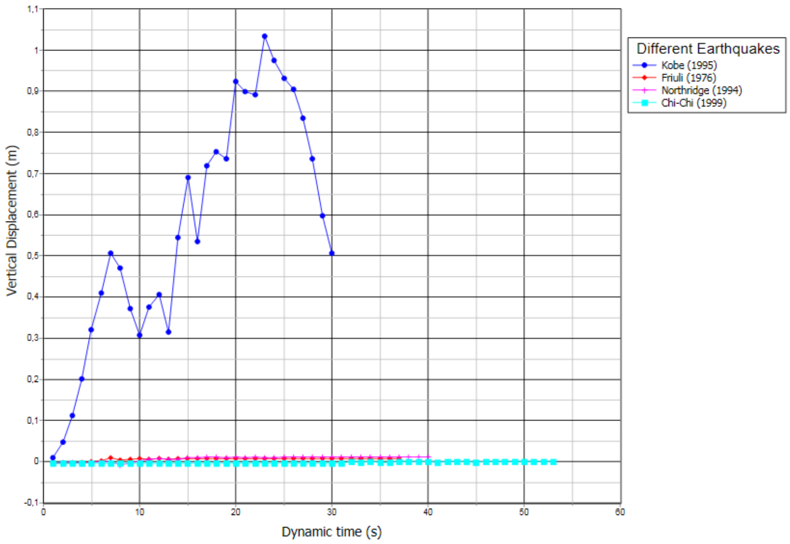

Figure 5.16 : Time-displacement graph in vertical direction for the point of top of the caisson.

5.4 Displacement Calculations with Analytical and Empirical Methods

Lateral displacements of caisson quay wall during 1995 Kobe earthquake also calculated with analytical and empirical methods which explained in Chapter 3. Displacements in horizontal direction also calculated with Richards-Elms (1977), Whitman-Liao (1979), Franklin-Chang (1985), Iai et al. (1997), Iai et al. (1999), LSI, Hamada (1994), Multi Linear Regression (MLR) and EPOLLS method. Results of all methods are given in Figure 5.17.

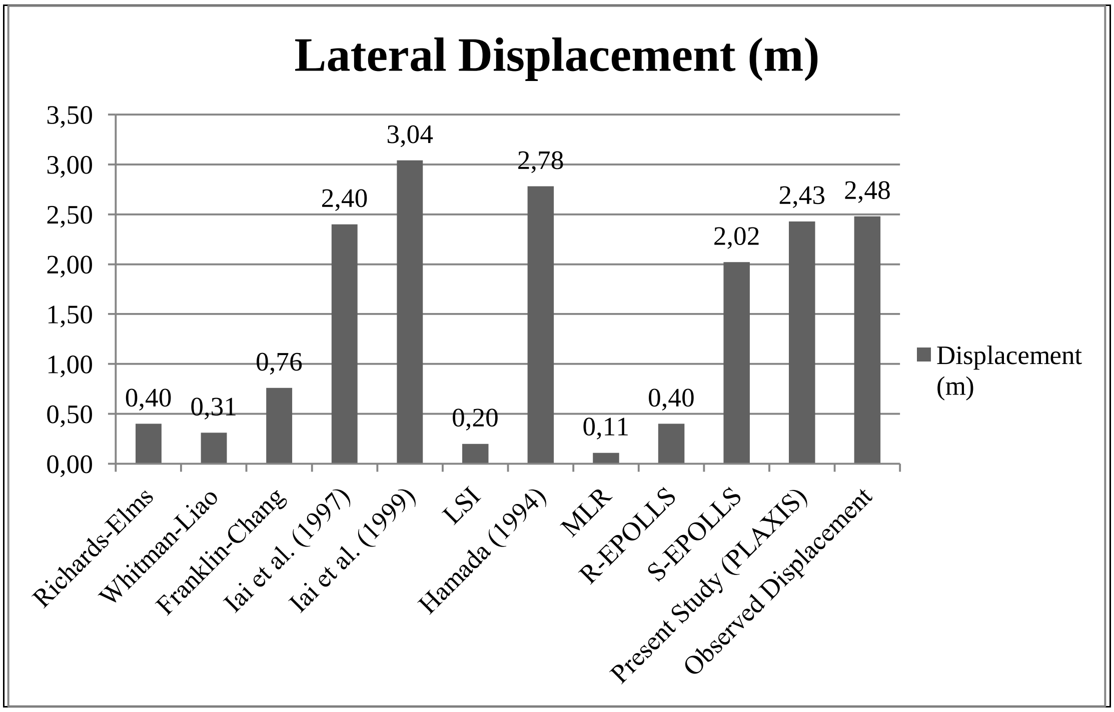

Figure 5.17 : Comparison of lateral displacements using all methods during 1995 Kobe earthquake.

Settlement below caisson during 1995 Kobe Earthquake is also calculated with empirical methods. Tokimatsu and Seed (1987), Ishihara and Yoshimine (1992) methods are used in settlement calculations. Results of calculations are given in Figure 5.18.

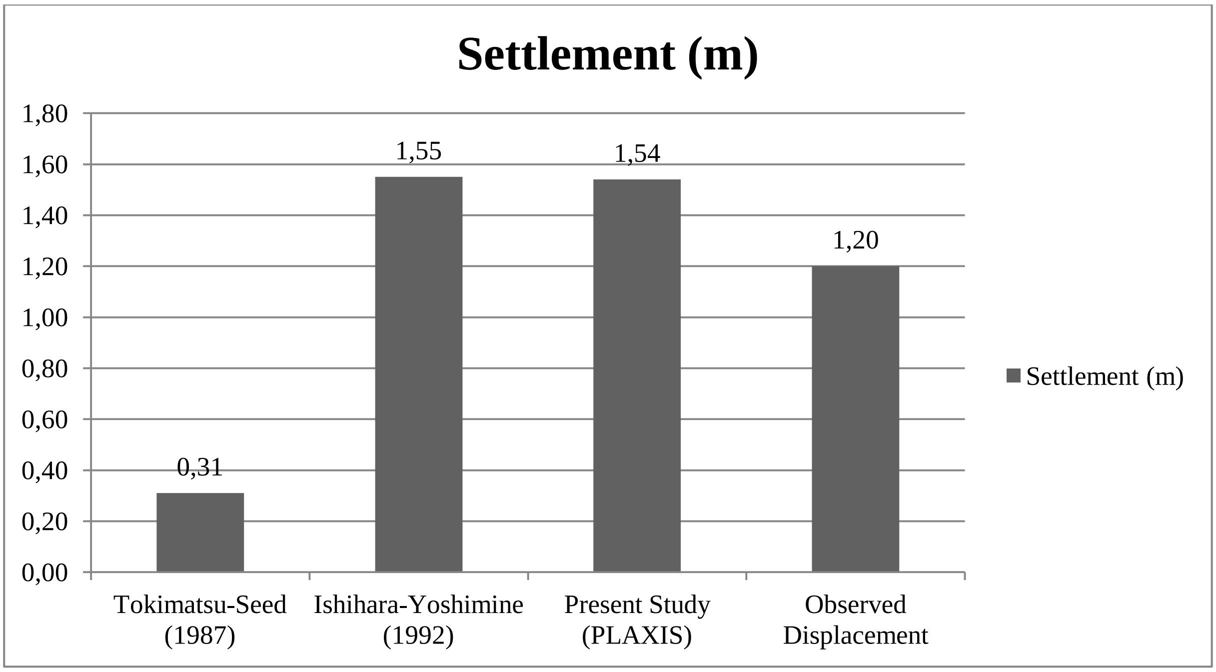

Figure 5.18 : Comparison of settlements using all methods during 1995 Kobe earthquake.

5.5 Conclusions

A quay wall which damaged in 1995 Kobe earthquake at Rokko Island is modeled in PLAXIS finite element programme. The behavior of wall during different earthquakes analyzed. Lateral displacements and settlements of quay wall using PLAXIS agrees with observed displacements. Also, different earthquakes such as Kocaeli (1999), Chi-Chi (1999), Northridge (1994) and Friuli (1976) applied to modeled wall and displacements are determined for every earthquake. Horizontal and vertical displacements of quay wall under different earthquakes analyzed.

Moreover, effect of soil improvement to displacements analyzed. Different layers are densified for different improvement cases. Two new soil layers are defined as medium sand and dense sand to model soil improvement. In the first case, backfill soil is densified. The relative density of backfill is increased from 35% to 50%. In the second case, foundation sand is densified. The relative density of foundation sand is improved from 40% to 70%. In the third case, foundation soil is improved partially below toe of caisson. Horizontal and vertical displacements of top of the caisson are reduced as a result of densification.

In addition, effect of different B/H ratios is analyzed. Three different B/H ratios, 0.66, 0.80 and 1.00 are analyzed. Horizontal and vertical displacement of caisson is calculated with the PLAXIS.

Furthermore, dynamic analysis of a damaged quay wall during 1993 Kushiro-oki earthquake in Kushiro Port is performed. Three different earthquake records are applied as dynamic multipliers, including Chi-Chi (1999), Northridge (1994) and Friuli (1976) earthquakes.

Also, lateral displacements of caisson quay wall during 1995 Kobe earthquake calculated with analytical and empirical methods which explained in Chapter 3. Displacements in horizontal direction calculated with Richards-Elms (1977), Whitman-Liao (1979), Franklin-Chang (1985), Iai et al. (1997), Iai et al. (1999), LSI, Hamada (1994), Multi Linear Regression (MLR) and EPOLLS method.

Lastly, settlements beneath caisson during 1995 Kobe Earthquake are also calculated with empirical methods. Tokimatsu and Seed (1987), Ishihara and Yoshimine (1992) methods are used in settlement calculations.

6. CONCLUSIONS AND RECOMMENDATIONS

Liquefaction is strength loss of a soil during undrained loading due to rapid excess pore pressure generation. Pore water pressure generation decreases the effective stress of soil. As a result of effective stress decrease, the strength and rigidity of soil decrease. Due to liquefaction, lateral spreading, flow failures, ground subsidence may be seen and airports, roads, railways, buried pipelines and bridges may be damaged.

Material characteristics determine liquefaction behavior of soils. Loose soils tend to flow liquefaction, if geometrical conditions are suitable. Also cyclic mobility or cyclic liquefaction may be observed. Dense soils may not liquefy during earthquake loading, however, if loading conditions are sufficient, they may soften due to excess pore pressure.

Liquefaction induced lateral spreading is the main cause of catastrophic damages in disastrous earthquakes. For that reason, mechanism of liquefaction and lateral spreading should be understood clearly and their impacts on engineering structures analyzed carefully during and after earthquake.

Lateral spreading causes large deformations on slopes and retaining structures. Several researchers have developed different methods to predict liquefaction induced lateral spreading, seismic quay wall displacements and settlements. These methods can be used to estimate potential damages on existing structures and can also be used on design process.

In present study, a quay wall which damaged severely in 1995 Kobe earthquake at Rokko Island is modeled using PLAXIS finite element programme. The behavior of wall during 1995 Kobe Earthquake is analyzed. Lateral displacements and settlements of quay wall calculated using PLAXIS agrees with observed displacements. Also, different earthquakes records such as Kocaeli (1999), Chi-Chi (1999), Northridge (1994) and Friuli (1976) applied to modeled wall and displacements are determined for every earthquake. Horizontal and vertical displacements of quay wall under different earthquakes are analyzed.

Moreover, effect of soil densification to displacements is analyzed. Different layers are densified for different improvement cases. Two new soil layers are defined as medium sand and dense sand to model soil improvement. In the first case, backfill soil is densified. The relative density of backfill is increased from 35% to 50%. In the second case, foundation sand is densified. The relative density of foundation sand is improved from 40% to 70%. In the third case, foundation soil is improved partially below toe of caisson. Horizontal and vertical displacements of top of the caisson are reduced as a result of densification. A densification of backfill reduces total displacements by 40%, densification of foundation soil reduces total displacements by 15%, and partial densification of foundation soil reduces total displacements by 10%.

In addition, effect of different B/H ratios is analyzed. Three different B/H ratios, 0.66, 0.80 and 1.00 are analyzed. Horizontal and vertical displacement of caisson is calculated with PLAXIS programme. It is seen that effect of B/H ratio is not an important parameter in liquefied cases.

Furthermore, dynamic analysis of a damaged quay wall during 1993 Kushiro-oki earthquake in Kushiro Port is performed. Three different earthquake records are applied as dynamic multipliers, including Chi-Chi (1999), Northridge (1994) and Friuli (1976) earthquakes. Horizontal and vertical displacements of caisson quay wall are calculated. According to results, displacements of wall are lesser than Rokko Island as layers are denser in Kushiro Port compared to Rokko Island.

Also, lateral displacements of caisson quay wall during 1995 Kobe earthquake calculated with analytical and empirical methods which are explained in Chapter 3. Displacements in horizontal direction calculated with Richards-Elms (1977), Whitman-Liao (1979), Franklin-Chang (1985), Iai et al. (1997), Iai et al. (1999), LSI, Hamada (1994), Multi Linear Regression (MLR) and EPOLLS method. Pseudo-static methods underestimate wall displacements as liquefaction behavior of soil during earthquake is ignored. LSI, MLR and R-EPOLLS also underestimate wall deformation. S-EPOLLS, Hamada (1994) and Iai et al. (1997) agree with wall displacements as liquefaction behavior of soil is considered. Iai et al. (1999) overestimates wall displacements.

Lastly, settlements beneath caisson during 1995 Kobe Earthquake are also calculated with empirical methods. Tokimatsu and Seed (1987), Ishihara and Yoshimine (1992) methods are used in settlement calculations. Tokimatsu and Seed method underestimates settlements due to liquefaction. Ishihara and Yoshimine (1992) method agrees with settlements.

In conclusion, Mononobe-Okabe method is not sufficient for quay wall design as it ignores liquefaction behavior. When seismic coefficients are reached, catastrophic wall damages occur. Local site effects should be evaluated and using field and laboratory test data, finite element analyses should be performed to understand wall behavior during earthquakes.

PLAXIS finite element program calculates lateral displacements accurately. However the program does not calculate vertical displacements accurately. In Rokko Island case, settlements are overestimated. In contrast to Rokko Island case, settlements are underestimated in Kushiro Port Case.

REFERENCES

Andrews, D. C. A., and Martin, G. R., (2000). Criteria for liquefaction of silty soils, *Proc., 12th World Conf. on Earthquake Engineering*, Upper Hutt, New Zealand, NZ Soc. for EQ Engrg., Paper No. 0312.

Atkinson, J. H. & Sallfors, G. (1991). Experimental determination of soil properties. *Proceedings of 10th European Conference of Soil Mechanics, Florence.*

Bartlett, S. F., and Youd, T. L., (1992a). Empirical prediction of lateral spread displacement, *Proc. 4th Japan-U.S. Workshop on Earthquake Resistant Design of Lifeline Facilities and Countermeasures for soil liquefaction*, Buffalo, NY, National Center for Earthquake Engineering Research Technical Report NCEER-92-0019, Eds. Hamada, M. and O'Rourke, T. D., August 12, 351-365.

Bartlett, S. F., and Youd, T. L., (1992b). Empirical analysis of horizontal ground displacement generated by liquefaction-induced lateral spreads, *National Center for Earthquake Engineering Research Technical Report NCEER-92-0021*, Buffalo, NY, August 17, 114-126.

Boulanger, R.W., and Idriss, I. M. (2004). Evaluating the potential for liquefaction or cyclic failure of silts and clays. *Report NO.UCD/CGM-04/01,*Center for Geotechnical Modeling, Department of Civil &Environmental Engineering University of California, Davis,California.

Bowles, J. E. (1988). Foundation Analysis and Design, 4th Edition, McGraw-Hill.

Brinkgreve, R. B. J. (2005). Selection of soil models and parameters for geotechnical engineering application. *Soil Constitutive Models*: pp. 69-98.

Brinkgreve, R. B. J. Engin, E., Engin, H.K. (2007). Validation of empirical formulas to derive model parameters for sands.

Celep, Z., Erken, A., Taşkın, B., İlki, A., (2011). Failures of masonry and concrete buildings during the March 8, 2010 Kovancılar and Palu (Elazığ) earthquakes in Turkey. *Engineering Failure Analysis, Elsevier.*

Chen, C. & Hwang, G. (2000). Preliminary Analysis for Quaywall movement in Taichung Harbour During the Septmeber 21, 1999, Chi-Chi Earthquake. *Earthquake Engineering and Engineering Seismology, Vol. 2, No. 1, 1 March 2000.*

Darendeli, M. (2001). Development of a new family of normalized modulus reduction and material damping curves. Ph.D. Thesis, Dept. of Civil Eng., Univ. of Texas, Austin.

Day, R. W. (2012). Geotechnical Earthquake Engineering Handbook, New York, The McGraw-Hill.

El Hosri, M. S., Biarez, H., Hicher, P. Y. (1984). Liquefaction characteristics of silty clay, *Proc., 8th World Conf. on Earthquake Engrg.*, Prentice-Hall, Englewood Cliffs, N.J., 3, 277–284.

Erken, A., Kaya, Z., Erdem, A. (2004a). Ground deformations in Adapazarı during 1999 Kocaeli earthquake. *13th World Conference on Earthquake Engineering Vancouver, B.C., Canada.*

Erken, A., Özay, R., Kaya, Z., Ülker, M. B. C., Elibol, B., (2004b). Depremler sırasında zeminlerin sıvılaşması ve taşıma gücü kayıpları. Türkiye Mühendislik Haberleri Sayı-431, 2004/3.

Franklin, A. G. and Chang F. K. (1977). Permanent displacement o f earth embankments by Newmark sliding Block Analysis. *Rep. 5, Misc. Paper S-71-17*, U.S. Army Corps of Engineers Waterway Experiment Station, Vicksburg, Miss.

Hamada, M., (2014). Engineering for earthquake disaster mitigation. Springer Tokyo.

Hamada, M., Sato, H., Kawakami, T., (1994). A consideration of the mechanism for liquefaction-related large ground displacement. *In: Proceedings from the Fifth US-Japan Workshop on Earthquake Resistant Design of Lifeline Facilities and Countermeasures against Soil Liquefaction*,Salt Lake City, USA, technical report NCEER-94-0026, 217-232.

Hatanaka, M. & Uchida, A. (1996). Empirical correlation between penetration resistance and internal friction angle of sandy soils. *Soils and Foundations, Vol. 36, No. 4, 1-9 December, Japanese Geotechnical Society.*

Hayashi, S., Kubo, K., Nakase, A. (1966). Damage to Harbour Structures by the Niigata Earthquake. Soils and foundations 6(1), 89-112, 1966-01.

Huang, C. C., (2009). Failures of soil structures during the 1999 Taiwan Chi-Chi earthquake. *Earthquake Geotechnical Case Histories For Performance Based Design.*

Housner, G. W., (1985). Liquefaction of soils during earthquakes, *Committee on Earthquake Engineering Commission on Engineering and Technical Systems National Research Council*, National Academy Pres, Washington, USA.

Iai, S., Ichii, K., Sato, H., Liu, H. (1999). Residual displacement of gravity quay walls - parameter study through effective stress analysis. *Proceedings of Seventh U.S.-Japan Workshop on Earthquake Resistant Design of Lifeline Facilities and Countermeasures Against Soil Liquefaction, MCEER*

Iai, S., Sugano, T., (2000). Shake table testing on seismic performance of gravity quay walls. *12th World Conference on Earthquake Engineering; Auckland, New Zealand.*

Inagaki, H., Iai, S., Sugano, T., Yamazaki, H., Inatomi, T. (1996). Performance of caisson type quay walls at Kobe Port. *Soils and Foundations January 1996, Japanese Geotechnical Society.*

Ichii, K., Iai, S., Sato, Y., Liu, H., (2002). Seismic performance evaluation charts for gravity type quay walls. *Structural Eng./Earthquake Eng., JSCE, Vol. 19.*

Idriss, I. M., Boulanger, R. W., (2007). SPT- and CPT-based relationships for the residual shear strength of liquefied soils. *Geotechnical, Geological and Earthquake Engineering, Volume 6 Springer.*

Inagaki, H., Iai, S., Sugano, T., Yamazaki, H., Inatomi, T. (1996). Performance of caisson type quay walls at Kobe Port. *Soils and Foundations January 1996, Japanese Geotechnical Society.*

Ishihara, K. and Yoshimine, M., (1992). Evaluation of settlements in sand deposits following liquefaction during earthquake, *Soils and Foundations*, 32, 173-188.

Ishihara, K. (1996). *Soil Behaviour in Earthquake Geotechnics*, 1rst ed., Oxford, Claredon Press.

Iwasaki, Y., Tai, M., . (1996). Strong motion records at Kobe Port Island. *Soils and Foundations January 1996, Japanese Geotechnical Society.*

Japanese Society of Civil Engineers. (1995). The Great Hanshin Earthquake: pp. 11, 270-272.

Jennings, P.C., Housner, G.W., (1971). The San Fernando, California, Earthquake February 9, 1971.

Kim, S., Jang, I., Chung, C., Kim, M., (2005). Evaluation of seismic displacements of quay walls. *Soil Dynamics and Earthquake Engineering.*

Kohama, E., Miura, K., Yoshida, N., Ohtsuka, N., Kurita, S., (1998). Instability of gravity type quay wall induced by liquefaction of backfill during earthquake. *Soils and Foundations December 1998, Japanese Geotechnical Society.*

Kuhlmeyer, R. L., Lysmer,J., (1973). Finite element method accuracy for wave propagations problems. *ASCE Journal Soil Mechanics and Foundation Engineering Div.1973;99(5):421–7.*

Kramer, S.L., (1996). Geotechnical earthquake engineering, Prentice Hall, Upper Saddle River, NJ.

Mayne, P. W., (2007). Cone Penetration Testing State-of-Practice. NCHRP Project 20-05, Topic 37-14.

Newmark, N. M., (1965). Effects of earthquakes on dams and embankments, Fifth Rankine Lecture, *Geotechnique*, 15(2), 139-159.

New York Transportation Department (2015). Geotechnical Design Procedure: Liquefaction Potential of Cohesionless Soils. *State of New York, Geotechnical Engineering Bureau.*

PIANC, International Navigation Association, (2001). Seismic Design Guidelines for Port Structures.

Pitilakis, K. & Moutsakis, A. (1989). Seismic Analysis and Behaviour of Gravity Retaining Walls – The Case of Kalamata Harbour Quay Wall. *Soils and Foundations, Vol. 29, No. 1, 1-17 March, Japanese Geotechnical Society.*

PLAXIS. (2012). Plaxis Material Models Manual. Plaxis bv P.O. Box 572, 2600 AN DELFT, Netherlands.

Richards R., and Elms D. G., (1979). Seismic behaviour of gravity retaining walls. *Proc. ASCE, J. Geotech. Engng Div.*

Rauch, A. F. (1997) EPOLLS: An empirical method for predicting surface displacements due to liquefaction-induced lateral spreading in earthquakes, *PhD Thesis*, Virginia Polytechnic Institute, Blacksburg, Virginia.

Robertson, P. K., List, B. R., Hofmann, B. A., (1994). CANLEX (Canadian Liquefaction Experiment):A one year update", *Proceedings from theFifth U.S.-Japan Workshop on Earthquake Resistant Design of Lifeline Facilities and Countermeasures Against Soil Liquefaction*, State University of Newyork at Buffalo, Eds. O'Rourke, T. D., Hamada, M., Technical Report NCEER-94-0026, 353-366.

Sato, M., Watanabe, H., Takeda, T., Shimada, M., (2000). Simplified method to evaluate caisson type quay wall movement. *12th World Conference on Earthquake Engineering; Auckland, New Zealand.*

Schanz, T. & Vermeer, P. A., (1998). On the stiffness of sands. Pre-failure deformation behaviour of geomaterials.

Seed, H. B., Idriss, I. M. and Arango, I., (1983). Evaluation of liquefaction potential using field performance data, *Journal of Geotechnical Engineering,* 109(GT3), 458-482.

Seed, R. B., Cetin, K. O., Moss, R. E. S., Kammerer, A. M., Wu, Pestana, J. M.,

Riemer, M. F., Sancio, R., B., Bray, J. D., Kayen, R. E. and Faris, A.,(2003). Recent advances in soıl liquefaction engineering: A unıfied and consıstent framework, *126th Annual ASCE Los Angeles Geotechnical Spring Seminar, Keynote Presentation*, H.M.S. Queen Mary, Long Beach, California, April 30.

Shibata, T., Oka, F., Ozawa, Y., (1996). Characteristics of ground deformation due to liquefaction. *Soils and Foundations January 1996, Japanese Geotechnical Society.*

Sugano, T., (2009). Quay wall displacements and deformation of reclaimed land during recent large earthquakes in Japan.

Terzaghi, K., Peck, R., (1967). Soil Mechanics in Engineering Practice, 2nd Edition. John Wiley, New York.

Tokimatsu, K., and Seed, H. B., (1987). Evaluation of settlements in sands due to earthquake shaking, Journal of Geotechnical Engineering, ASCE, 113, 861-878.

Tokimatsu, K., (2009). Case histories of pile foundation subjected to ground displacements in the 1995 Hyogoken-Nambu earthquake. *Earthquake Geotechnical Case Histories For Performance Based Design.*

Towhata, I., Ghalandarzadeh, A., Sundarraj, K. P., Vargas-Monge, W., (1996). Dynamic failures of subsoils observed in waterfront areas. *Soils and Foundations January 1996, Japanese Geotechnical Society.*

Towhata, I. (2008). Geotechnical Earthquake Engineering. *Springer-Verlag Berlin Heidelberg.*

Tsuchida, H., (1970). Prediction and countermeasure against liquefaction in sand deposits. *Proceedings of the Seminar of the Port and Harbour Research Institute, vol. 3, pp. 1–3, Ministry of Transport,* Yokosuka, Japan, 1970.

Wang, W. S., (1979). Some findings in soil liquefaction. *Water conservancy and hydroelectric power scientific research ınstitute,* Beijing, China.

Wang, L., Liu, H., Jiang, P. (2011). Validation on prediction method of seismic residual horizontal deformation of caisson quay wall in liquefied foundation by 1g-shaking table test. *Geotechnical Engineering Div. ASCE*, 216.

Whitman, R. V., and Liao, S. (1985). Seismic design of gravity retaining walls. *Proc., 8th World Conf. on Earthquake Engrg.*, San Francisco, Vol. III, 533–540.

Youd, T.L. (1973). Liquefaction, Flow and Associated Ground Failure. *Geolological Survey Circular,* United States Department of Interior.

Youd, T. L., (1984).Geologic Effects - Liquefaction and Associated Ground Failure, *Proceedings of the Geologic and Hydrologic Hazards Training Program, Open-File Report 84-760,* U.S. Geological Survey, Menlo Park, California.

Youd, T. L. and Perkins, D. M., (1987). Mapping of liquefaction severity index, *Journal of Geotechnical Engineering*, **113**, 1374-1392.

Youd, T.L., Idriss, I.M., Andrus, R.D., Arango, I., Castro, G., Christian, J.T., Dobry, R., Finn, W.D.L., Harder, L.F.,Hynes, M.E., Ishihara, K., Koester, J.P., Liao, S.S.C.,Marcuson, W.F., III, Martin, G.R., Mitchell, J.K., Moriwaki, Y., Power, M.S., Robertson, P.K., Seed, R.B., and Stokoe, K. H., II, (2001) Liquefaction resistance of soils: Summary report from the 1996 NCEER and 1998 NCEER/NSF workshops on evaluation of liquefaction resistance of soils, *Journal of* 311 *Geotechnical and Geoenvironmental Engineering, ASCE,* 127 (10), 817-833.

Youd, T. L., Hansen, C. M. and Bartlett, S. F., (2002). Revised multilinear regression equations for predicting of lateral spread displacement, *Journal of Geotechnical and Geoenvironmental Engineering, ASCE,* **128**, 1007-1017.

Yüksel, Y., Alpar, B., Yalçıner, A. C., Çevik, E., Ozguven, O., Çelikoğlu, Y. (2002). Effects of the eastern Marmara Earthquake on marine structures and coastal areas. *Water & Maritime Engineering, No. 156, June 2002.*

APPENDICES

APPENDIX A: Pore water pressures and effective pressures

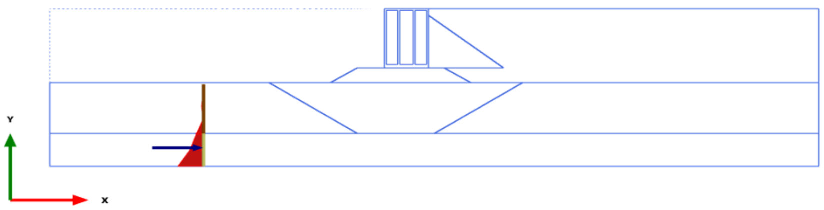

Excess pore pressures p_{excess} (scaled up 0,0500 times) (Pressure = negative)
Maximum value = -0,5478 kN/m^2
Minimum value = -133,6 kN/m^2
Equivalent force is -929,6 kN/m at position (40,000, -4,348) m

Figure A.1 : Excess pore pressure distribution under sea side at the end of the earthquake.

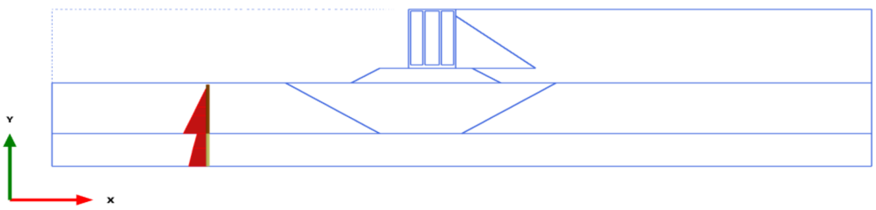

Principal effective stress σ'_3 (scaled up 0,0500 times)
Maximum value = 3,492 kN/m^2
Minimum value = -118,9 kN/m^2

Figure A.2 : Effective stress distribution under sea side at the end of the earthquake.

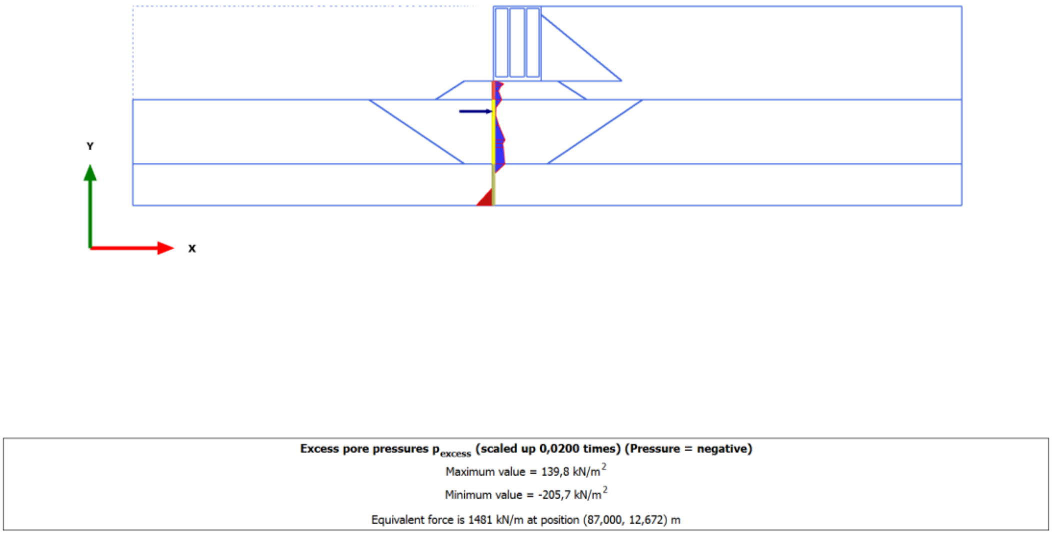

Figure A.3 : Excess pore pressure distribution below quay wall at the end of the earthquake.

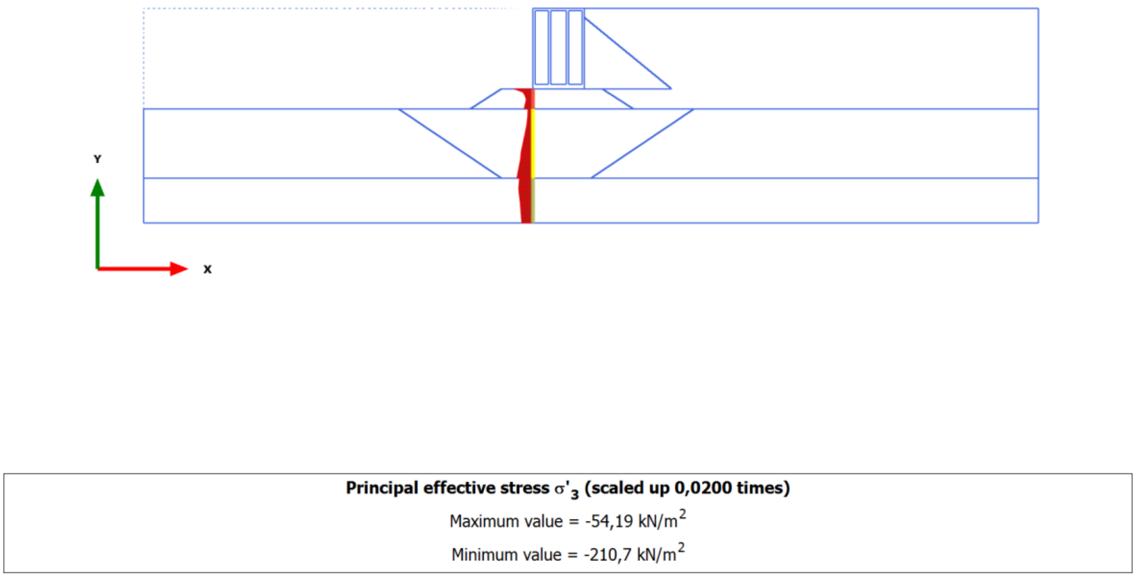

Figure A.4 : Effective stress distribution below quay wall at the end of the earthquake.

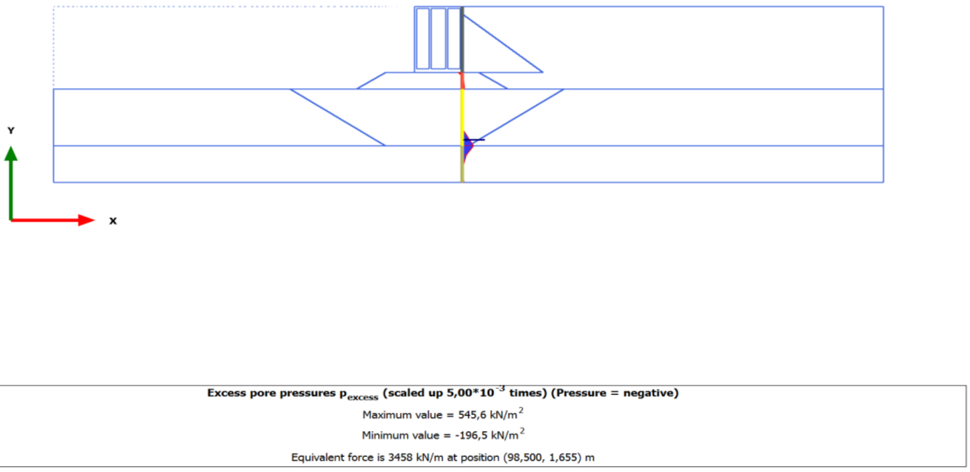

Figure A.5 : Excess pore pressure distribution below quay wall at the end of the earthquake.

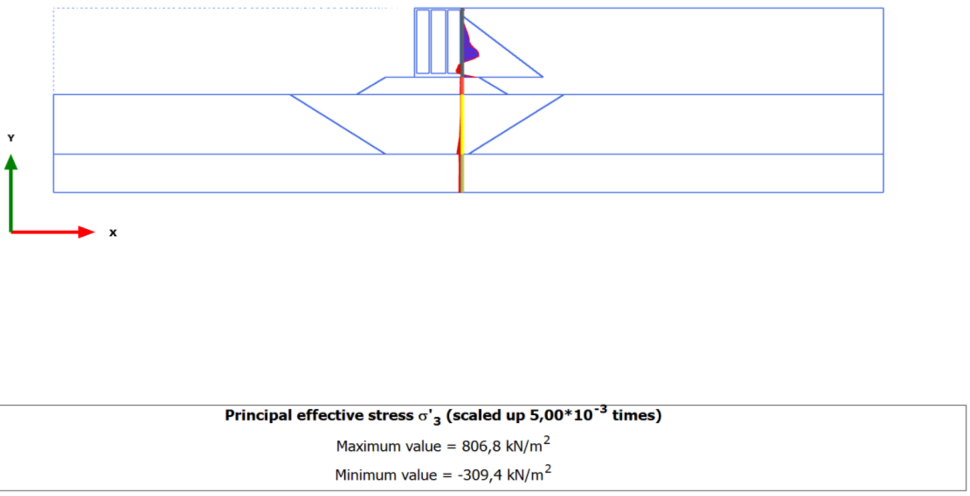

Figure A.6 : Effective stress distribution below quay wall at the end of the earthquake.

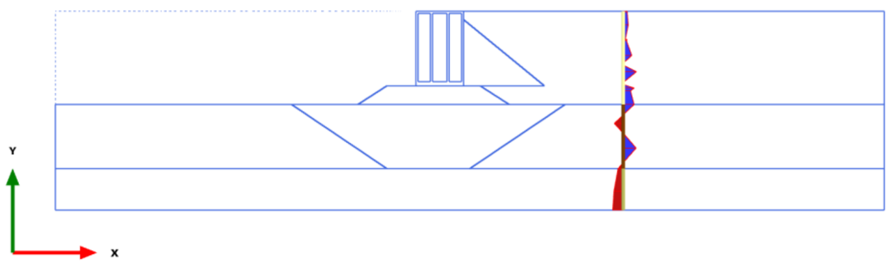

Excess pore pressures p_{excess} (scaled up 0,100 times) (Pressure = negative)

Maximum value = 32,03 kN/m^2

Minimum value = -25,42 kN/m^2

Figure A.7 : Excess pore pressure distribution backfill at the end of the earthquake.

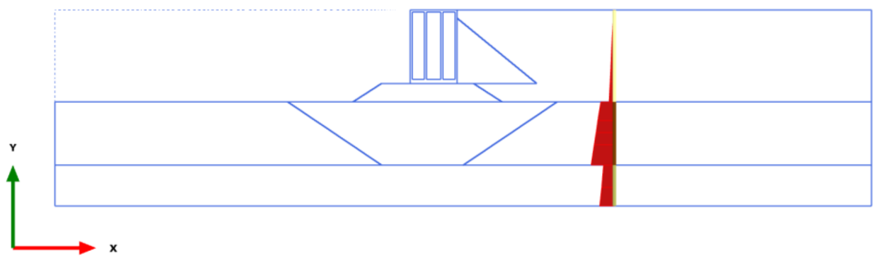

Principal effective stress σ'_3 (scaled up 0,0200 times)

Maximum value = -4,710 kN/m^2

Minimum value = -284,4 kN/m^2

Figure A.8 : Effective stress distribution backfill at the end of the earthquake.

CURRICULUM VITAE

Name Surname: Doruk DİKER

Place and Date of Birth: Diyarbakır – 14/04/1990

E-Mail: dorukdiker@gmail.com

EDUCATION:

B.Sc.: Istanbul Technical University (2013)

PROFESSIONAL EXPERIENCE AND REWARDS:

1) **Internship:** İstanbul İl Özel İdaresi (2011)
2) **Internship:** İstanbul İl Özel İdaresi (2012)